

Light hadron spectroscopy with two flavors of $O(a)$ -improved dynamical quarks

JLQCD Collaboration: S. Aoki¹, R. Burkhalter^{1,2}, M. Fukugita³, S. Hashimoto⁴, K-I. Ishikawa², N. Ishizuka^{1,2}, Y. Iwasaki^{1,2}, K. Kanaya^{1,2}, T. Kaneko⁴, Y. Kuramashi⁴, M. Okawa⁵, T. Onogi⁶, N. Tsutsui⁴, A. Ukawa^{1,2}, N. Yamada⁴, and T. Yoshié^{1,2}

¹*Institute of Physics, University of Tsukuba, Tsukuba, Ibaraki 305-8571, Japan*

²*Center for Computational Physics, University of Tsukuba, Tsukuba, Ibaraki 305-8577, Japan*

³*Institute for Cosmic Ray Research, University of Tokyo, Kashiwa 277-8582, Japan*

⁴*High Energy Accelerator Research Organization (KEK), Tsukuba, Ibaraki 305-0801, Japan*

⁵*Department of Physics, Hiroshima University,*

Higashi-Hiroshima, Hiroshima 739-8526, Japan

⁶*Yukawa Institute for Theoretical Physics, Kyoto University, Kyoto 606-8502, Japan*

(Dated: October 31, 2018)

We present a high statistics study of the light hadron spectrum and quark masses in QCD with two flavors of dynamical quarks. Numerical simulations are carried out using the plaquette gauge action and the $O(a)$ -improved Wilson quark action at $\beta = 5.2$, where the lattice spacing is found to be $a = 0.0887(11)$ fm from ρ meson mass, on a $20^3 \times 48$ lattice. At each of five sea quark masses corresponding to $m_{\text{PS}}/m_V \simeq 0.8-0.6$, we generate 12000 trajectories using the symmetrically pre-conditioned Hybrid Monte Carlo algorithm. Finite spatial volume effects are investigated employing $12^3 \times 48$, $16^3 \times 48$ lattices. We also perform a set of simulations in quenched QCD with the same lattice actions at a similar lattice spacing to those for the full QCD runs. In the meson sector we find clear evidence of sea quark effects. The J parameter increases for lighter sea quark masses, and the full QCD meson masses are systematically closer to experiment than in quenched QCD. Careful finite-size studies are made to ascertain that these are not due to finite-size effects. Evidence of sea quark effects is less clear in the baryon sector due to larger finite-size effects. We also calculate light quark masses and find $m_{ud}^{\overline{\text{MS}}}(2 \text{ GeV}) = 3.223 \left(\begin{smallmatrix} +0.046 \\ -0.069 \end{smallmatrix} \right)$ MeV and $m_s^{\overline{\text{MS}}}(2 \text{ GeV}) = 84.5 \left(\begin{smallmatrix} +12.0 \\ -1.7 \end{smallmatrix} \right)$ MeV which are about 20% smaller than in quenched QCD.

I. INTRODUCTION

Lattice QCD calculation of the light hadron mass spectrum has witnessed significant progress in recent years [1, 2, 3]. In the quenched approximation in which the quark vacuum polarization effects are ignored, the CP-PACS Collaboration performed a precise calculation of hadron masses, in which the estimated accuracy reached the level of a few percent in the continuum limit [4]. They found that the quenched spectrum shows a significant and systematic deviation from experiment; the K^*-K hyperfine splitting is smaller by about 10% than experiment. The decuplet baryon mass splittings are also small, and the octet baryon masses are themselves smaller than experiment.

Since this work, the focus of efforts has shifted toward full QCD simulations including vacuum polarization effects of dynamical quarks. A number of simulations now exist, pursued by the SESAM-T χ L [5, 6, 7], UKQCD [8, 9], CP-PACS [10, 11] and QCDSF-UKQCD [12] Collaborations for two flavors using the Wilson-type quark action, and by the MILC Collaboration [13, 14] for two and three flavors using the Kogut-Susskind(KS) quark action. In particular the CP-PACS calculation [10, 11] made a first attempt toward execution of the chiral and continuum extrapolations within the single set of simulations, as pioneered by the GF11 Collaboration [15] in their quenched spectrum study. The chief finding of this work was that the K^*-K hyperfine splitting agrees much better with experiment in two-flavor full QCD than in quenched QCD, and that light quark masses decrease by about 25% by the inclusion of dynamical u and d quarks.

A subtle point with the CP-PACS results is that the dynamical sea quark effects become manifest only after the continuum extrapolation. Further studies are required to consolidate effects of dynamical sea quarks. The CP-PACS simulation used a renormalization group (RG) improved gauge action [16], but the $O(a)$ -improved Wilson quark action [17] with only tadpole-improved [18] clover coefficient. This leaves scaling violation of $O(g^2a)$. The use of non-perturbatively determined clover coefficient removing all of $O(a)$ errors should be much better to control the continuum extrapolation [19]. Studies along this direction were previously carried out by the UKQCD and QCDSF Collaborations using the plaquette gauge action. However, sea quark effects are not clear in their results of hadron masses, albeit encouraging evidence is seen in the static quark potential [9, 12].

In the present work, we explore sea quark effects in hadron and quark masses in two-flavor QCD using the plaquette gauge action and the non-perturbatively $O(a)$ -improved Wilson quark action. Our simulations are performed at a single lattice spacing $a^{-1} \simeq 2$ GeV at $\beta = 5.2$ using a $20^3 \times 48$ lattice. We also carry out

calculations in quenched QCD with the same action and similar simulation parameters to those in full QCD in order to make a direct comparison between full and quenched QCD. Preliminary results of these calculations have been reported in Refs. [20, 21, 22, 23].

We pay particular attention to two points which are important for an unambiguous identification of sea quark effects. One is the finite spatial volume effect whose magnitude is believed to be more pronounced in full QCD simulations than in quenched QCD [24]. An increase of hadron masses due to this effect could mimic sea quark effects. There are only a few studies of finite-size effects in full QCD for the Wilson-type quark action [6, 8]. This leads us to perform a systematic investigation of finite-size effects employing $12^3 \times 48$, $16^3 \times 48$ and $20^3 \times 48$ lattices.

Another point is the chiral extrapolation. With currently available computer power and simulation algorithms, the sea quark mass which can be explored with the Wilson-type quark action is limited to values corresponding to $m_{\text{PS,sea}}/m_{\text{V,sea}} \gtrsim 0.6$. The long extrapolation to the physical u and d quark masses may involve sizable systematic errors, potentially blurring, or artificially enhancing, sea quark effects. This can be avoided if one examines sea quark effects at the quark masses actually simulated. In this study, therefore, sea quark effects are examined in detail not only at the physical quark mass but also at our simulation points.

We have also made efforts to accumulate high statistics of 12000 trajectories each at five values of sea quark masses. Our implementation of the symmetric preconditioning of the lattice clover-Dirac operator [25, 26] speeded up the configuration generation by a factor two by allowing a doubly larger step size over the even-odd preconditioning.

This paper is organized as follows. We describe details of configuration generation in full and quenched QCD in Sec. II. Method of measurement of hadron masses and the static quark potential is explained in Sec. III. Finite-size effects on hadron masses are discussed in Sec. IV. Section V is devoted to detailed description of the chiral extrapolation of our hadron mass data. We examine sea quark effects in light hadron masses in Sec. VI. Results of the decay constants and quark masses are presented in Secs. VII and VIII. Our conclusion is given in Sec. IX.

II. SIMULATION METHOD

A. Simulation parameters and algorithm

We carry out numerical simulations of lattice QCD with two flavors of degenerate dynamical quarks which are identified with the up and down quarks. We use the standard plaquette action for gauge fields defined by

$$S_g = \frac{\beta}{6} \sum_{x,\mu\nu} \text{Tr} U_{x,\mu\nu}, \quad (1)$$

where $U_{x,\mu\nu}$ is the product of gauge link variables $U_{x,\mu}$ around the plaquette given by

$$U_{x,\mu\nu} = U_{x,\mu} U_{x+\hat{\mu},\nu} U_{x+\hat{\mu},\mu}^\dagger U_{x,\nu}^\dagger. \quad (2)$$

The $O(a)$ -improved Wilson action [17] defined by

$$S_q = \sum_{x,y} \bar{q}_x D_{xy} q_y \quad (3)$$

$$D_{xy} = \delta_{xy} - K \sum_{\mu} \left\{ (1 - \gamma_{\mu}) U_{x,\mu} \delta_{x+\hat{\mu},y} + (1 + \gamma_{\mu}) U_{x,\mu}^\dagger \delta_{x,y+\hat{\mu}} \right\} - \frac{1}{2} K c_{\text{SW}} \sigma_{\mu\nu} F_{x,\mu\nu} \delta_{xy} \quad (4)$$

is used for the quark part. The field strength tensor on the lattice is defined by

$$F_{x,\mu\nu} = \frac{1}{8i} \left\{ (U_{x,\mu\nu} + U_{x,-\mu\nu} + U_{x,-\mu-\nu} + U_{x,\mu-\nu}) - (\text{h.c.}) \right\}, \quad (5)$$

where (h.c.) denotes the hermitian conjugate of the preceding bracket, and $\sigma_{\mu\nu} = (i/2) [\gamma_{\mu}, \gamma_{\nu}]$. The clover coefficient c_{SW} is set to the non-perturbative value determined by the ALPHA Collaboration [27].

Our simulations are performed at a single value of $\beta=5.2$. The lattice spacing fixed from m_{ρ} at the physical sea quark mass is found to be 0.0887(11) fm. Our value of β is slightly off the range $\beta=12.0-5.4$ where the

ALPHA Collaboration carried out a non-perturbative determination of c_{SW} . We set $c_{\text{SW}} = 2.02$ by extrapolating their parametrization formula of the non-perturbative c_{SW} as a function of the bare coupling. We performed an independent non-perturbative determination of c_{SW} at $\beta = 5.2$ and confirmed that our preliminary result $c_{\text{SW}} = 1.98(7)$ is consistent with 2.02 within the error [28].

We employ three lattice sizes that differ in spatial volumes, $N_s^3 \times N_t = 12^3 \times 48$, $16^3 \times 48$ and $20^3 \times 48$. The hadron spectrum and quark masses at the physical point are calculated using the data on the largest lattice. The data on the two smaller lattices are used to investigate finite-size effects on hadron masses.

On each lattice size, we adopt five values of the sea quark mass corresponding to the hopping parameter $K_{\text{sea}} = 0.1340, 0.1343, 0.1346, 0.1350$ and 0.1355 . This choice covers $m_{\text{PS,sea}}/m_{\text{V,sea}} = 0.6-0.8$, and enables us to extrapolate our data to the physical sea quark mass. These simulation parameters are summarized in Table I.

We note that the UKQCD Collaboration also performed a set of simulations using the same lattice action at $a^{-1} \simeq 2$ GeV [9]. There are, however, some differences in the choice of β and K_{sea} : The UKQCD simulations shift β with the sea quark mass keeping the Sommer scale r_0/a [29] fixed, while our simulations are performed at fixed β . Another difference is the range of the sea quark mass covered in the two simulations. We explore light sea quark masses down to $m_{\text{PS,sea}}/m_{\text{V,sea}} \simeq 0.6$, whilst UKQCD's lightest point is around $m_{\text{PS,sea}}/m_{\text{V,sea}} \simeq 0.7$. Although the UKQCD Collaboration made another simulation at a smaller sea quark mass $m_{\text{PS,sea}}/m_{\text{V,sea}} \simeq 0.6$ at a spatial extent of $N_s = 16$ ($N_s a \simeq 1.6$ fm), finite-size effects seem to be significant there (see discussion in Sec. IV).

Gauge configurations are generated using the Hybrid Monte Carlo (HMC) algorithm [30, 31]. We use simulation programs with three variants of HMC for the $O(a)$ -improved Wilson action:

- HMC with the even/odd preconditioning [32] only for the inversion of the quark matrix D_{xy} . This algorithm is used in the simulations on the $16^3 \times 48$ lattice.
- HMC with the asymmetric preconditioning for the lattice action (A-HMC) [25, 26, 33]. Whole simulations on the $12^3 \times 48$ lattice are performed with this algorithm.
- HMC with the symmetric preconditioning for the action (S-HMC) [25, 26], which shows the best performance among the three algorithms.

Our main simulation on the $20^3 \times 48$ lattices is initially started with the A-HMC algorithm, but is later switched to the S-HMC to speed up the calculations. The trajectory length in each HMC step is fixed to the unit length. We use the conventional leap-frog integration scheme for the molecular dynamics equation. The step size $\Delta\tau$ is chosen to achieve an acceptance of 60–80%.

The even/odd preconditioned BiCGStab algorithm [34] is used for the quark matrix inversion to solve the equation $D_{xy}G_y = B_x$. We take the stopping condition of the form $\|DG - B\| < \Delta$ in the HMC program. A modified form $\|DG - B\|/\|B\| < \Delta$ is used in the A-HMC and S-HMC programs. The value of Δ in the evaluation of the fermionic force is determined so that the reversibility over unit length is satisfied to a relative level better than 10^{-13} for the Hamiltonian. We use a stricter stopping condition in the calculation of the Hamiltonian in the Metropolis accept/reject test. Table I shows our choice of Δ together with the average number of the BiCGStab iteration in the quark matrix inversion for the force calculation, N_{inv} .

We accumulate 12000 HMC trajectories at each sea quark mass on the $20^3 \times 48$ lattice. The statistics on smaller lattices are 3000 trajectories. Measurements of light hadron masses and the static quark potential are carried out at every 10 HMC trajectories. Details of the measurement method will be described in the next section.

All simulations are performed on the parallel computer HITACHI SR8000 model F1 installed at KEK. This machine consists of 100 nodes and has a peak speed of 1.2 TFLOPS and 448 GB of main memory in total. The CPU time needed per unit HMC trajectory on the full machine is listed in Table I. The total time for configuration generation on each lattice size is 8.6 days on $12^3 \times 48$, 58 days on $16^3 \times 48$, and 130 days on $20^3 \times 48$ lattices. Additional 100 days are spent for the measurement of the hadron masses and the static potential.

B. Simulation in quenched QCD

While many calculations of the hadron spectrum have been performed in quenched QCD, comparisons between our full QCD results and quenched results from other simulations may be subject to systematic uncertainties due to the difference in the simulation details. We therefore carry out a set of quenched calculations of the hadron spectrum using the same lattice actions and simulation parameters as those for full QCD runs.

Our simulations are performed at $\beta = 6.0$, where the lattice spacing fixed from m_ρ equals 0.1074(14) fm. We take $c_{\text{SW}} = 1.769$ which is the value determined non-perturbatively by the ALPHA Collaboration [35]. Three lattice sizes $12^3 \times 48$, $16^3 \times 48$ and $20^3 \times 48$ are employed in order to investigate finite-size effects.

Gauge configurations are generated with a combination of the heat-bath and the over-relaxation algorithms. We call four heat-bath sweeps with a succeeding over-relaxation step an iteration. We accumulate statistics of 60000 iterations on each lattice size. Hadron masses and the static potential are calculated at every 200 iterations.

III. MEASUREMENT

A. Hadron Masses

In measurements in full QCD, we use six values of the valence quark mass corresponding to the hopping parameter $K_{\text{val},i} (i = 1, \dots, 6) = 0.1340, 0.1343, 0.1346, 0.1350, 0.1355$ and 0.1358 , which cover the range of $m_{\text{PS, val}}/m_{\text{V, val}} \simeq 0.5 - 0.8$. At each sea quark mass, therefore, there is one value of $K_{\text{val},i}$, which equals K_{sea} and is identified as the light quark mass. Other five values of $K_{\text{val},i}$ correspond to the mass of strange quarks treated in the quenched approximation. In the following, we use the abbreviation ‘‘diagonal data’’ to represent hadron correlators or masses with a quark mass combination in which all valence quark masses are equal to the sea quark mass.

We employ meson operators defined by

$$M(x) = \bar{q}_x^{(f)} \Gamma q_x^{(g)}, \quad \Gamma = I, \gamma_5, \gamma_\mu, \gamma_5 \gamma_\mu, \quad (6)$$

where f and g are flavor indices and x is the coordinates on the lattice. Meson correlators $\langle M(x)M(0)^\dagger \rangle$ are calculated for the following eleven combinations of valence quark masses

$$\begin{aligned} & (K_{\text{val},i}, K_{\text{val},i}) \quad (i = 1, \dots, 6), \\ & (K_{\text{sea}}, K_{\text{val},i}) \quad (i = 1, \dots, 6, K_{\text{sea}} \neq K_{\text{val},i}). \end{aligned} \quad (7)$$

The former is identified with a degenerate light or strange meson and the latter with a non-degenerate light-strange meson. This choice of the valence quark masses enables us to calculate the full spectrum of strange and non-strange mesons.

For baryons, we use the same operators as those employed in Ref. [11]. Namely, the octet baryon operator is defined as

$$O^{fgh}(x) = \epsilon^{abc} \left(q_x^{(f)aT} C \gamma_5 q_x^{(g)b} \right) q_x^{(h)c}, \quad (8)$$

where a, b, c are color indices and $C = \gamma_4 \gamma_2$ is the charge conjugation matrix. We measure baryon correlators with two types of flavor structure (Σ - and Λ -like baryons),

$$\Sigma : -\frac{1}{\sqrt{2}} \left(O^{[fh]g} + O^{[gh]f} \right), \quad (9)$$

$$\Lambda : \frac{1}{\sqrt{6}} \left(O^{[fh]g} - O^{[gh]f} - 2O^{[fg]h} \right), \quad (10)$$

where $O^{[fgh]} = O^{fgh} - O^{gfh}$. Decuplet baryon correlators are calculated using an operator defined by

$$D^{fgh}(x) = \epsilon^{abc} \left(q_x^{(f)aT} C \gamma_\mu q_x^{(g)b} \right) q_x^{(h)c} \quad (11)$$

with symmetrized flavor structure

$$\begin{aligned} O^{fff}, \quad & \frac{1}{\sqrt{3}} (D^{ffg} + D^{fgf} + D^{gff}), \\ & \frac{1}{\sqrt{6}} (D^{fgh} + D^{hfg} + D^{ghf} + D^{fhg} + D^{gfh} + D^{hgf}). \end{aligned} \quad (12)$$

We take quark mass combinations of $(K_{\text{val},i}, K_{\text{val},i}, K_{\text{val},i})$ ($i = 1, \dots, 6$), $(K_{\text{sea}}, K_{\text{val},i}, K_{\text{val},i})$ and $(K_{\text{sea}}, K_{\text{sea}}, K_{\text{val},i})$ ($i = 1, \dots, 6, K_{\text{sea}} \neq K_{\text{val},i}$) for the baryon correlators.

In order to construct the smeared hadron operators, we measure the wave function of the pseudoscalar (PS) meson

$$\phi(\mathbf{r}) = \frac{\sum_{\mathbf{x}} \langle \bar{q}(\mathbf{x}, t) \gamma_5 q(\mathbf{x} + \mathbf{r}, t) P(\mathbf{0}, 0)^\dagger \rangle}{\sum_{\mathbf{x}} \langle P(\mathbf{x}, t) P(\mathbf{0}, 0)^\dagger \rangle}, \quad (13)$$

where P is the PS meson operator, Eq. (6), with $\Gamma = \gamma_5$ and t fixed to 12. The measurement is performed at each sea quark mass and lattice size using a subset of gauge configurations (30 configurations every 100 trajectories). We parameterize $\phi(\mathbf{r})$ using a polynomial approximation $\phi(\mathbf{r}) = 1 + \sum_{n=1,8} c_n |\mathbf{r}|^n$ and use it as the smearing function. We employ three types of the meson operator : i) local operator, ii) smeared operator $M(x) = \sum_{\mathbf{r}} \phi(\mathbf{r}) \bar{q}(\mathbf{x}, t) \Gamma q(\mathbf{x} + \mathbf{r}, t)$, iii) doubly smeared operator $M(x) = \sum_{\mathbf{r}, \mathbf{r}'} \phi(\mathbf{r}) \phi(\mathbf{r}') \bar{q}(\mathbf{x} + \mathbf{r}, t) \Gamma q(\mathbf{x} + \mathbf{r}', t)$. Additionally, we use ‘‘triply smeared operator’’

$$O^{fgh}(x) = \sum_{\mathbf{r}_1, \mathbf{r}_2, \mathbf{r}_3} \phi(\mathbf{r}_1) \phi(\mathbf{r}_2) \phi(\mathbf{r}_3) \epsilon^{abc} (q^{aT}(\mathbf{x} + \mathbf{r}_1, t) C \Gamma q^b(\mathbf{x} + \mathbf{r}_2, t)) q^c(\mathbf{x} + \mathbf{r}_3, t) \quad (14)$$

for baryons. Hadron correlators are measured with a) point source and sink operators, b) smeared source and point sink, and c) smeared source and sink operators. We fix configurations to the Coulomb gauge, since b) and c) are not gauge invariant.

We observe that, when valence quarks are lighter than sea quarks, the hadron correlator takes an exceptionally large value on a small number of configurations. This might be caused by a fluctuation of the lowest eigenvalue of the Dirac operator of the $O(a)$ -improved Wilson action. If the PS meson correlator on the i -th gauge configuration takes a value larger than 20 times the statistical average, which is evaluated without that configuration, at a certain time slice

$$\langle P(x) P(0)^\dagger \rangle_i > \frac{20}{N_{\text{conf}} - 1} \sum_{k=1, k \neq i}^{N_{\text{conf}}} \langle P(x) P(0)^\dagger \rangle_k \quad (15)$$

where N_{conf} is the total number of configurations, we consider it as an exceptional configuration and remove it from the following analysis. The number of the removed configurations is given in Table I.

In order to reduce the statistical fluctuation of hadron correlators on the $20^3 \times 48$ lattice, we repeat the measurement for two choices of the location of the hadron source, $t_{\text{src}} = 1$ and $N_t/2 + 1 (= 25)$, and take the average over the two sources:

$$\frac{1}{2} \left(\langle M(t_{\text{src}} + t) M(t_{\text{src}})^\dagger \rangle_{t_{\text{src}}=1} + \langle M(t_{\text{src}} + t) M(t_{\text{src}})^\dagger \rangle_{t_{\text{src}}=25} \right). \quad (16)$$

We find that this procedure reduces the statistical error of hadron correlators by typically 20%, which suggests that the statistics is increased effectively by a factor of 1.5. For further reduction of the statistical fluctuation, we take the average over three polarization states for vector mesons, two spin states for octet baryons and four spin states for decuplet baryons.

Figures 1–4 show examples of effective mass plots. We find that the best plateau of the effective mass is obtained from hadron correlators with the point sink and the doubly smeared source for mesons and the triply smeared one for baryons. Therefore, hadron masses are extracted from these types of correlators.

We carry out χ^2 fits to hadron correlators by taking account of correlations among different time slices. A single hyperbolic cosine form is assumed for mesons, and a single exponential form for baryons. The lower cut of the fit range t_{min} is determined by inspecting stability of the fitted mass. The upper cut (t_{max}) dependence of the fit results is small and, therefore, we fix t_{max} to $N_t/2$ for all hadrons. Our choice of fit ranges and resulting hadron masses are summarized in Tables XXIX–XXXIV in Appendix A. Statistical errors of hadron masses are estimated with the jack-knife procedure. We adopt the bin size of 100 trajectories by inspecting the bin size dependence of the jack-knife error as discussed in Sec.III C.

In Fig. 5, we test double exponential fits to extract hadron masses at $K_{\text{sea}} = K_{\text{val}} = 0.1355$. While these fits are unstable and lead to a large error for the mass of the first excited state, the result for the ground state mass is consistent with that from the single exponential fit. The situation is similar at other sea and valence quark masses. This suggests that the hadron masses in Tables XXIX – XXXIV and the light hadron spectrum calculated from these results have small contamination from excited states.

Hadron correlators in quenched QCD are calculated in an analogous manner. We use six values of K_{val} , 0.13260, 0.13290, 0.13331, 0.13384, 0.13432 and 0.13465, corresponding to $m_{\text{PS, val}}/m_{\text{V, val}} \simeq 0.50 - 0.80$ and the hadron operators and smearing procedure same as those in the full QCD study. A difference is that we can take more combinations of valence quark masses than in full QCD, since any value of the six valence quark masses can be identified with either light or strange quark mass. We take all combinations $(K_{\text{val}, i}, K_{\text{val}, j})$ ($i, j = 1, \dots, 6$) for mesons, and somewhat restricted choices $(K_{\text{val}, i}, K_{\text{val}, j}, K_{\text{val}, k})$ ($i, j, k = 1, \dots, 6$) for baryons. Statistical errors are estimated with the jack-knife procedure with bin size of 200 iterations. The exceptional configurations are discarded with the same criterion as defined in Eq. (15). Results of hadron masses are collected in Tables XXXV – XL in Appendix A.

B. Static quark potential

We calculate the static quark potential in order to determine the Sommer scale [29] which we use in our analysis of hadron masses. For this purpose, the temporal Wilson loops $W(r, t)$ up to $t = 16$ and $r = (\sqrt{3}N_s/2)$ are measured both in full and quenched QCD simulations. We apply the smearing procedure of Ref. [36] up to twelve steps and the measurements are carried out every four steps.

The static quark potential $V(r)$ is determined from the correlated fit of the form

$$W(r, t) = C(r) \exp[-V(r)t]. \quad (17)$$

We take the fit range $[t_{\text{min}}, t_{\text{max}}] = [3, 7]$ in all simulations in full and quenched QCD by inspecting the t dependence of the effective potential

$$V_{\text{eff}}(r, t) = \ln[W(r, t)/W(r, t+1)]. \quad (18)$$

Examples of V_{eff} are plotted in Fig. 6. For each r , the number of smearing steps is fixed to its optimum value at which the overlap to the ground state $C(r)$ takes the largest value.

As shown in Fig.7, we do not observe any clear indication of the string breaking. Therefore $V(r)$ is fitted to the form

$$V(r) = V_0 - \frac{\alpha}{r} + \sigma r + \delta V(r), \quad (19)$$

where $\delta V(r)$ is the lattice correction to the Coulomb term calculated perturbatively from one lattice-gluon exchange diagram [37]

$$\delta V(r) = -g_c \left(G(\mathbf{r}) - \frac{1}{r} \right), \quad (20)$$

$$G(\mathbf{r}) = 4\pi \sum_{\mathbf{k}} \frac{\cos[\mathbf{k}\mathbf{r}]}{4 \sum_{i=1}^3 \sin^2[k_i/2]}. \quad (21)$$

The Sommer scale r_0 defined through [29]

$$r_0^2 \left. \frac{dV(r)}{dr} \right|_{r=r_0} = 1.65 \quad (22)$$

is then determined from the parametrization of the corrected potential $V(r) - \delta V(r)$:

$$r_0 = \sqrt{\frac{1.65 - \alpha}{\sigma}}. \quad (23)$$

The lower cut of the fit range in Eq. (19), r_{min} , is determined by inspecting the r_{min} dependence of r_0 . We observe that r_0 is relatively stable for $r_{\text{min}} \in [\sqrt{2}, 2\sqrt{2}]$ as shown in Fig.8. With $r_{\text{min}} < \sqrt{2}$, χ^2/dof takes an unacceptably large value due to the violation of rotational symmetry, while α becomes ill-determined with

$r_{\min} > 2\sqrt{2}$. We therefore take $r_{\min} = \sqrt{5}$. While the r_{\max} dependence of r_0 is rather mild, the covariance matrix becomes ill-determined with r_{\max} greater than $9\sqrt{2}$ on $20^3 \times 48$, $7\sqrt{2}$ on $16^3 \times 48$ and $6\sqrt{2}$ on $12^3 \times 48$. We therefore fix r_{\max} to these values.

We repeat the fits, Eqs. (17) and (19), with other choices of the range: $t_{\min} = 4$ or $r_{\min} \in [\sqrt{2}, 2\sqrt{2}]$. The largest deviations in the fit parameters and r_0 are included into their systematic errors. Other systematic errors due to the choice of t_{\max} , the optimum number of the smearing steps and r_{\max} are small and ignored. Fit parameters in Eq. (19) and r_0 are summarized in Table II for full QCD, and in Table III for quenched QCD.

C. Autocorrelation

The autocorrelation in our full QCD data is studied by calculating the cumulative autocorrelation time

$$\tau_{\mathcal{O}}^{\text{cum}}(\Delta t_{\max}) = \frac{1}{2} + \sum_{\Delta t=1}^{\Delta t_{\max}} \rho_{\mathcal{O}}(\Delta t), \quad (24)$$

where $\rho_{\mathcal{O}}(t)$ is the autocorrelation function

$$\rho_{\mathcal{O}}(\Delta t) = \frac{\Gamma_{\mathcal{O}}(\Delta t)}{\Gamma_{\mathcal{O}}(0)}, \quad (25)$$

$$\Gamma_{\mathcal{O}}(\Delta t) = \langle (\mathcal{O}(t) - \langle \mathcal{O} \rangle) (\mathcal{O}(t + \Delta t) - \langle \mathcal{O} \rangle) \rangle \quad (26)$$

and we take $\Delta t_{\max} = 200$.

In Table IV, we summarize $\tau_{\mathcal{O}}^{\text{cum}}$ in the A-HMC and S-HMC simulations on the $20^3 \times 48$ lattices for three quantities: i) the plaquette which is measured at every trajectory, ii) the PS meson propagator at $t=12$, iii) the temporal Wilson loop with $(r, t) = (5, 4)$. The results do not show any systematic differences in $\tau_{\mathcal{O}}^{\text{cum}}$ between the A-HMC and S-HMC runs. The plaquette shows the largest autocorrelation with $\tau_{\text{plaq}}^{\text{cum}} = 10-30$, which is similar to those found in the UKQCD simulation [9] using the same lattice action and similar simulation parameters. We obtain smaller values of $\tau_{\mathcal{O}}^{\text{cum}}$ for the other two quantities. This is contrary to a naive expectation that these long-distance observables have a longer autocorrelation than the local quantity like the plaquette. This suggests that the size of noise arising from short correlation modes is larger than that of the longest mode in these observables and our statistics are not sufficient to extract $\tau_{\mathcal{O}}^{\text{cum}}$ of the longest but weak mode.

The statistical error including the effect of autocorrelation is given by $\sqrt{2\tau_{\mathcal{O}}^{\text{cum}}}$ times the naive error. Therefore, the above observation tells us that the bin size in the jack-knife procedure of 60 HMC trajectories or larger is a safe choice to take account of the autocorrelation in our data.

The bin size dependence of the jack-knife error of hadron masses and the static potential is plotted in Figs. 9 and 10. We use errors obtained from uncorrelated fits because, with large bin sizes, the number of bins would not be sufficiently large to determine the covariance matrix reliably. For both hadron masses and the static potential, the jack-knife error reaches its plateau at bin size of 50–100 trajectories, which is roughly consistent with the above estimate from $\tau_{\mathcal{O}}^{\text{cum}}$. The situation is similar on smaller volumes $16^3 \times 48$ and $12^3 \times 48$. We therefore take the bin size of 100 trajectories in the error analysis in full QCD.

We also investigate the bin size dependence of the jack-knife error in quenched QCD. As shown in Figs. 11 and 12, the bin size of 200 iterations is reasonable.

Another point of interest is the sea quark mass dependence of the autocorrelation. A natural expectation is that smaller sea quark mass leads to a larger correlation length and hence a longer autocorrelation. This expectation is supported by the CP-PACS observation in Ref. [11], where they used the RG-improved gauge and clover quark actions. However, our result of $\tau_{\text{plaq}}^{\text{cum}}$ in the S-HMC simulations, which is determined more precisely than that for the A-HMC due to the higher statistics, shows the contrary sea quark mass dependence: $\tau_{\text{plaq}}^{\text{cum}}$ decreases as the sea quark mass decreases. This is consistent with the UKQCD's observation in Ref. [9]. We also note that $\tau_{\text{plaq}}^{\text{cum}}$ in our simulations is much larger than in the CP-PACS's runs particularly at the heaviest sea quark masses $m_{\text{PS,sea}}/m_{\text{V,sea}} \simeq 0.8$ ($K_{\text{sea}} = 0.1340$).

In our determination of non-perturbative c_{SW} at $\beta = 5.2$ [28], we find that the expectation value of the plaquette varies rapidly around $K_{\text{sea}} \simeq 0.132$, where the plaquette shows the strongest autocorrelation in the investigated region $K \in [0.100, 0.136]$. Since such a behavior, somewhat similar to a phase transition, is not observed at higher β , we consider the unexpected behavior of the plaquette to be an artifact due to finite lattice

spacing. This artifact is probably absent or well suppressed with the CP-PACS's choice of the improved actions. At sufficiently small lattice spacings, we then expect that $\tau_{\text{plaq}}^{\text{cum}}$ shows the natural sea quark mass dependence, namely larger $\tau_{\text{plaq}}^{\text{cum}}$ for lighter sea quark masses. We also expect that, even at $\beta=5.2$, $\tau_{\text{plaq}}^{\text{cum}}$ will increase if the sea quark mass becomes sufficiently small compared to that corresponding to $K_{\text{sea}}=0.132$.

IV. FINITE-SIZE EFFECTS

Finite-size effects (FSE) are one of the major sources of systematic errors in lattice calculations. Since our largest volume size $\simeq (1.8 \text{ fm})^3$ is still not so large, it is important to check FSE in our data. We discuss how much FSE is present in our data on the largest lattice using data on three spatial volumes $12^3 \times 48$, $16^3 \times 48$ and $20^3 \times 48$.

In Figs. 13–15, we plot diagonal data of hadron masses as a function of the spatial volume inverse. For $m_{\text{PS,sea}}/m_{\text{V,sea}} \gtrsim 0.7$, including the quenched case, hadron masses obtained on the $16^3 \times 48$ and $20^3 \times 48$ lattices are consistent with each other within two standard deviations. On the other hand, hadron masses decrease monotonously up to $V=20^3$ at the lightest sea quark mass corresponding to $m_{\text{PS,sea}}/m_{\text{V,sea}} \simeq 0.6$.

The magnitude of FSE also depends on the valence quark mass. Figure 16 shows the valence quark mass dependence of the relative mass shift between the two larger lattices for PS mesons and octet baryons. We observe that, except at the lightest sea quark mass, the mass shift is at most a few percent level in the whole range of the simulated valence quark mass. The situation is similar for vector mesons and decuplet baryons. Therefore, we conclude that the size of FSE on our largest lattice is small over our range of valence quark masses down to the second lightest sea quark mass.

The mass shift is non-negligible at the lightest sea quark mass. While the magnitude is of the order of a few percent for the heaviest valence quarks, it clearly increases as the valence quark mass decreases.

We consider that the observed FSE is caused by valence quarks wrapping around the lattice in spatial directions (namely squeezing of hadrons into the small box) rather than wrapping of virtual pions. As shown in Fig. 13, the magnitude of FSE caused by the effects of virtual pions (long dashed line) [38] given by $m_{\text{PS}}(L) - m_{\text{PS}}(L=\infty) \sim \exp[-m_{\text{PS}}(L=\infty)L]$ with $L=N_s a$ is too small compared to observed effects.

A qualitative understanding of the observed FSE is as follows. The wrapping of valence quarks is suppressed by the center $Z(3)$ symmetry in quenched QCD [24]. In full QCD, $Z(3)$ symmetry is broken by the wrapping of sea quarks in the spatial directions, whose magnitude increases toward lighter sea quark. A possible reason why FSE is significant only at our lightest sea quark mass would be that the $Z(3)$ breaking turns on rather quickly around the lightest sea quarks.

The enhancement of FSE toward the lighter valence quarks leads to a decrease of the slope $dm_{\text{had}}/dm_{\text{PS}}^2$ in Fig. 17 and, hence, underestimation of hadron mass splittings, such as the K^*-K hyperfine splitting. The mass splittings are expected to be increased by sea quark effects, since these are underestimated in quenched QCD as well established in Ref. [4]. Therefore, FSE makes sea quark effects less clear. It is crucial to check how large FSE is in our hadron mass data at the lightest sea quark mass on the largest lattice.

Figures 13 and 14 show that the volume dependence of our data is well described by a power law

$$m_{\text{had}}(L) = m_{\text{had}}(L=\infty) + c/L^3 \quad (27)$$

as found in Ref. [39] using the KS fermion. The relative size of FSE on the largest lattice

$$\Delta m = \frac{m(L=20a) - m_{\text{had}}(L=\infty)}{m(L=20a)} \quad (28)$$

is estimated from this ansatz and is plotted in Fig. 18. We find that, for PS and vector mesons, Δm is about 5 % for diagonal data and is reduced to a few percent at $K_{\text{val}}=0.1350$, which roughly corresponds to the strange quark mass m_s . It is expected, however, that the volume dependence (27) turns into a milder form $\exp[-m_{\text{PS}}L]$ for sufficiently large volumes. The actual size of FSE should be smaller than the above estimation, say, a few percent. Since this is smaller than the typical size of quenching errors, which is 5–10%, we consider that the examination of sea quark effects is feasible in the meson sector, particularly in strange meson masses.

Finite-size effects are more pronounced for baryon masses as observed in Fig. 18. For diagonal data, Δm is roughly comparable with typical quenching errors in the baryon spectrum of the order of 5–10 %. Sea quark effects in the light baryon masses, such as m_N and m_Δ , may become unclear by the contamination of FSE.

We note, however, that Δm decreases for heavier valence quark masses. The examination of sea quark effects becomes more feasible for strange baryon masses like m_{Ξ} and m_{Ω} .

Figure 19 shows Δm for the diagonal data of the octet baryon mass as a function of N_s . We find that the size of $N_s \approx 30$, which corresponds to $L \approx 2.7$ fm, is required to suppress Δm to a few percent level. The required size becomes slightly smaller, $L \approx 2.4$ fm, for the valence quark mass around m_s . These sizes are larger than our largest spatial lattice size $L \simeq 1.8$ fm. Further simulations on such large lattices will be needed to obtain a definite conclusion on sea quark effects in the baryon spectrum.

Tables II and III show that FSE in r_0 are much smaller than in hadron masses. While the central value on 20^3 is systematically higher than that on 16^3 in both full and quenched QCD, the difference is about 1 % and not significant with the accuracy of our data. The size of FSE is small, namely a few percent level, even on 12^3 . Therefore FSE in r_0 on the largest lattice can be safely neglected both in full and quenched QCD.

V. CHIRAL EXTRAPOLATION

The hadron spectrum in full QCD is calculated using hadron masses measured on the $20^3 \times 48$ lattice. This requires a parametrization of the mass data as a function of sea and valence quark masses in order to extrapolate (up-down) or interpolate (strange) quark masses to their physical values. We make this parametrization by combined fits to masses of a given hadron at all sea quark masses. We test the following two methods for the combined fit:

- A The effective lattice spacing, determined from r_0 for instance, may vary as a function of the sea quark mass. In order to separate this effect from the physical quark mass dependence, we carry out the chiral extrapolation using dimensionless quantities such as $(r_0(K_{\text{sea}})m_{\text{had}}(K_{\text{sea}}; K_{\text{val},1}, K_{\text{val},2}))$, where $m_{\text{had}}(K_{\text{sea}}; K_{\text{val},1}, K_{\text{val},2})$ represents the measured hadron mass composed of valence quark masses corresponding to $K_{\text{val},1}$ and $K_{\text{val},2}$ on the gauge configurations generated at K_{sea} . We refer to this way as “method-A”.
- B It is also possible to fit hadron masses in lattice units, as was done by the SESAM [5] and the CP-PACS [11] Collaborations. We call this “method-B”.

A detailed description of the two methods will be given in Secs. V A and V B. They should yield a consistent hadron spectrum, since fit forms in method-B can be reproduced from those in method-A by expanding r_0 as a function of sea quark mass. This consistency is examined in Sec. V B.

A. chiral extrapolation using r_0 (method-A)

Chiral perturbation theory (ChPT) [40] provides a guide to obtain a controlled chiral limit of hadron mass data. For the quark mass dependence of diagonal data of the PS meson mass, ChPT predicts the presence of logarithmic singularities. At the one-loop level, the ChPT prediction reads

$$\frac{m_{\text{PS}}^2}{2B_0m_q} = 1 + \frac{1}{N_f}y \ln[y] + Ay \quad (29)$$

where $y = 2B_0m_q/(4\pi f)^2$ and A is a linear combination of the low energy constants α_i of ChPT Lagrangian : $A = (2\alpha_8 - \alpha_5) + N_f(2\alpha_6 - \alpha_4)$. The mass ratio on the left hand-side, m_{PS}^2/m_q , is plotted as a function of $m_q \propto y$ in Fig. 20. As we already reported [21, 23], our data show no hint of the curvature predicted by the chiral logarithm. The fit of Eq. (29), assuming f to be a free parameter, gives $f \sim 6$ GeV, which is much larger than its experimental value 93 MeV. On the other hand, the fit gives an unacceptably large $\chi^2/\text{dof} = O(100)$, if we fix f to the experimental value.

A similar test using formulae from partially quenched ChPT (PQChPT) [41] also shows that the coefficient of the chiral logarithm term obtained from our data is much smaller than the prediction from PQChPT [21, 23, 42]. A possible reason for the absence of the chiral logarithm is that the sea quark mass in our simulations is still too large and higher order corrections of ChPT should be included to describe the data.

In this study, therefore, we use simple polynomial fitting forms in terms of the quark mass for the chiral extrapolation. The systematic error due to the chiral extrapolation is estimated by testing several different

polynomial forms. However, the inconsistency between our data and ChPT suggests that the extrapolation may have larger uncertainty than this estimation. This point will be examined in detail in a separate paper [42].

Since the sea quark mass in our simulations is not so small as discussed above, it is important to check the convergence property of the polynomial expansion of hadron masses in our range of the sea quark mass. We carry out both quadratic and cubic chiral fits to diagonal data of PS and vector meson masses:

$$(r_0(K_{\text{sea}}) m_{\text{PS}}(K_{\text{sea}}; K_{\text{sea}}, K_{\text{sea}}))^2 = B_{\text{diag}}^{\text{PS}} \mu_{\text{q,sea}} + C_{\text{diag}}^{\text{PS}} \mu_{\text{q,sea}}^2 + D_{\text{diag}}^{\text{PS}} \mu_{\text{q,sea}}^3, \quad (30)$$

$$r_0(K_{\text{sea}}) m_{\text{V}}(K_{\text{sea}}; K_{\text{sea}}, K_{\text{sea}}) = A_{\text{diag}}^{\text{V}} + B_{\text{diag}}^{\text{V}} \mu_{\text{PS,sea}} + C_{\text{diag}}^{\text{V}} \mu_{\text{PS,sea}}^2 + D_{\text{diag}}^{\text{V}} \mu_{\text{PS,sea}}^3, \quad (31)$$

where $\mu_{\text{q,diag}}$ and $\mu_{\text{PS,sea}}$ are the quark mass defined through the vector Ward identity (VWI) and the PS meson mass normalized by r_0 :

$$\mu_{\text{q,sea}} = r_0(K_{\text{sea}}) m_{\text{q,sea}}, \quad (32)$$

$$m_{\text{q,sea}} = \frac{1}{2} \left(\frac{1}{K_{\text{sea}}} - \frac{1}{K_c} \right), \quad (33)$$

$$\mu_{\text{PS,sea}} = (r_0(K_{\text{sea}}) m_{\text{PS,sea}})^2, \quad (34)$$

$$m_{\text{PS,sea}} = m_{\text{PS}}(K_{\text{sea}}; K_{\text{sea}}, K_{\text{sea}}). \quad (35)$$

Fit parameters and χ^2/dof are collected in Tables V and VI. The coefficient of the cubic term is small and consistent with zero for both Eqs. (30) and (31). Consequently, the quadratic and cubic fits show a good consistency with each other in the whole range of the quark mass and toward the chiral limit, as seen in Fig. 21. These observations suggest that the polynomial expansion up to the quadratic order is sufficient to describe the quark mass dependence of our data of meson masses in the method-A.

We carry out a combined fit to PS meson masses as a function of sea and valence quark masses using the quadratic form

$$\begin{aligned} & (r_0(K_{\text{sea}}) m_{\text{PS}}(K_{\text{sea}}; K_{\text{val},1}, K_{\text{val},2}))^2 \\ &= B_s^{\text{PS}} \mu_{\text{q,sea}} + B_v^{\text{PS}} \mu_{\text{q,val}} + C_s^{\text{PS}} \mu_{\text{q,sea}}^2 + C_v^{\text{PS}} \mu_{\text{q,val}}^2 + C_{sv}^{\text{PS}} \mu_{\text{q,sea}} \mu_{\text{q,val}}, \end{aligned} \quad (36)$$

where $\mu_{\text{q,sea}}$ is defined in Eq. (32) and

$$\mu_{\text{q,val}} = r_0(K_{\text{sea}}) m_{\text{q,val}}, \quad (37)$$

$$m_{\text{q,val}} = \frac{1}{2} (m_{\text{q,val},1} + m_{\text{q,val},2}), \quad (38)$$

$$m_{\text{q,val},i} = \frac{1}{2} \left(\frac{1}{K_{\text{val},i}} - \frac{1}{K_c} \right) \quad (i = 1, 2). \quad (39)$$

The presence of the monomial term in $m_{\text{q,sea}}$ means that the PS meson mass does not vanish in the chiral limit $m_{\text{q,val}} = 0$ for non-zero values of $m_{\text{q,sea}}$. This is because the value of K_{val} where the PS meson mass vanishes depends on the sea quark mass due to explicit violation of chiral symmetry with the Wilson-type quark action.

We employ uncorrelated fits in the combined chiral extrapolations although the data with the same sea quark mass are expected to be correlated. Therefore, the obtained χ^2/dof can be considered only as a guide to judge the quality of the fit. Figure 22 shows that this fit form describes our data well. Parameters of the fit are summarized in Table VII. We note that K_c determined from the diagonal fit Eq. (30) and the combined fit Eq. (36) are consistent with each other, as they should be.

The most general quadratic fit ansatz for the PS meson masses should include an additional cross term

$$(r_0(K_{\text{sea}}) m_{\text{PS}}(K_{\text{sea}}; K_{\text{val},1}, K_{\text{val},2}))^2 = \text{“r.h.s of Eq. (36)”} + C_{sv}^{\text{PS}} \mu_{\text{q,val},1} \mu_{\text{q,val},2}, \quad (40)$$

where $\mu_{\text{q,val},i} = r_0(K_{\text{sea}}) m_{\text{q,val},i}$. However, the coefficient is small as shown in fit parameters in Table VII, and hence does not change the hadron spectrum. We use this fit to estimate the systematic error due to the choice of the fitting function.

For the vector meson, we find that the following form describes our data well

$$r_0(K_{\text{sea}}) m_{\text{V}}(K_{\text{sea}}; K_{\text{val},1}, K_{\text{val},2}) = A^{\text{V}} + B_s^{\text{V}} \mu_{\text{PS,sea}} + B_v^{\text{V}} \mu_{\text{PS,val}} + C_{sv}^{\text{V}} \mu_{\text{PS,sea}} \mu_{\text{PS,val}}, \quad (41)$$

where $\mu_{\text{PS,sea}}$ is defined in Eq. (34) and

$$\mu_{\text{PS,val}} = (r_0(K_{\text{sea}}) m_{\text{PS,val}})^2, \quad (42)$$

$$m_{\text{PS,val}}^2 = \frac{1}{2} (m_{\text{PS,val},1}^2 + m_{\text{PS,val},2}^2), \quad (43)$$

$$m_{\text{PS,val},i} = m_{\text{PS}}(K_{\text{sea}}; K_{\text{val},i}, K_{\text{val},i}). \quad (44)$$

For a more general fit of form

$$r_0(K_{\text{sea}}) m_{\text{V}}(K_{\text{sea}}; K_{\text{val},1}, K_{\text{val},2}) = \text{“r.h.s of Eq. (41)”} + C_{\text{s}}^{\text{V}} \mu_{\text{PS,sea}}^2 + C_{\text{v}}^{\text{V}} \mu_{\text{PS,val}}^2, \quad (45)$$

the additional parameters C_{s}^{V} and C_{v}^{V} are not well-determined as seen in Table VIII. We use the former fit, which is shown in Fig. 23, to calculate the hadron spectrum, and the latter to estimate systematic error of the chiral extrapolation.

We also carry out a partially quenched fit to vector meson masses at each sea quark mass. We use a linear form, which is obtained from Eq. (41) by dropping all terms describing the sea quark mass dependence

$$m_{\text{V}}(K_{\text{sea}}; K_{\text{val},1}, K_{\text{val},2}) = A_{\text{PQ}}^{\text{V}} + B_{\text{PQ}}^{\text{V}} m_{\text{PS,val}}^2. \quad (46)$$

Parameters given in Table IX are used to calculate the J parameter at each sea quark mass.

The chiral extrapolation of octet baryon masses is carried out using a quadratic form based on the leading order prediction of ChPT [43], which was also used in Ref. [11]. We carry out the simultaneous fit to the Σ - and Λ -like octet baryon masses using the functions

$$\begin{aligned} & r_0(K_{\text{sea}}) m_{\text{oct},\Sigma}(K_{\text{sea}}; K_{\text{val},1}, K_{\text{val},2}, K_{\text{val},2}) \\ &= A^{\text{O}} + B_{\text{s}}^{\text{O}} \mu_{\text{PS,sea}} + (F_{\text{v}}^{\text{O}} - D_{\text{v}}^{\text{O}}) \mu_{\text{PS,val},1} + 2F_{\text{v}}^{\text{O}} \mu_{\text{PS,val},2} + C_{\text{s}}^{\text{O}} \mu_{\text{PS,sea}}^2 + (C_{\text{v}}^{\text{O}} + C_{\text{v}}^{\text{O},\Sigma}) \mu_{\text{PS,val},1}^2 \\ &+ (C_{\text{v}}^{\text{O}} - C_{\text{v}}^{\text{O},\Sigma}) \mu_{\text{PS,val},2}^2 + (C_{\text{sv}}^{\text{O}} + C_{\text{sv}}^{\text{O},\Sigma}) \mu_{\text{PS,sea}} \mu_{\text{PS,val},1} + (C_{\text{sv}}^{\text{O}} - C_{\text{sv}}^{\text{O},\Sigma}) \mu_{\text{PS,sea}} \mu_{\text{PS,val},2}, \end{aligned} \quad (47)$$

$$\begin{aligned} & r_0(K_{\text{sea}}) m_{\text{oct},\Lambda}(K_{\text{sea}}; K_{\text{val},1}, K_{\text{val},2}, K_{\text{val},2}) \\ &= A^{\text{O}} + B_{\text{s}}^{\text{O}} \mu_{\text{PS,sea}} + \left(F_{\text{v}}^{\text{O}} + \frac{D_{\text{v}}^{\text{O}}}{3} \right) \mu_{\text{PS,val},1} + 2 \left(F_{\text{v}}^{\text{O}} - \frac{2}{3} D_{\text{v}}^{\text{O}} \right) \mu_{\text{PS,val},2} \\ &+ C_{\text{s}}^{\text{O}} \mu_{\text{PS,sea}}^2 + (C_{\text{v}}^{\text{O}} + C_{\text{v}}^{\text{O},\Lambda}) \mu_{\text{PS,val},1}^2 + (C_{\text{v}}^{\text{O}} - C_{\text{v}}^{\text{O},\Lambda}) \mu_{\text{PS,val},2}^2 + (C_{\text{sv}}^{\text{O}} + C_{\text{sv}}^{\text{O},\Lambda}) \mu_{\text{PS,sea}} \mu_{\text{PS,val},1} \\ &+ (C_{\text{sv}}^{\text{O}} - C_{\text{sv}}^{\text{O},\Lambda}) \mu_{\text{PS,sea}} \mu_{\text{PS,val},2}, \end{aligned} \quad (48)$$

where $\mu_{\text{PS,val},i} = (r_0(K_{\text{sea}}) m_{\text{PS,val},i})^2$.

The decuplet baryon masses are well described by the following form

$$r_0(K_{\text{sea}}) m_{\text{dec}}(K_{\text{sea}}; K_{\text{val},1}, K_{\text{val},2}, K_{\text{val},2}) = A^{\text{D}} + B_{\text{s}}^{\text{D}} \mu_{\text{PS,sea}} + B_{\text{v}}^{\text{D}} \mu_{\text{PS,val}} + C_{\text{sv}}^{\text{D}} \mu_{\text{PS,sea}} \mu_{\text{PS,val}}, \quad (49)$$

where $\mu_{\text{PS,val}}$ stands for the average of three valence quark masses

$$\mu_{\text{PS,val}} = (r_0(K_{\text{sea}}) m_{\text{PS,val}})^2, \quad (50)$$

$$m_{\text{PS,val}}^2 = \frac{1}{3} (m_{\text{PS,val},1}^2 + 2m_{\text{PS,val},2}^2). \quad (51)$$

Figures 24 and 25 show the fit for octet and decuplet baryon masses. Parameters are summarized in Tables X and XI. We also test the following forms to estimate systematic error of the baryon spectrum due to the choice of the fitting form

$$\begin{aligned} & r_0(K_{\text{sea}}) m_{\text{oct}}(K_{\text{sea}}; K_{\text{val},1}, K_{\text{val},2}, K_{\text{val},2}) \\ &= \text{“r.h.s of Eqs. (47) and (48)”} + C_{\text{vv}}^{\text{O}} \mu_{\text{PS,val},1} \mu_{\text{PS,val},2}, \end{aligned} \quad (52)$$

$$\begin{aligned} & r_0(K_{\text{sea}}) m_{\text{dec}}(K_{\text{sea}}; K_{\text{val},1}, K_{\text{val},2}, K_{\text{val},2}) \\ &= \text{“r.h.s of Eq. (49)”} + C_{\text{s}}^{\text{D}} \mu_{\text{PS,sea}}^2 + C_{\text{v}}^{\text{D}} \mu_{\text{PS,val}}^2. \end{aligned} \quad (53)$$

We carry out the chiral extrapolation of $r_0(K_{\text{sea}})$ in order to determine r_0 at the physical sea quark mass, which is required to calculate the hadron spectrum in the method-A. We use a linear form

$$\frac{1}{r_0} = A_{r_0} + \frac{B_{r_0}}{K_{\text{sea}}}. \quad (54)$$

As seen in Fig. 26 and Table XII, this fit describes our data well and gives a reasonable value of $\chi^2/\text{dof} \sim 1.5$.

B. chiral extrapolation in lattice units (method-B)

In order to study the convergence properties of polynomial fit forms in the method-B, we carry out quadratic and cubic diagonal fits to PS and vector meson masses

$$m_{\text{PS}}(K_{\text{sea}}; K_{\text{sea}}, K_{\text{sea}})^2 = B_{\text{diag}}^{\text{PS}} m_{\text{q,sea}} + C_{\text{diag}}^{\text{PS}} m_{\text{q,sea}}^2 + D_{\text{diag}}^{\text{PS}} m_{\text{q,sea}}^3, \quad (55)$$

$$m_{\text{V}}(K_{\text{sea}}; K_{\text{sea}}, K_{\text{sea}}) = A_{\text{diag}}^{\text{V}} + B_{\text{diag}}^{\text{V}} m_{\text{PS,sea}}^2 + C_{\text{diag}}^{\text{V}} m_{\text{PS,sea}}^4 + D_{\text{diag}}^{\text{V}} m_{\text{PS,sea}}^6. \quad (56)$$

Fit parameters are summarized in Tables XIII and XIV.

Fit curves of the quadratic and cubic fits to vector meson masses are shown in Fig. 27. While quadratic and cubic fits describe our data reasonably well at quark masses used in the simulation, they develop a deviation toward the chiral limit and for heavy quarks.

Figure 28 compares the relative magnitude of the linear and quadratic terms in the quadratic diagonal fit to PS meson mass in the method-A and B. As the quark mass increases, the magnitude of the quadratic contribution in the method-B increases more rapidly than in the method-A; it is no longer a small correction at the simulated quark masses ($m_{\text{q,diag}} \simeq 0.015 - 0.055$). A similar situation is observed in the chiral fit to vector meson masses as shown in Fig. 29.

We come to conclude that the chiral expansions of meson masses in lattice units, Eqs. (55) and (56), have poor convergence properties compared to those in unit of r_0 , Eqs. (30) and (31) in the method-A, and the cubic term should not be ignored in the method-B. We directly confirm this point in Fig. 30, where the fit results for vector mesons from the method-A are converted to lattice units using Eq. (54) and compared with the fits of method-B. The cubic fit in the method-B shows a good consistency with the quadratic fit in the method-A, while the quadratic fit in method-B does not.

The combined chiral fit including cubic terms is not very stable because it contains a number of free parameters. In this study, therefore, we do not use the method-B to extract the physical hadron spectrum.

Before we turn to details of the determination of the hadron spectrum, let us make additional comments on the failure of the method-B with our data. Figure 31 shows the chiral fit of r_0 as a function of $m_{\text{PS,sea}}^2$

$$r_0(K_{\text{sea}}) = A'_{r_0} + B'_{r_0} m_{\text{PS,sea}}^2 + C'_{r_0} m_{\text{PS,sea}}^4 + D'_{r_0} m_{\text{PS,sea}}^6. \quad (57)$$

Fit parameters in Table XV show that a large contribution of higher order terms is present also in this fit. By substituting this parametrization of r_0 to Eqs. (30) and (31) (diagonal fits in the method-A), the large higher order corrections appear in Eqs. (55) and (56) (diagonal fits in the method-B). Conversely, why the method-A works well is that large contributions of higher order terms in hadron masses and r_0 cancel with each other at least partially.

We note that the method-B works well in the CP-PACS's study [11], where they took similar simulation parameters but with different lattice actions, namely the RG-improved gauge action and the tadpole improved clover quark action. We compare the CP-PACS data of $r_0 m_{\text{V}}$ at $\beta=2.2$ and ours in Fig. 32. A good consistency in the whole range of the quark mass suggests that two groups' data are in the scaling region. However, we find that the CP-PACS data of r_0 in lattice units show much milder dependence on the sea quark mass than ours. This is the reason why the method-B works well in the CP-PACS study, but does not with our data. It is, of course, not surprising that different lattice actions lead to different sea quark mass dependences of hadron masses and r_0 in the lattice units. However, as discussed above, the much stronger dependence with our choice of the lattice action is practically problematic, if one carries out the chiral extrapolation in lattice units.

C. calculation of hadron spectrum

The hadron spectrum at the physical quark mass is determined as follows. The pion and ρ meson masses normalized by r_0 are determined by tuning their ratio $(r_0 m_{\pi})/(r_0 m_{\rho})$ to its experimental value, i.e., by solving the equation,

$$\frac{(r_0 m_{\pi})}{A^{\text{V}} + (B_{\text{S}}^{\text{V}} + B_{\text{V}}^{\text{V}}) (r_0 m_{\pi})^2 + C_{\text{SV}}^{\text{V}} (r_0 m_{\pi})^4} = \frac{m_{\pi, \text{exp}}}{m_{\rho, \text{exp}}}, \quad (58)$$

where we denote the experimental value of hadron mass by $m_{\text{had,exp}}$, and r_0 represents the Sommer scale at the physical sea quark mass. The hopping parameter corresponding to the physical light quark mass, K_{ud} , is fixed by solving

$$\{ \text{r.h.s of Eq. (36) with } K_{\text{sea}} = K_{\text{val},1} = K_{\text{val},2} = K_{ud} \} = (r_0 m_\pi)^2. \quad (59)$$

Then we determine r_0 , which is required to convert $r_0 m_\pi$ and $r_0 m_\rho$ to m_π and m_ρ , from K_{ud} and Eq. (54).

We test two meson mass inputs to fix the strange quark mass:

- In the first method, we use the kaon mass as input. The hopping parameter corresponding to the strange quark mass, K_s , is determined by solving

$$\frac{\sqrt{\text{r.h.s of Eq. (36)}}}{r_0 m_\rho} = \frac{m_{K,\text{exp}}}{m_{\rho,\text{exp}}}, \quad (60)$$

where we set $K_{\text{sea}} = K_{\text{val},1} = K_{ud}$ and $K_{\text{val},2} = K_s$ in the r.h.s of Eq. (36). Then the mass of the “ η_s ” meson, that is an unphysical $\bar{s}s$ PS meson, is determined from Eq. (36), and used to calculate strange vector meson and strange baryon masses. We refer to this meson mass input as K -input.

- In the second method, we use the ϕ meson mass as input assuming that it is a pure $\bar{s}s$ vector meson. The η_s meson mass is fixed from

$$\frac{\text{r.h.s of Eq. (41)}}{r_0 m_\rho} = \frac{m_{\phi,\text{exp}}}{m_{\rho,\text{exp}}}, \quad (61)$$

where we set $m_{\text{PS,sea}} = m_\pi$ and $m_{\text{PS,val},1} = m_{\text{PS,val},2} = m_{\eta_s}$. We determine K_s from m_{η_s} and Eq. (36). This input is called ϕ -input.

The full spectrum of non-strange and strange hadrons is determined by substituting K_{ud} , m_π , K_s , m_{η_s} and r_0 to Eqs. (36), (41), (47), (48) and (49). We use the lattice spacing a determined from m_ρ to convert the hadron masses in lattice units to those in physical units. We note that this estimate of the scale a is subject to a systematic uncertainty due to the use of the polynomial fitting forms for the chiral extrapolation. However, if we use r_0 as the input to set the scale, we obtain a consistent result for a within errors. The results of K_{ud} , K_s and a^{-1} are collected in Table XVI.

We repeat the above analysis using each of the alternative fit forms Eqs. (40), (45) (52) and (53). The largest deviation in the hadron spectrum among these analyses is taken as the systematic error due to the choice of the chiral fit forms.

For the chiral extrapolation of r_0 , we find that an alternative form

$$r_0(K_{\text{sea}}) = A'_{r_0} + B'_{r_0} \mu_{\text{PS,sea}}^2 \quad (62)$$

also describes our data well. However, the hadron spectrum calculated using this fit is completely consistent with those using Eq. (54). We therefore ignore the systematic error due to the choice of the fit form Eq. (54).

The systematic error of the measured value of $r_0(K_{\text{sea}})$ leads to an additional uncertainty in the result of the hadron spectrum. We perform the calculation of the spectrum with $r_0(K_{\text{sea}})$ shifted by its systematic error at one value of K_{sea} . This calculation is repeated for all K_{sea} and the largest deviation in the spectrum is included into the systematic error.

D. chiral extrapolation in quenched QCD

The chiral extrapolations in quenched QCD are performed using fit forms which are obtained from those used in the full QCD analysis by dropping all terms describing the sea quark mass dependence. Namely, fitting forms for meson masses are

$$m_{\text{PS}}(K_{\text{val},1}, K_{\text{val},2})^2 = B_{\text{q}}^{\text{PS}} m_{\text{q,val}} + C_{\text{q}}^{\text{PS}} m_{\text{q,val}}^2, \quad (63)$$

$$m_{\text{V}}(K_{\text{val},1}, K_{\text{val},2}) = A_{\text{q}}^{\text{V}} + B_{\text{q}}^{\text{V}} m_{\text{PS,val}}^2. \quad (64)$$

The following fitting forms are used for baryon masses

$$m_{\text{oct},\Sigma}(K_{\text{val},1}, K_{\text{val},2}, K_{\text{val},2}) = A_{\text{q}}^{\text{O}} + (F_{\text{q}}^{\text{O}} - D_{\text{q}}^{\text{O}}) m_{\text{PS, val},1}^2 + 2F_{\text{q}}^{\text{O}} m_{\text{PS, val},2}^2 + (C_{\text{q}}^{\text{O}} + C_{\text{q}}^{\text{O},\Sigma}) m_{\text{PS, val},1}^4 + (C_{\text{q}}^{\text{O}} - C_{\text{q}}^{\text{O},\Sigma}) m_{\text{PS, val},2}^4, \quad (65)$$

$$m_{\text{oct},\Lambda}(K_{\text{val},1}, K_{\text{val},2}, K_{\text{val},2}) = A_{\text{q}}^{\text{O}} + \left(F_{\text{q}}^{\text{O}} + \frac{D_{\text{q}}^{\text{O}}}{3}\right) m_{\text{PS, val},1}^2 + 2\left(F_{\text{q}}^{\text{O}} - \frac{2}{3}D_{\text{q}}^{\text{O}}\right) m_{\text{PS, val},2}^2 + (C_{\text{q}}^{\text{O}} + C_{\text{q}}^{\text{O},\Lambda}) m_{\text{PS, val},1}^4 + (C_{\text{q}}^{\text{O}} - C_{\text{q}}^{\text{O},\Lambda}) m_{\text{PS, val},2}^4, \quad (66)$$

$$m_{\text{dec}}(K_{\text{val},1}, K_{\text{val},2}, K_{\text{val},2}) = A_{\text{q}}^{\text{D}} + B_{\text{q}}^{\text{D}} m_{\text{PS, val}}^2. \quad (67)$$

These forms fit to our data very well as shown in Fig. 33. Fit parameters are summarized in Table XVII. The hadron spectrum is calculated in an analogous way to that for full QCD. Resulting values of K_{ud} , K_s and a^{-1} are summarized in Table XVIII.

VI. SEA QUARK EFFECTS ON HADRON SPECTRUM

A. Sea quark effects at simulated quark mass

Figure 34 compares the valence quark mass dependence of the vector meson mass at each sea quark mass in full QCD and in quenched QCD. We observe that quenched data have a significantly smaller slope than experimental points. This leads to the underestimation of the K^*-K hyperfine splitting in quenched QCD.

The slopes in full QCD data are clearly larger than in quenched QCD, and increase for decreasing sea quark mass. This is reflected in a negative value of C_{sv}^{V} for Eq. (41) in Table VIII. This sea quark effect leads to a better agreement of the meson spectrum in full QCD with experiment than in quenched QCD.

The J parameter [44] defined by

$$J = m_{\text{V}} \left. \frac{dm_{\text{V}}}{dm_{\text{PS}}^2} \right|_{m_{\text{PS}}/m_{\text{V}}=m_{\text{K}}/m_{\text{K}^*}} \quad (68)$$

is useful to quantify the sea quark effect. Numerical results of J calculated from the partially quenched chiral fit Eq. (46) are given in Table XIX. In Fig. 35, we plot J in full QCD (filled circles) as a function of the sea quark mass together with the quenched result (open circle in the right panel). We observe that J in full QCD is close to the quenched value at heavy sea quark masses corresponding to $m_{\text{PS}}/m_{\text{V}} \geq 0.75$ and increases as the sea quark masses decreases.

In the same figure, we also plot J reproduced from the combined chiral fit Eq. (41) (dashed lines). The result is consistent with J from the partially quenched fit, as it should be, and shows a similar sea quark mass dependence. We observe that J extrapolated to the physical sea quark mass is closer to the phenomenological value [44]

$$J = m_{\text{K}^*} \frac{m_{\text{K}^*} - m_{\rho}}{m_{\text{K}}^2 - m_{\pi}^2} = 0.48(2) \quad (69)$$

than in quenched QCD.

Figure 35 also shows J calculated from our results of the meson spectrum (see Table XX) using the above alternative definition Eq. (69) (filled square). The result is in good agreement with other determinations, showing the magnitude of the sea quark effect in J to be stable against the definition of J .

In Sec. IV, we pointed out that FSE decreases the slope $dm_{\text{V}}/dm_{\text{PS}}^2$. This is confirmed numerically in $dm_{\text{V}}/dm_{\text{PS}}^2$ determined from the partially quenched chiral fit Eq. (46) at the lightest sea quark mass: $dm_{\text{V}}/dm_{\text{PS}}^2$ is 0.906(14) on 20^3 , 0.814(88) on 16^3 and 0.68(30) on 12^3 . The slope would be larger if we increase the spatial size beyond 20^3 . Therefore, the observed sea quark mass dependence of the slope and J is a genuine effect of dynamical quarks and not an artifact of FSE.

A similar effect of sea quarks can be found in decuplet baryon masses as shown in Fig. 36. However, a significant deviation still exists in the slope between full QCD data and the experimental spectrum. We consider

that a larger slope in full QCD is still partly masked by FSE on the 20^3 volume; volume as large as 30^3 would be needed to reduce FSE to a few % level as discussed in Sec. IV.

We emphasize that the evidence of sea quark effects observed in this subsection does not suffer from possibly large systematic errors due to the chiral extrapolation and the choice of inputs to fix the scale and quark masses: the increase of the slopes, dm_V/dm_{PS}^2 and dm_{dec}/m_{PS}^2 , is observed without any chiral extrapolation and inputs. The sea quark mass dependence of J is obtained by a short extrapolation or an interpolation to a relatively heavy valence quark mass corresponding to $m_{PS}/m_V = m_K/m_{K^*}$.

B. hadron spectrum

The meson spectrum in full and quenched QCD is summarized in Table XX. Since our fitting functions to vector meson masses, Eqs. (41) and (64), are linear in terms of the valence quark mass, m_{K^*} with ϕ -input equals $(m_{\rho,\text{exp}} + m_{\phi,\text{exp}})/2$ in both full and quenched QCD. The deviation of this value from the experimental mass $m_{K^*,\text{exp}}$ is only 0.2%.

A clear difference between full and quenched QCD is observed in other meson masses as shown in Fig. 37. While the quenched meson spectrum shows a significant deviation from experiment, sea quark effects reduce the deviation by about 40%. This closer agreement of the meson spectrum with experiment is a consequence of the sea quark effects observed in the previous subsection.

In Fig. 38, m_{K^*} with the K -input in full QCD is compared with the CP-PACS results obtained with the RG-improved gauge and clover quark actions [11]. We observe that our m_{K^*} is consistent with the CP-PACS' result at a similar lattice spacing, and is at the lower edge of their estimate in the continuum limit. In the same figure, we also make a comparison in quenched QCD with the CP-PACS results obtained with the plaquette gauge and the Wilson quark actions in Ref. [4]. Two groups' results show a good agreement with each other. These observations suggest that the scaling violation is small in our data both in full and quenched QCD and, hence, the closer agreement of the meson spectrum in full QCD with experiment is a genuine effect of sea quarks.

The baryon masses in full and quenched QCD are listed in Table XXI. These masses are compared with experiment in Fig. 39. For heavier baryons, such as Σ , Ξ and Ω , full QCD results show a closer agreement with experiment than in quenched QCD. The sea quark effect is, however, less clear for lighter baryons. This is partly due to FSE in full QCD data which is more pronounced for lighter valence quarks.

In Fig. 40, m_N and m_Ξ with the K -input are compared with the CP-PACS results [4, 11]. While the full QCD results of two groups show a reasonable agreement with each other, the CP-PACS results in the continuum limit in quenched QCD are systematically smaller than ours. This suggests that our quenched data has non-negligible scaling violation, which is another source making sea quark effects less clear. Therefore, further investigations of FSE in full QCD and scaling violation in quenched QCD are required to obtain a clear conclusion on sea quark effects in the baryon spectrum.

We now turn to theoretical predictions which can be derived from our data. The first is the mass of the η_s meson, for which our full QCD data predict $m_{\eta_s} = 0.6948(3)(+8/-1)(+2)$ GeV with the K -input, and $0.7381(46)(+57)(+40/-46)$ GeV with the ϕ -input, where the first error is statistical, and the second and third ones are due to the choice of the fitting form and a systematic uncertainty of r_0 . These results are to be compared with those in quenched QCD, 0.6988(9) GeV (K -input) and 0.7719(58) GeV (ϕ -input). While the values themselves do not differ by going from quenched to full QCD, the difference between the two inputs is reduced by about 40% in full QCD. This reflects the closer agreement of the meson spectrum in full QCD.

Another interesting prediction is the physical value of r_0 . Our full QCD simulation gives $r_0 = 0.497(6)(-9)(+11/-12)$ fm, where the meaning of three errors are the same to those of m_{η_s} . We note that this is close to the phenomenological estimate in the original paper [29], $r_0 = 0.49$ fm. The quenched simulation gives $0.5702(75)(50)$ fm, where the first error is statistical and the second comes from the systematic uncertainty of the measurement. About a 14 % difference between full and quenched QCD arises from the following two sea quark effects. One is the difference of the physical value of r_0 itself due to the change of the shape of the static quark potential. The other source is the reduction of the quenching error in m_ρ in full QCD, which is used to fix the lattice scale.

VII. DECAY CONSTANTS

The PS meson decay constants are calculated using the fourth component of the improved axial vector current, which is defined by

$$A_4^{\text{imp}} = A_4 + c_A \Delta_4 P \quad (70)$$

with the symmetric lattice derivative Δ_4 . We extract the amplitude of the $\langle A_4^{\text{imp}}(t)P(0)^\dagger \rangle$ correlator, C_A^{LS} , by the correlated fit of the form

$$\langle A_4^{\text{imp}}(t)P(0)^\dagger \rangle = C_A^{\text{LS}} \{ \exp[-m_{\text{PS}} t] - \exp[-m_{\text{PS}} (N_t - t)] \} \quad (71)$$

with m_{PS} fixed to the results given in Appendix A. We use the local operator for A_4^{imp} , while the double smearing is applied to P . The amplitude of the $\langle P(t)P(0)^\dagger \rangle$ operator with the doubly smeared source and the sink operators, C_P^{SS} , is extracted assuming a single hyperbolic cosine form.

The renormalized decay constant is calculated by

$$f_{\text{PS}} = 2KZ_A (1 + b_A m_{\text{q, val}}) C_A^{\text{LS}} \sqrt{\frac{2}{m_{\text{PS}} C_P^{\text{SS}}}}. \quad (72)$$

Since non-perturbatively determined values for Z_A , b_A and c_A are not available for two-flavor QCD, we adopt one-loop perturbative values in Refs. [45, 46, 47, 48, 49, 50] with the tadpole improvement. We calculate $\alpha_P(3.40/a)$ from the plaquette average $\langle U_P \rangle$ according to [51, 52]

$$-\ln[\langle U_P \rangle] = \frac{4\pi}{3} \alpha_P(3.40/a) \{ 1 - (1.1905 - 0.2266 N_f) \alpha_P \}. \quad (73)$$

Then, $\alpha_P(3.40/a)$ is evolved to the optimum scale ($q_{Z_A}^* = 1.803/a$ for Z_A , $q_{b_A}^* = 2.289/a$ for b_A and $q_{c_A}^* = 2.653/a$ for c_A [53]) using the universal two-loop beta function and is used as the expansion parameter of tadpole improved perturbation theory.

The consistent chiral extrapolation of the decay constant should include the chiral logarithmic term as predicted by ChPT [40]. However, our data do not show the characteristic curvature of the chiral logarithm as discussed in Sec.V A (and also in Refs. [21, 23]). We therefore use the following polynomial form for the chiral extrapolation leaving the problem of the chiral logarithm and associated uncertainty for future publication [42]

$$r_0(K_{\text{sea}}) f_{\text{PS}}(K_{\text{sea}}; K_{\text{val},1}, K_{\text{val},2}) = A^{\text{f}} + B_s^{\text{f}} \mu_{\text{PS, sea}} + B_v^{\text{f}} \mu_{\text{PS, val}} + C_{\text{sv}}^{\text{f}} \mu_{\text{PS, sea}} \mu_{\text{PS, val}}. \quad (74)$$

The fit is plotted in Fig. 41 with parameters summarized in Table XXII. Pion and kaon decay constants, f_π and f_K , are calculated by tuning $\mu_{\text{PS, sea}}$ to $(r_0 m_\pi)^2$ and substituting $(r_0 m_\pi)^2$ or $(r_0 m_{\eta_s})^2$ for $\mu_{\text{PS, val}, i}$ ($i=1, 2$) in $\mu_{\text{PS, val}}$. The systematic errors due to the choice of the fitting function and the uncertainty of r_0 are estimated in a way similar to those described in Sec. V C. In the estimation of the former error, we use

$$r_0(K_{\text{sea}}) f_{\text{PS}}(K_{\text{sea}}; K_{\text{val},1}, K_{\text{val},2}) = \text{“r.h.s of Eq. (74)”} + C_s^{\text{f}} \mu_{\text{PS, sea}}^2 + C_v^{\text{f}} \mu_{\text{PS, val}}^2 \quad (75)$$

and Eqs. (40) and (45) as the alternative fitting functions for the chiral extrapolation.

In quenched QCD, we use the chiral extrapolation form

$$f_{\text{PS}}(K_{\text{val},1}, K_{\text{val},2}) = A_q^{\text{f}} + B_q^{\text{f}} m_{\text{PS, val}}^2. \quad (76)$$

and obtain parameters summarized in Table XXIII. For Z_A , b_A and c_A , we test the one-loop perturbative value and the non-perturbative one in Ref. [54].

Our results of the decay constants are summarized in Table XXIV. A comparison between full and quenched QCD results obtained by the one-loop matching is made in Fig. 42. We observe that f_π is consistent with the experimental value within two standard deviations in both full and quenched QCD. While f_K in quenched QCD is significantly smaller than the experimental value, the deviation is reduced by sea quark effects and the full QCD result becomes consistent with experiment.

The results obtained with one-loop renormalization factors are subject to higher order corrections. However, as shown in Table XXIV for the quenched results, the difference between the perturbative and non-perturbative matchings is not large. This is because the $O(a)$ correction to the improved current in Eq. (70) is not large, and

the non-perturbative values for Z_A and b_A are close to those in tadpole improved perturbation theory. We may therefore expect that the uncertainty due to the perturbative matching is small also in the full QCD results.

It is expected that various systematic uncertainties, including the scaling violation, would partially cancel in the ratio f_K/f_π . This expectation is supported by the good agreement of the quenched results between the perturbative and non-perturbative matching, which suggests that higher order corrections to the renormalization factors almost cancel in the ratio. Therefore the ratio is useful to discuss sea quark effects. Comparison of this quantity shows that the full QCD values are significantly closer to the experimental value $\simeq 1.22$ by about two standard deviations than in quenched QCD.

VIII. QUARK MASSES

We calculate the up-down and strange quark masses through the axial vector Ward identity (AWI). The bare quark mass at simulation points is obtained by

$$m_q^{\text{AWI}} = \frac{m_{\text{PS}} C_A^{\text{LS}}}{2C_P^{\text{LS}}}, \quad (77)$$

where C_A^{LS} and C_P^{LS} are the amplitudes of $\langle A_4^{\text{imp}}(t)P(0)^\dagger \rangle$ and $\langle P(t)P(0)^\dagger \rangle$ with the doubly smeared source and the local sink operators.

We then carry out the chiral fit of the PS meson mass as a function of the AWI bare quark mass. The fitting function is obtained from Eq. (36) with the replacement of the VWI masses with the AWI ones. We also drop all monomial terms in the sea quark mass, since the PS meson mass vanishes in the chiral limit $m_{\text{q, val}}^{\text{AWI}} = 0$ even for non-zero sea quark masses [41]. The adopted form is

$$\begin{aligned} & (r_0(K_{\text{sea}}) m_{\text{PS}}(K_{\text{sea}}; K_{\text{val},1}, K_{\text{val},2}))^2 \\ &= B_v^{\text{PS,AWI}} \mu_{\text{q, val}}^{\text{AWI}} + C_v^{\text{PS,AWI}} (\mu_{\text{q, val}}^{\text{AWI}})^2 + C_{\text{sv}}^{\text{PS,AWI}} \mu_{\text{q, sea}}^{\text{AWI}} \mu_{\text{q, val}}^{\text{AWI}}, \end{aligned} \quad (78)$$

where

$$\mu_{\text{q, sea}}^{\text{AWI}} = r_0(K_{\text{sea}}) m_q^{\text{AWI}}(K_{\text{sea}}; K_{\text{sea}}, K_{\text{sea}}), \quad (79)$$

$$\mu_{\text{q, val}}^{\text{AWI}} = r_0(K_{\text{sea}}) m_{\text{q, val}}^{\text{AWI}}, \quad (80)$$

$$m_{\text{q, val}}^{\text{AWI}} = \frac{1}{2} (m_{\text{q, val},1}^{\text{AWI}} + m_{\text{q, val},2}^{\text{AWI}}), \quad (81)$$

$$m_{\text{q, val},i}^{\text{AWI}} = m_q^{\text{AWI}}(K_{\text{sea}}; K_{\text{val},i}, K_{\text{val},i}). \quad (82)$$

Our data and fit are shown in Fig. 43.

We adopt the fit (78) because it is consistent with that in terms of the VWI quark mass (Eq. (36)). However, a function with fewer terms

$$(r_0(K_{\text{sea}}) m_{\text{PS}}(K_{\text{sea}}; K_{\text{val},1}, K_{\text{val},2}))^2 = B_v^{\text{PS,AWI}} \mu_{\text{q, val}}^{\text{AWI}} + C_{\text{sv}}^{\text{PS,AWI}} \mu_{\text{q, sea}}^{\text{AWI}} \mu_{\text{q, val}}^{\text{AWI}} \quad (83)$$

also gives an acceptable χ^2/dof . We use this as an alternative fit in our estimation of the systematic error due to the choice of the fitting function (see below). Parameters of these two fits are summarized in Table XXV.

The bare AWI masses of the up-down and strange quarks are fixed in a way analogous to that described in Sec. V C by using Eq. (78) instead of Eq. (36). The matching to the $\overline{\text{MS}}$ scheme is made at the scale $\mu = 2/a$ using the one-loop renormalization constant [46, 47, 48, 49, 50] with the tadpole improvement. We use $\alpha_P(q_{Z_A}^*)$, $\alpha_P(q_{b_A}^*)$ as the expansion parameter in the one-loop expression of Z_A and b_A , while we set $q^* = 2/a$ for other coefficients for which q^* is not known. The $\overline{\text{MS}}$ quark mass is evolved to $\mu = 2$ GeV using the four-loop beta function [55, 56].

The VWI quark mass may differ from the AWI one because of explicit violation of chiral symmetry at finite lattice spacings. The difference between the AWI and VWI masses, therefore, gives insight into the size of scaling violation in our results. This leads us to repeat the calculation of quark masses using the VWI definition. The bare quark mass is calculated from K_c , K_{ud} and K_s in Tables VII and XVI. The $\overline{\text{MS}}$ mass is obtained by the one-loop matching at $\mu = 2/a$ and the four-loop running to $\mu = 2$ GeV. The resulting AWI and VWI masses are summarized in Table XXVI.

For a calculation of quark masses in quenched QCD, the chiral extrapolation is carried out using a quadratic fit form obtained from Eq. (78) by dropping the third term which represents the sea quark mass dependence

$$m_{\text{PS}}(K_{\text{val},1}, K_{\text{val},2})^2 = B_{\text{q}}^{\text{PS,AWI}} \mu_{\text{q,val}}^{\text{AWI}} + C_{\text{q}}^{\text{PS,AWI}} (\mu_{\text{q,val}}^{\text{AWI}})^2. \quad (84)$$

Obtained parameters are listed in Table XXVII. We use either one-loop or non-perturbative value in Refs. [35, 57, 58, 59] for the renormalization factors. Numerical results are summarized in Table XXVIII.

In Figure 44, our full QCD results are compared with estimates by the CP-PACS [10, 11] and the QCDSF-UKQCD Collaborations [60]. We observe good agreement for the AWI masses among the three groups even at the finite lattice spacing of $a^{-1} \sim 2$ GeV. These results are consistent also with the CP-PACS's result extrapolated to the continuum limit. This suggests that various uncertainties, such as scaling violation and higher order corrections to renormalization factors, are likely to be canceled in the ratio defining the AWI mass (Eq. (77)).

On the other hand, such a cancellation is not expected in the VWI mass. Indeed there is a sizable difference between our AWI and VWI results. We also observe that our and the CP-PACS results of VWI m_{ud} show a large discrepancy of about 18 % (6 standard deviations). These observations suggest that the scaling violation in our results of the VWI masses is not small.

In both full and quenched QCD, therefore, we quote the AWI masses as the central value. We adopt K -input for m_s . The difference between m_s with K - and ϕ -inputs is treated as the systematic error due to the choice of the meson mass input to fix m_s .

Additional systematic errors due to the choice of the chiral fit form and the uncertainty of the measured value of r_0 are included in our final results in full QCD. These errors are estimated in a similar way to that described in Sec. V C by using Eqs. (40), (45) and (83) as alternative fit forms.

Adding all errors in quadrature, we obtain

$$m_{ud}^{\overline{\text{MS}}}(2 \text{ GeV}) = 3.223 \left(\begin{smallmatrix} +0.046 \\ -0.069 \end{smallmatrix} \right) \quad (85)$$

$$m_s^{\overline{\text{MS}}}(2 \text{ GeV}) = 84.5 \left(\begin{smallmatrix} +12.0 \\ -1.7 \end{smallmatrix} \right) \quad (86)$$

$$m_s/m_{ud} = 26.13 \left(\begin{smallmatrix} +3.65 \\ -0.02 \end{smallmatrix} \right) \quad (87)$$

in two-flavor QCD and

$$m_{ud}^{\overline{\text{MS}}}(2 \text{ GeV}) = 4.020 (0.077) \quad (88)$$

$$m_s^{\overline{\text{MS}}}(2 \text{ GeV}) = 104.1 \left(\begin{smallmatrix} +24.1 \\ -1.6 \end{smallmatrix} \right) \quad (89)$$

$$m_s/m_{ud} = 25.90 \left(\begin{smallmatrix} +5.98 \\ -0.13 \end{smallmatrix} \right). \quad (90)$$

in quenched QCD using the one-loop matching. The scaling violation is expected to be small and hence is ignored here. This point, however, should be checked in future studies.

There is an additional uncertainty arising from the use of the perturbative value for c_A , $Z_{A,P}$, and $b_{A,P}$. Comparing the quenched result of Eqs. (88)–(90) with those obtained by the non-perturbative matching given by

$$m_{ud}^{\overline{\text{MS}}}(2 \text{ GeV}) = 3.522 (0.66) \text{ MeV} \quad (91)$$

$$m_s^{\overline{\text{MS}}}(2 \text{ GeV}) = 91.9 \left(\begin{smallmatrix} +21.3 \\ -1.4 \end{smallmatrix} \right) \text{ MeV} \quad (92)$$

$$m_s/m_{ud} = 26.08 \left(\begin{smallmatrix} +6.02 \\ -0.13 \end{smallmatrix} \right), \quad (93)$$

we observe a systematic error of about 13 %. In quenched QCD the non-perturbative estimate of $Z_A/Z_P = 1.19$ is very close to that in one-loop perturbation theory 1.22, since higher order corrections in Z_A and Z_P partially cancel with each other. The non-perturbative value $b_A - b_P = 0.171$ deviates significantly from that at one-loop -0.011 . The $O(am_q)$ term, however, is a small correction in our data. Most of the 13 % difference originates from the large deviation between the non-perturbative value $c_A = -0.083$ in Ref. [35] and its one-loop value -0.013 . Therefore, a non-perturbative determination of c_A in full QCD is an important task toward a more precise calculation of the quark masses in future studies.

In Fig. 45, we compare the quark masses in full and quenched QCD. The chief observation is that sea quark effects reduce the light and strange quark masses by about 20 %. The magnitude of the sea quark effect is roughly consistent with the CP-PACS observation in Refs. [10, 11].

The quark mass ratio m_s/m_{ud} in full QCD is consistent with the quenched value, because the sea quark effects in m_{ud} and m_s almost cancel with each other in the ratio. We note that $m_s/m_{ud} \simeq 26$ is in a good agreement with the estimate of one-loop chiral perturbation theory 24.4(1.5) [61].

Another important observation is that the deviation in m_s between K - and ϕ -inputs is reduced by effects of sea quarks: the deviation is 21 % ($\simeq 24$ MeV) in quenched QCD and 13 % ($\simeq 12$ MeV) in full QCD. This reflects the closer agreement of the meson spectrum in full QCD with experiment. The remaining deviation may be attributed to quenching of strange quarks and scaling violation.

IX. CONCLUSIONS

In this paper we have presented a high statistics study of the hadron spectrum and quark masses in two-flavor QCD using the plaquette gauge action and the fully $O(a)$ -improved Wilson quark action. We find firm evidence of sea quark effects at the simulated quark masses: the slopes dm_V/dm_{PS}^2 and $dm_{\text{dec}}/dm_{\text{PS}}^2$ are larger than in quenched QCD and the J parameter increases for lighter sea quarks. These findings do not suffer from systematic errors arising from the chiral extrapolation with respect to the sea quark mass, which is a major uncertainty particularly in recent studies with the Wilson-type quark action. Note that the use of a volume $La \geq 1.8$ fm at smaller sea quark masses $m_{\text{PS,sea}}/m_{V,\text{sea}} \simeq 0.6-0.7$ is an important factor to control finite-size errors and in reaching our observations.

The sea quark effect observed at the simulated quark masses means that the strange meson and baryon masses in full QCD show a better agreement with experiment than in quenched QCD. A similar reduction of quenching errors is also observed in the ratio f_K/f_π . We also find that the sea quark effects lead to about 20 % reduction of quark masses.

For baryons finite-size effects are large for the volume we used, which render sea quark effects unclear for lighter baryons. Further investigations on larger spatial volumes, of the order of 3 fm at the lightest sea quark mass, are needed to observe sea quark effects in the light baryons.

The present work is carried out at a single lattice spacing of $a^{-1} = 2.221(28)$ GeV. The $O(a)$ -improved Wilson quark action we employed is designed to have reduced scaling violation, and experiences in quenched QCD [62] support this expectation. Nonetheless scaling study of both the hadron spectrum and quark masses with this action is needed to establish the sea quark effects in the spectral quantities on a quantitative basis.

Another important subject in future is simulations at much lighter sea quark mass, in particular below the $\rho \rightarrow \pi\pi$ threshold. Such simulations will lead to a better control of the chiral extrapolation. This would also give insight into the chiral logarithmic singularity in the PS meson mass and decay constant, which we have not observed in our data.

Acknowledgments

This work is supported by the Supercomputer Project No.79 (FY2002) of High Energy Accelerator Research Organization (KEK), and also in part by the Grant-in-Aid of the Ministry of Education (Nos. 11640294, 12640253, 12740133, 13135204, 13640259, 13640260, 14046202, 14740173). N.Y. is supported by the JSPS Research Fellowship.

APPENDIX A: HADRON MASSES

Measured hadron masses are summarized in Tables XXIX–XXXIV for full QCD, and Tables XXXV–XL for quenched QCD. Our choice of the fitting range and resulting value of χ^2/dof are also shown in these tables.

[1] S. Aoki, Nucl. Phys. B (Proc. Suppl.) **94**, 3 (2001).

- [2] D. Toussaint, Nucl. Phys. B (Proc. Suppl.) **106**, 111 (2002).
- [3] T. Kaneko, Nucl. Phys. B (Proc. Suppl.) **106**, 133 (2002).
- [4] S.Aoki *et al.* (CP-PACS Collaboration), Phys. Rev. Lett. **84**, 238 (2000).
- [5] N. Eicker *et al.* (SESAM Collaboration), Phys. Rev. D **59**, 014509 (1999).
- [6] T. Lippert, *et al.* (T χ L Collaboration), Nucl. Phys. B (Proc. Suppl.) **60A**, 311 (1998).
- [7] N. Eicker, Th. Lippert, B. Orth and K. Schilling (SESAM-T χ L Collaboration), Nucl. Phys. B (Proc. Suppl.) **106**, 209 (2002).
- [8] C.R. Allton *et al.* (UKQCD Collaboration), Phys. Rev. D **60**, 034507 (1999).
- [9] C.R. Allton *et al.* (UKQCD Collaboration), Phys. Rev. D **65**, 054502 (2002).
- [10] A. Ali Khan *et al.* (CP-PACS Collaboration), Phys. Rev. Lett. **85**, 4674 (2000).
- [11] A. Ali Khan *et al.* (CP-PACS Collaboration), Phys. Rev. D **65**, 054505 (2002).
- [12] H. Stüben, (QCDSF-UKQCD Collaboration), Nucl. Phys. B (Proc. Suppl.) **94**, 273 (2001).
- [13] C. Bernard *et al.* (MILC Collaboration), Nucl. Phys. B (Proc. Suppl.) **73**, 198 (1999); *ibid.* **60A**, 297 (1998) and references therein.
- [14] C. Bernard *et al.* (MILC Collaboration), Phys. Rev. D **64** 054506 (2001); hep-lat/0208041.
- [15] F. Butler, H. Chen, J. Sexton, A. Vaccarino and D. Weingarten, Nucl. Phys. B **430**, 179 (1994).
- [16] Y. Iwasaki, Nucl. Phys. B **258**, 141 (1985); Univ. of Tsukuba report UTHEP-118 (1983), unpublished.
- [17] B. Sheikholeslami and R. Wohlert, Nucl. Phys. B **259**, 572 (1985).
- [18] G.P. Lepage and P.B. Mackenzie, Phys. Rev. D **48**, 2250 (1993).
- [19] M. Lüscher, S. Sint, R. Sommer and P. Weisz, Nucl. Phys. B **478**, 365 (1996).
- [20] S. Aoki *et al.* (JLQCD Collaboration), Nucl. Phys. B (Proc. Suppl.) **94**, 233 (2001).
- [21] S. Aoki *et al.* (JLQCD Collaboration), Nucl. Phys. B (Proc. Suppl.) **106**, 224 (2002).
- [22] T. Kaneko *et al.* (JLQCD Collaboration), hep-lat/0209057.
- [23] S. Hashimoto *et al.* (JLQCD Collaboration), hep-lat/0209091.
- [24] S. Aoki *et al.*, Phys. Rev. D **50**, 486 (1994).
- [25] K. Jansen and C. Liu, Comput. Phys. Commun. **99**, 221 (1997).
- [26] S. Aoki *et al.* (JLQCD Collaboration), Phys. Rev. D **65**, 094507 (2002).
- [27] K. Jansen and R. Sommer (ALPHA Collaboration), Nucl. Phys. B **530**, 185 (1998).
- [28] JLQCD Collaboration, in preparation.
- [29] R. Sommer, Nucl. Phys. B **411**, 839 (1994).
- [30] S. Duane, A.D. Kennedy, B.J. Pendleton, and D. Roweth, Phys. Lett. B **195**, 216 (1987).
- [31] S. Gottlieb, W. Liu, D. Toussaint, R.L. Renken and R.L. Sugar, Phys. Rev. D **35**, 2531 (1987).
- [32] T.A. DeGrand, Comput. Phys. Commun. **52**, 161 (1988).
- [33] X-Q. Luo, Comput. Phys. Commun. **94**, 119 (1996).
- [34] H. van der Vorst, SIAM J. Sc. Stat. Comp. **13**, 631 (1992).
- [35] M. Lüscher, S. Sint, R. Sommer, P. Weisz and U. Wolff, Nucl. Phys. B **491**, 323 (1997).
- [36] G.S. Bali and K. Schilling, Phys. Rev. D **46**, 2636 1992.
- [37] C.B. Lang and C. Rebbi, Phys. Lett. B **115**, 137 (1982).
- [38] M. Lüscher, Commun. Math. Phys. **104**, 177 (1986).
- [39] M. Fukugita *et al.*, Phys. Lett. B **294**, 380 (1992); Phys. Rev. D **47**, 4739 (1993).
- [40] J. Gasser and H. Leutwyler, Annals Phys. **158**, 142 (1984); Nucl. Phys. B **250**, 465 (1985).
- [41] S.R. Sharpe, Phys. Rev. D **56**, 7052 (1997).
- [42] JLQCD Collaboration, in preparation.
- [43] V. Bernard, N. Kaiser and U.G. Meissner, Z. Phys. C **60**, 111 (1993).
- [44] P. Lacock and C. Michael (UKQCD Collaboration), Phys. Rev. D **52**, 5213 (1995).
- [45] M. Lüscher and P. Weisz, Nucl. Phys. B **479**, 429 (1996).
- [46] E. Gabrielli, G. Martinelli, C. Pittori, G. Heatlie and C.T. Sachrajda, Nucl. Phys. B **362**, 475 (1991).
- [47] S. Sint, P. Weisz, Nucl. Phys. B **502**, 251 (1997).
- [48] S. Aoki, K. Nagai, Y. Taniguchi and A. Ukawa, Phys. Rev. D **58**, 074505 (1998).
- [49] Y. Taniguchi and A. Ukawa, Phys. Rev. D **58**, 114503 (1998).
- [50] S. Aoki, R. Frezzotti, P. Weisz, Nucl. Phys. B **540**, 501 (1999).
- [51] K-I. Ishikawa and S. Hashimoto, private notes (2001).
- [52] G.S. Bali and P. Boyle, hep-lat/0210033.
- [53] J. Harada, S. Hashimoto, A.S. Kronfeld and T. Onogi, hep-lat/0208004.
- [54] T. Bhattacharya, R. Gupta, W. Lee, S. Sharpe, Phys. Rev. D **63**, 074505 (2001); Nucl. Phys. B (Proc.Suppl.) **106**, 789 (2002).
- [55] K.G. Chetyrkin, Phys. Lett. B404, 161 (1997).
- [56] J.A.M. Vermaseren, S.A. Larin and T. van Ritbergen, Phys. Lett. B405, 327 (1997).
- [57] M. Lüscher, S. Sint, R. Sommer and H. Wittig, Nucl. Phys. B **491**, 344 (1997).
- [58] S. Capitani, M. Lüscher, R. Sommer and H. Wittig (ALPHA Collaboration), Nucl. Phys. B **544**, 669 (1999).
- [59] M. Guagnelli *et al.* (ALPHA Collaboration), Nucl. Phys. B **595**, 44 (2001).
- [60] D.Pleiter (QCDSF-UKQCD Collaboration), Nucl. Phys. B (Proc. Suppl.) **94**, 265 (2001).
- [61] H. Leutwyler, Phys. Lett. B **378**, 313 (1996).
- [62] K.C. Bowler *et al.* (UKQCD Collaboration), Phys. Rev. D **62**, 054506 (2000).

TABLE I: Run parameters in simulations of two-flavor QCD. The step size $\Delta\tau$ is given by the inverse of the number of the molecular dynamics steps (#MD). We denote the tolerance parameter in the stopping condition for the quark matrix inversion in calculations of the force and Hamiltonian by Δ_f and Δ_H , respectively. CPU time required per trajectory on the full machine is written in units of minute. Number of measurement is denoted by N_{meas} and the number of the exceptional configurations is written in the bracket.

$12^3 \times 48$, A-HMC					
K_{sea}	0.1340	0.1343	0.1346	0.1350	0.1355
#MD	68	72	80	110	175
accept.	0.667(8)	0.667(10)	0.668(10)	0.772(6)	0.799(9)
Δ_f	10^{-8}	10^{-8}	10^{-8}	10^{-8}	10^{-8}
Δ_H	10^{-14}	10^{-14}	10^{-14}	10^{-14}	10^{-14}
N_{inv}	64.1(2)	74.5(2)	88.6(3)	117.6(5)	203.0(1.0)
time/traaj	0.291	0.351	0.465	0.829	2.20
N_{traaj}	3000	3000	3000	3000	3000
N_{meas}	300(2)	300(0)	300(1)	300(2)	300(7)
$m_{\text{PS}}/m_{\text{V}}$	0.792(15)	0.753(18)	0.749(14)	0.705(24)	0.608(63)
$16^3 \times 48$, HMC					
K_{sea}	0.1340	0.1343	0.1346	0.1350	0.1355
#MD	160	160	200	200	320
accept.	0.799(8)	0.744(10)	0.804(10)	0.702(9)	0.688(10)
Δ_f	10^{-18}	10^{-18}	10^{-18}	10^{-18}	10^{-18}
Δ_H	10^{-20}	10^{-20}	10^{-20}	10^{-20}	10^{-20}
N_{inv}	105.9(2)	124.0(2)	148.0(5)	203.0(7)	362.2(1.9)
time/traaj	1.92	2.21	3.86	5.25	14.7
N_{traaj}	3000	3000	3000	3000	3000
N_{meas}	300(1)	300(0)	300(0)	300(3)	300(0)
$m_{\text{PS}}/m_{\text{V}}$	0.802(5)	0.779(12)	0.752(8)	0.707(13)	0.586(21)
$20^3 \times 48$, A-HMC					
K_{sea}	0.1340	0.1343	0.1346	0.1350	0.1355
#MD	100	100	115	135	250
accept.	0.673(7)	0.627(8)	0.670(8)	0.663(9)	0.755(8)
Δ_f	10^{-8}	10^{-8}	10^{-8}	10^{-8}	10^{-8}
Δ_H	10^{-14}	10^{-14}	10^{-14}	10^{-14}	10^{-14}
N_{inv}	64.3(1)	74.4(1)	88.2(2)	118.2(2)	214.9(8)
time/traaj	1.57	1.79	2.44	3.75	12.5
N_{traaj}	3000	3000	3000	3000	3000
N_{meas}	300(2)	300(0)	300(1)	300(0)	300(0)
$m_{\text{PS}}/m_{\text{V}}$	0.802(5)	0.773(5)	0.745(18)	0.705(5)	0.586(8)
$20^3 \times 48$, S-HMC					
K_{sea}	0.1340	0.1343	0.1346	0.1350	0.1355
#MD	80	100	100	100	160
accept.	0.676(5)	0.771(5)	0.749(4)	0.666(6)	0.678(7)
Δ_f	10^{-8}	10^{-8}	10^{-8}	10^{-8}	10^{-8}
Δ_H	10^{-14}	10^{-14}	10^{-14}	10^{-14}	10^{-14}
N_{inv}	69.3(1)	81.0(1)	96.9(1)	131.5(2)	243.6(5)
time/traaj	1.08	1.53	1.78	2.35	6.64
N_{traaj}	9000	9000	9000	9000	9000
N_{meas}	900(4)	900(2)	900(6)	900(10)	900(7)
$m_{\text{PS}}/m_{\text{V}}$	0.799(1)	0.779(1)	0.753(2)	0.709(2)	0.600(4)

TABLE II: Parameters in Eq. (19) and r_0 in full QCD. The first error is statistical. The second and third ones are the systematic error due to the choice of t_{\min} and r_{\min} .

$12^3 \times 48$					
K_{sea}	V_0	α	g_c	σ	r_0
0.1340	0.549(19)(71)(37)	0.301(13)(19)(21)	0.76(5)(24)(12)	0.0922(19)(30)(16)	3.826(24)(35)(27)
0.1343	0.552(14)(43)(47)	0.288(9)(32)(44)	0.74(5)(8)(11)	0.0838(10)(49)(36)	4.031(15)(76)(33)
0.1346	0.568(14)(23)(34)	0.288(10)(16)(64)	0.67(4)(5)(8)	0.0772(15)(18)(32)	4.200(29)(23)(42)
0.1350	0.603(10)(17)(13)	0.296(8)(7)(19)	0.57(3)(7)(4)	0.0675(11)(14)(14)	4.481(27)(59)(17)
0.1355	0.658(10)(14)(29)	0.333(7)(24)(21)	0.47(3)(1)(7)	0.0514(11)(25)(25)	5.059(45)(80)(77)
$16^3 \times 48$					
K_{sea}	V_0	α	g_c	σ	r_0
0.1340	0.567(9)(18)(60)	0.268(8)(3)(45)	0.82(3)(9)(19)	0.0919(10)(7)(44)	3.880(14)(11)(31)
0.1343	0.597(9)(5)(47)	0.288(8)(13)(38)	0.75(3)(2)(14)	0.0811(10)(18)(36)	4.098(16)(25)(34)
0.1346	0.612(7)(23)(35)	0.296(6)(21)(25)	0.71(3)(5)(12)	0.0737(8)(28)(22)	4.287(19)(49)(24)
0.1350	0.644(9)(8)(20)	0.317(7)(5)(17)	0.62(3)(7)(10)	0.0624(8)(9)(15)	4.621(21)(25)(26)
0.1355	0.667(7)(10)(22)	0.331(5)(17)(18)	0.57(3)(1)(13)	0.0515(6)(18)(10)	5.059(23)(59)(32)
$20^3 \times 48$					
K_{sea}	V_0	α	g_c	σ	r_0
0.1340	0.626(3)(12)(38)	0.302(3)(10)(27)	0.79(1)(3)(16)	0.0866(4)(17)(25)	3.946(5)(24)(17)
0.1343	0.631(3)(3)(39)	0.303(3)(1)(28)	0.77(1)(1)(17)	0.0785(3)(6)(25)	4.143(6)(16)(23)
0.1346	0.643(2)(21)(33)	0.304(2)(15)(26)	0.71(1)(7)(13)	0.0716(3)(22)(21)	4.336(6)(43)(24)
0.1350	0.662(2)(4)(20)	0.312(2)(6)(16)	0.64(1)(1)(9)	0.0623(2)(16)(13)	4.635(7)(49)(20)
0.1355	0.687(2)(6)(16)	0.330(2)(8)(17)	0.56(1)(1)(12)	0.0509(2)(18)(13)	5.092(8)(76)(33)

TABLE III: Parameters in Eq. (19) and r_0 in quenched QCD.

lattice	V_0	α	g_c	σ	r_0
$12^3 \times 48$	0.568(7)(17)(10)	0.276(5)(8)(13)	0.318(21)(36)(42)	0.0519(6)(17)(10)	5.149(24)(72)(22)
$16^3 \times 48$	0.592(4)(12)(4)	0.278(3)(9)(11)	0.324(15)(29)(27)	0.0497(4)(11)(2)	5.255(15)(42)(15)
$20^3 \times 48$	0.610(4)(5)(14)	0.287(3)(7)(18)	0.319(15)(9)(49)	0.0484(4)(2)(15)	5.309(16)(1)(47)

TABLE IV: Autocorrelation time for plaquette ($\tau_{\text{plaq}}^{\text{cum}}$), PS meson propagator ($\tau_{\text{PS}}^{\text{cum}}$) and Wilson loop ($\tau_{\text{W}}^{\text{cum}}$) for A-HMC and S-HMC simulations. All numbers are written in units of HMC trajectory.

K_{sea}	0.1340	0.1343	0.1346	0.1350	0.1355
A-HMC					
$\tau_{\text{plaq}}^{\text{cum}}$	11.4(1.5)	35.4(9.8)	21.9(4.7)	10.3(2.4)	13.6(2.2)
$\tau_{\text{PS}}^{\text{cum}}$	13.7(2.6)	13.5(3.1)	17.6(4.3)	7.7(0.9)	8.5(3.1)
$\tau_{\text{W}}^{\text{cum}}$	5.0(0.4)	5.9(0.8)	5.9(1.1)	4.6(0.7)	6.2(0.9)
S-HMC					
K_{sea}	0.1340	0.1343	0.1346	0.1350	0.1355
$\tau_{\text{plaq}}^{\text{cum}}$	32.6(6.1)	30.7(4.8)	20.0(3.1)	18.9(2.7)	12.0(1.3)
$\tau_{\text{PS}}^{\text{cum}}$	16.4(2.0)	16.1(2.2)	13.8(2.0)	14.6(6.2)	10.4(1.3)
$\tau_{\text{W}}^{\text{cum}}$	6.3(2.5)	4.9(0.5)	5.1(0.3)	5.2(0.5)	5.2(0.3)

TABLE V: Parameters of diagonal fits to PS meson masses in method-A. We put “-” in some columns in this and the following tables when the corresponding term is not included in the fit.

χ^2/dof	K_c	$B_{\text{diag}}^{\text{PS}}$	$C_{\text{diag}}^{\text{PS}}$	$D_{\text{diag}}^{\text{PS}}$
0.01	0.136026(11)	25.97(63)	4.5(2.4)	-
0.01	0.136025(43)	26.0(4.0)	4(31)	2(72)

TABLE VI: Parameters of diagonal fits to vector meson masses in method-A.

χ^2/dof	A_{diag}^V	B_{diag}^V	C_{diag}^V	D_{diag}^V
0.06	1.867(36)	0.248(17)	-0.0083(19)	–
0.04	1.90(10)	0.224(81)	-0.002(21)	-0.0005(17)

TABLE VII: Parameters of combined chiral fits to PS meson masses in terms of VWI quark mass.

χ^2/dof	K_c	B_s^{PS}	B_v^{PS}	C_s^{PS}	C_v^{PS}	C_{sv}^{PS}	C_{vv}^{PS}
0.33	0.1360187(95)	9.64(51)	16.694(93)	7.5(1.8)	2.39(13)	-6.68(41)	–
0.33	0.1360185(95)	9.62(51)	16.751(95)	7.6(1.8)	1.61(21)	-6.78(41)	0.63(11)

TABLE VIII: Parameters of combined chiral fits to vector meson masses.

χ^2/dof	A^V	B_s^V	B_v^V	C_s^V	C_v^V	C_{sv}^V
0.55	1.914(24)	0.0349(51)	0.1895(45)	–	–	-0.00554(96)
0.23	1.877(33)	0.051(14)	0.1953(55)	-0.0028(16)	-0.00159(41)	-0.00389(65)

TABLE IX: Parameters of partially quenched chiral fits to vector meson masses.

K_{sea}	χ^2/dof	A_{PQ}^V	B_{PQ}^V
0.1340	0.10(5)	0.5306(23)	0.6361(53)
0.1343	0.08(5)	0.5067(23)	0.6648(58)
0.1346	0.04(3)	0.4835(27)	0.6940(84)
0.1350	0.14(10)	0.4394(29)	0.786(10)
0.1355	0.27(20)	0.3885(34)	0.906(14)

TABLE X: Parameters of combined chiral fits to octet baryon masses.

χ^2/dof	A^{O} $C_v^{\text{O},\Sigma}$	B_s^{O} $C_v^{\text{O},\Lambda}$	F_v^{O} $C_{sv}^{\text{O},\Sigma}$	D_v^{O} $C_{sv}^{\text{O},\Lambda}$	C_s^{O}	C_v^{O}	C_{sv}^{O}	C_{vv}^{O}
0.82	2.512(50) 0.00047(23)	0.018(23) 0.00374(26)	0.1286(32) 0.00057(35)	-0.0344(34) 0.00014(39)	0.0001(28)	-0.00621(39)	-0.00148(54)	–
0.66	2.489(51) 0.00074(25)	0.020(23) 0.00395(27)	0.1315(34) 0.00044(35)	-0.0342(34) 0.00006(39)	-0.0008(28)	-0.00520(32)	-0.00088(54)	-0.00356(34)

TABLE XI: Parameters of combined chiral fits to decuplet baryon masses.

χ^2/dof	A^{D}	B_s^{D}	B_v^{D}	C_s^{D}	C_v^{D}	C_{sv}^{D}
0.92	3.317(65)	0.038(15)	0.268(13)	–	–	-0.0055(29)
0.92	3.327(85)	0.049(36)	0.253(16)	-0.0012(43)	0.0020(13)	-0.0059(19)

TABLE XII: Parameters of chiral extrapolation of r_0^{-1} .

χ^2/dof	A_{r_0}	B_{r_0}
1.5	-4.867(35)	0.6861(48)

TABLE XIII: Parameters of diagonal fits to PS meson masses in method-B.

χ^2/dof	$K'_{c,\text{diag}}$	$B'_{\text{diag}}^{\text{PS}}$	$C'_{\text{diag}}^{\text{PS}}$	$D'_{\text{diag}}^{\text{PS}}$
2.5	0.136020(10)	4.67(11)	39.1(1.3)	–
1.9	0.135976(23)	5.47(42)	15(13)	252(142)

TABLE XIV: Parameters of diagonal fits to vector meson masses in method-B.

χ^2/dof	$A'_{\text{diag}}{}^V$	$B'_{\text{diag}}{}^V$	$C'_{\text{diag}}{}^V$	$D'_{\text{diag}}{}^V$
1.4	0.3523(45)	1.481(38)	-1.000(73)	–
0.1	0.3379(89)	1.73(13)	-2.19(59)	1.71(80)

TABLE XV: Parameters of chiral extrapolation of r_0 in terms of PS meson mass squared.

χ^2/dof	A'_{r_0}	B'_{r_0}	C'_{r_0}	D'_{r_0}
0.01	5.629(34)	-8.41(56)	16.3(2.7)	-15.2(3.8)

TABLE XVI: Hopping parameters corresponding to the light (K_{ud}) and the strange quark mass with K - ($K_s(K)$) and ϕ -input ($K_s(\phi)$) in full QCD. The lattice cutoff determined from ρ meson mass is also written. Error is statistical only.

K_{ud}	$K_s(K)$	$K_s(\phi)$	a^{-1} [GeV]
0.1359896(90)	0.134857(29)	0.134711(44)	2.221(28)

TABLE XVII: Fit parameters of chiral extrapolations in quenched QCD.

	χ^2/dof	$K_{c,q}$	B_q^{PS}	C_q^{PS}			
m_{PS}^2	0.18	0.135315(12)	2.859(35)	3.09(31)			
	χ^2/dof	A_q^V	B_q^V				
m_V	0.04	0.4146(54)	0.797(22)				
	χ^2/dof	A_q^O	F_q^O	D_q^O	C_q^O	$C_q^{O,\Sigma}$	$C_q^{O,\Lambda}$
m_{oct}	0.66	0.538(14)	0.521(47)	-0.158(44)	-0.36(17)	-0.059(92)	0.255(95)
	χ^2/dof	A_q^D	B_q^D				
m_{dec}	0.03	0.712(14)	1.123(59)				

TABLE XVIII: Hopping parameters corresponding to the light (K_{ud}) and the strange quark mass with K - ($K_s(K)$) and ϕ -input ($K_s(\phi)$) in quenched QCD.

K_{ud}	$K_s(K)$	$K_s(\phi)$	a^{-1} [GeV]
0.135245(11)	0.133571(43)	0.133214(76)	1.834(24)

TABLE XIX: J parameter calculated by Eq. (68). We obtain $J = 0.4242(61)$ at $K_{\text{sea}} = K_{ud}$ with the alternative definition (69).

K_{sea}	0.1340	0.1343	0.1346	0.1350	0.1355	K_{ud}	quenched
J	0.3827(22)	0.3818(21)	0.3801(34)	0.3932(32)	0.4018(37)	0.4153(62)	0.3735(66)

TABLE XX: Strange vector meson masses in GeV units in full and quenched QCD. The meson mass input to fix the strange quark mass is written in the brackets in the first column. The first error is statistical. The second and third ones are systematic error due to the choice of chiral fit forms and systematic uncertainty of r_0 . The deviation from the experimental spectrum is denoted by Δm .

	$m(N_f=2)$	$\Delta m(N_f=2)$	$m(N_f=0)$	$\Delta m(N_f=0)$
$K^*(K)$	0.8791(14)($^{+3}_{-1}$)($^{+14}_{-12}$)	-1.9%	0.8706(16)	-2.9%
$\phi(K)$	0.9899(28)($^{+5}_{-28}$)($^{+29}_{-24}$)	-2.9%	0.9727(32)	-4.7%
$K(\phi)$	0.5272(31)($^{+40}_{-7}$)($^{+26}_{-31}$)	+5.8%	0.5466(39)	+9.4%
$K^*(\phi)$	0.89390(0)(+173)(0)	-0.2%	0.89390(0)	-0.2%

TABLE XXI: Baryon spectrum in GeV units in full and quenched QCD.

	$m(N_f=2)$	$\Delta m(N_f=2)$	$m(N_f=0)$	$\Delta m(N_f=0)$
N	1.015(19)($^{+18}_{-9}$)($^{+10}_{-7}$)	+7.7%	1.004(26)	+6.7%
$\Sigma(K)$	1.185(17)($^{+16}_{-10}$)($^{+8}_{-5}$)	-0.7%	1.162(20)	-2.6%
$\Lambda(K)$	1.143(18)($^{+16}_{-9}$)($^{+9}_{-6}$)	+2.4%	1.120(20)	+0.4%
$\Xi(K)$	1.291(16)(+14)($^{+7}_{-4}$)	-1.8%	1.260(14)	-4.3%
$\Sigma(\phi)$	1.204(17)(+18)($^{+6}_{-3}$)	+1.0%	1.194(19)	+0.1%
$\Lambda(\phi)$	1.159(17)(+18)($^{+7}_{-4}$)	+3.8%	1.146(19)	+2.7%
$\Xi(\phi)$	1.325(16)(+18)($^{+3}_{-1}$)	+0.7%	1.315(11)	+0.02%
Δ	1.328(25)(+24)($^{+11}_{-7}$)	+7.5%	1.318(26)	+6.7%
$\Sigma^*(K)$	1.433(21)($^{+22}_{-1}$)($^{+10}_{-7}$)	+3.5%	1.414(22)	+2.2%
$\Xi^*(K)$	1.537(17)($^{+20}_{-5}$)($^{+9}_{-6}$)	+0.4%	1.510(18)	-1.4%
$\Omega(K)$	1.642(14)($^{+18}_{-6}$)($^{+8}_{-6}$)	-1.8%	1.606(14)	-4.1%
$\Sigma^*(\phi)$	1.447(20)($^{+24}_{-2}$)($^{+8}_{-5}$)	+4.4%	1.436(20)	+3.7%
$\Xi^*(\phi)$	1.566(15)($^{+24}_{-5}$)($^{+5}_{-3}$)	+2.2%	1.554(14)	+1.4%
$\Omega(\phi)$	1.684(11)($^{+23}_{-7}$)($^{+3}_{-1}$)	+0.7%	1.671(10)	-0.1%

TABLE XXII: Parameters of combined chiral fits to PS meson decay constant in full QCD.

χ^2/dof	A^f	B_s^f	B_v^f	C_s^f	C_v^f	C_{sv}^f
0.001	0.3415(71)	0.0075(18)	0.0349(18)	-	-	-0.00128(42)
0.001	0.344(11)	0.0019(55)	0.0398(18)	0.00046(70)	-0.00105(19)	-0.00069(23)

TABLE XXIII: Parameters of chiral extrapolation to PS meson decay constant in quenched QCD.

χ^2/dof	A_q^f	B_q^f
0.06	0.07221(94)	0.1246(42)

TABLE XXIV: Pseudoscalar decay constants in full and quenched QCD calculated with one-loop and non-perturbative (NP) matchings. Decay constants are written in GeV units. The first error is statistical. The second and third ones for full QCD results are systematic error due to the choice of chiral fit forms and uncertainty of measured value of r_0 .

	one-loop c_A , Z_A and b_A		NP c_A , Z_A and b_A
	$N_f=2$	$N_f=0$	$N_f=0$
f_π	0.1372(31)(+25) $\binom{+11}{-7}$	0.1337(24)	0.1287(23)
$f_K(K)$	0.1576(23)(+28) $\binom{+8}{-5}$	0.1497(20)	0.1438(19)
$f_K(\phi)$	0.1603(21)(+29) $\binom{+5}{-3}$	0.1533(17)	0.1473(17)
$f_K(K)/f_\pi$	1.148(11) $\binom{+12}{-5}$ $\binom{+2}{-3}$	1.1195(63)	1.1174(63)
$f_K(\phi)/f_\pi$	1.168(13) $\binom{+13}{-3}$ $\binom{+4}{-6}$	1.1468(90)	1.1443(89)

TABLE XXV: Parameters of combined chiral fits to PS meson masses in terms of AWI quark mass in full QCD.

χ^2/dof	$B_v^{\text{PS,AWI}}$	$C_v^{\text{PS,AWI}}$	$C_{sv}^{\text{PS,AWI}}$
0.21	18.08(12)	0.33(19)	-3.01(38)
0.22	18.13(11)	–	-2.89(39)

TABLE XXVI: Quark masses in two-flavor QCD in $\overline{\text{MS}}$ scheme at $\mu=2$ GeV. Values of m_{ud} and m_s are in MeV units. The meson mass input to fix m_s is written in brackets. The quoted errors are statistical only.

	m_{ud}	$m_s(K)$	$m_s(\phi)$	$m_s(K)/m_{ud}$	$m_s(\phi)/m_{ud}$
AWI	3.223(43)	84.5(1.1)	96.4(2.2)	26.133(24)	29.78(38)
VWI	2.488(57)	98.2(1.1)	110.4(2.3)	39.36(73)	44.21(93)

TABLE XXVII: Parameters of chiral fit to PS meson masses in terms of AWI quark mass in quenched QCD.

χ^2/dof	$B_q^{\text{PS,AWI}}$	$C_q^{\text{PS,AWI}}$
0.22	2.974(44)	1.31(61)

TABLE XXVIII: Quark masses in quenched QCD in $\overline{\text{MS}}$ scheme at $\mu=2$ GeV calculated in quenched QCD. Values of m_{ud} and m_s are in MeV units. Choice of input to fix m_s is written in brackets.

	m_{ud}	$m_s(K)$	$m_s(\phi)$	$m_s(K)/m_{ud}$	$m_s(\phi)/m_{ud}$
one-loop matching					
AWI	4.020(77)	104.1(1.6)	128.2(3.3)	25.90(13)	31.88(56)
VWI	4.628(77)	114.2(1.6)	136.9(3.2)	24.673(88)	29.57(42)
non-perturbative matching					
AWI	3.522(66)	91.9(1.4)	113.1(2.9)	26.08(13)	32.11(56)
VWI	4.315(72)	106.5(1.5)	127.7(3.0)	24.681(87)	29.58(42)

TABLE XXIX: Meson masses on $12^3 \times 48$ lattice in $N_f=2$ full QCD.

K_{sea}	$K_{\text{val},1}$	$K_{\text{val},2}$	$[t_{\min}, t_{\max}]$	χ^2/dof	m_{PS}	$[t_{\min}, t_{\max}]$	χ^2/dof	mv
0.1340	0.1340	0.1340	9,24	2.7	0.619(10)	9,24	2.1	0.782(12)
0.1340	0.1343	0.1343	9,24	2.9	0.592(11)	9,24	2.3	0.762(13)
0.1340	0.1346	0.1346	9,24	2.9	0.564(12)	9,24	2.5	0.742(13)
0.1340	0.1350	0.1350	9,24	2.6	0.525(12)	9,24	2.7	0.714(14)
0.1340	0.1355	0.1355	9,24	2.1	0.4709(95)	9,24	2.6	0.679(14)
0.1340	0.1358	0.1358	9,24	1.9	0.4344(79)	9,24	2.4	0.660(13)
0.1340	0.1340	0.1343	9,24	2.8	0.606(11)	9,24	2.2	0.772(13)
0.1340	0.1340	0.1346	9,24	3.0	0.592(11)	9,24	2.3	0.762(13)
0.1340	0.1340	0.1350	9,24	3.0	0.574(12)	9,24	2.4	0.749(13)
0.1340	0.1340	0.1355	9,24	2.7	0.550(12)	9,24	2.5	0.731(13)
0.1340	0.1340	0.1358	9,24	2.4	0.535(11)	9,24	2.5	0.720(14)
0.1343	0.1340	0.1340	9,24	2.2	0.5766(55)	9,24	2.6	0.748(13)
0.1343	0.1343	0.1343	9,24	2.2	0.5474(51)	9,24	2.7	0.728(14)
0.1343	0.1346	0.1346	9,24	2.1	0.5174(48)	9,24	2.6	0.704(16)
0.1343	0.1350	0.1350	9,24	2.2	0.4755(50)	9,24	1.8	0.665(19)
0.1343	0.1355	0.1355	9,24	2.4	0.4173(61)	9,24	0.9	0.626(16)
0.1343	0.1358	0.1358	9,24	2.9	0.3798(69)	9,24	1.3	0.613(19)
0.1343	0.1343	0.1340	9,24	2.2	0.5621(53)	9,24	2.7	0.738(13)
0.1343	0.1343	0.1346	9,24	2.1	0.5325(49)	9,24	2.7	0.716(14)
0.1343	0.1343	0.1350	9,24	2.2	0.5124(47)	9,24	2.5	0.699(16)
0.1343	0.1343	0.1355	9,24	2.2	0.4867(49)	9,24	1.9	0.675(18)
0.1343	0.1343	0.1358	9,24	2.2	0.4704(56)	9,24	1.3	0.661(18)
0.1346	0.1340	0.1340	9,24	4.0	0.5595(39)	9,24	2.5	0.7122(93)
0.1346	0.1343	0.1343	9,24	4.7	0.5304(49)	9,24	2.6	0.6917(97)
0.1346	0.1346	0.1346	9,24	4.5	0.5011(70)	9,24	2.6	0.669(11)
0.1346	0.1350	0.1350	9,24	3.0	0.4596(80)	9,24	2.8	0.636(15)
0.1346	0.1355	0.1355	9,24	2.0	0.4000(56)	9,24	4.6	0.601(19)
0.1346	0.1358	0.1358	9,24	1.6	0.3561(67)	9,24	3.7	0.576(24)
0.1346	0.1346	0.1340	9,24	4.7	0.5305(49)	9,24	2.5	0.6916(95)
0.1346	0.1346	0.1343	9,24	4.7	0.5158(59)	9,24	2.6	0.681(10)
0.1346	0.1346	0.1350	9,24	3.7	0.4809(80)	9,24	2.6	0.653(12)
0.1346	0.1346	0.1355	9,24	2.6	0.4544(74)	9,24	2.9	0.631(16)
0.1346	0.1346	0.1358	9,24	2.0	0.4371(60)	9,24	3.7	0.620(19)
0.1350	0.1340	0.1340	10,24	2.9	0.5304(61)	10,24	0.9	0.671(13)
0.1350	0.1343	0.1343	10,24	2.8	0.4998(65)	10,24	0.8	0.650(14)
0.1350	0.1346	0.1346	10,24	2.6	0.4681(69)	10,24	0.8	0.629(16)
0.1350	0.1350	0.1350	10,24	2.4	0.4239(71)	10,24	0.7	0.602(18)
0.1350	0.1355	0.1355	10,24	1.8	0.3634(63)	10,24	0.7	0.574(17)
0.1350	0.1358	0.1358	10,24	1.4	0.3233(56)	10,24	0.9	0.564(19)
0.1350	0.1350	0.1340	10,24	2.6	0.4791(68)	10,24	0.7	0.637(15)
0.1350	0.1350	0.1343	10,24	2.6	0.4629(70)	10,24	0.7	0.626(16)
0.1350	0.1350	0.1346	10,24	2.5	0.4464(71)	10,24	0.7	0.615(17)
0.1350	0.1350	0.1355	10,24	2.1	0.3948(67)	10,24	0.6	0.587(19)
0.1350	0.1350	0.1358	10,24	1.7	0.3768(61)	10,24	0.7	0.580(17)
0.1355	0.1340	0.1340	10,24	2.0	0.4825(57)	11,24	1.5	0.621(13)
0.1355	0.1343	0.1343	10,24	1.9	0.4530(60)	11,24	1.4	0.601(14)
0.1355	0.1346	0.1346	10,24	1.8	0.4230(66)	11,24	1.3	0.581(15)
0.1355	0.1350	0.1350	10,24	1.7	0.3821(84)	11,24	1.4	0.556(21)
0.1355	0.1355	0.1355	10,24	1.4	0.328(14)	11,24	1.2	0.541(48)
0.1355	0.1358	0.1358	10,24	1.5	0.287(26)	11,24	0.9	0.560(82)
0.1355	0.1355	0.1340	10,24	1.6	0.4111(92)	11,24	1.2	0.577(20)
0.1355	0.1355	0.1343	10,24	1.6	0.3948(97)	11,24	1.3	0.566(22)
0.1355	0.1355	0.1346	10,24	1.6	0.378(10)	11,24	1.3	0.556(25)
0.1355	0.1355	0.1350	10,24	1.6	0.356(11)	11,24	1.4	0.546(31)
0.1355	0.1355	0.1358	10,24	1.4	0.309(20)	11,24	1.0	0.546(64)

TABLE XXX: Baryon masses on $12^3 \times 48$ lattice in $N_f=2$ full QCD.

K_{sea}	$K_{\text{val},1}$	$K_{\text{val},2}$	$K_{\text{val},3}$	$[t_{\min}, t_{\max}]$	χ^2/dof	m_{Σ}	$[t_{\min}, t_{\max}]$	χ^2/dof	m_{Λ}	$[t_{\min}, t_{\max}]$	χ^2/dof	m_{dec}
0.1340	0.1340	0.1340	0.1340	10,24	1.7	1.153(12)	–	–	–	10,24	1.6	1.220(37)
0.1340	0.1343	0.1343	0.1343	10,24	1.7	1.122(16)	–	–	–	10,24	1.5	1.191(39)
0.1340	0.1346	0.1346	0.1346	10,24	1.7	1.089(24)	–	–	–	10,24	1.4	1.164(39)
0.1340	0.1350	0.1350	0.1350	10,24	1.6	1.040(33)	–	–	–	10,24	1.3	1.131(36)
0.1340	0.1355	0.1355	0.1355	10,24	1.8	0.971(41)	–	–	–	10,24	1.4	1.096(32)
0.1340	0.1358	0.1358	0.1358	10,24	1.8	0.922(43)	–	–	–	10,24	1.5	1.077(38)
0.1340	0.1340	0.1340	0.1343	10,24	1.8	1.142(13)	10,24	1.6	1.143(13)	10,24	1.6	1.209(37)
0.1340	0.1340	0.1340	0.1346	10,24	1.8	1.132(15)	10,24	1.5	1.134(14)	10,24	1.6	1.199(38)
0.1340	0.1340	0.1340	0.1350	10,24	1.9	1.118(18)	10,24	1.4	1.121(18)	10,24	1.5	1.186(38)
0.1340	0.1340	0.1340	0.1355	10,24	1.9	1.100(21)	10,24	1.2	1.104(22)	10,24	1.5	1.173(37)
0.1340	0.1340	0.1340	0.1358	10,24	1.9	1.089(23)	10,24	1.0	1.094(23)	10,24	1.7	1.170(38)
0.1340	0.1343	0.1343	0.1340	10,24	1.6	1.133(14)	10,24	1.7	1.132(14)	10,24	1.6	1.199(38)
0.1340	0.1346	0.1346	0.1340	10,24	1.6	1.112(19)	10,24	1.8	1.110(19)	10,24	1.5	1.180(39)
0.1340	0.1350	0.1350	0.1340	10,24	1.5	1.083(26)	10,24	1.8	1.080(25)	10,24	1.3	1.156(37)

TABLE XXX: (Continued)

K_{sea}	$K_{\text{val},1}$	$K_{\text{val},2}$	$K_{\text{val},3}$	$t_{\text{min}}, t_{\text{max}}$	χ^2/dof	m_{Σ}	$t_{\text{min}}, t_{\text{max}}$	χ^2/dof	m_{Λ}	$t_{\text{min}}, t_{\text{max}}$	χ^2/dof	m_{dec}
0.1340	0.1355	0.1355	0.1340	10,24	1.4	1.043(35)	10,24	1.7	1.039(28)	10,24	1.5	1.136(34)
0.1340	0.1358	0.1358	0.1340	10,24	1.6	1.020(40)	10,24	1.8	1.017(28)	10,24	1.6	1.129(33)
0.1343	0.1340	0.1340	0.1340	10,24	1.7	1.132(23)	–	–	–	10,24	1.7	1.216(27)
0.1343	0.1343	0.1343	0.1343	10,24	1.8	1.094(23)	–	–	–	10,24	1.5	1.187(27)
0.1343	0.1346	0.1346	0.1346	10,24	2.0	1.055(25)	–	–	–	10,24	1.3	1.159(28)
0.1343	0.1350	0.1350	0.1350	10,24	2.3	0.998(25)	–	–	–	10,24	1.1	1.125(33)
0.1343	0.1355	0.1355	0.1355	10,24	2.4	0.921(32)	–	–	–	10,24	1.3	1.099(51)
0.1343	0.1358	0.1358	0.1358	10,24	1.3	0.876(43)	–	–	–	10,24	2.0	1.117(83)
0.1343	0.1343	0.1343	0.1340	10,24	1.7	1.107(23)	10,24	1.9	1.107(23)	10,24	1.6	1.193(26)
0.1343	0.1343	0.1343	0.1346	10,24	1.9	1.081(24)	10,24	1.7	1.082(23)	10,24	1.5	1.174(26)
0.1343	0.1343	0.1343	0.1350	10,24	2.2	1.063(25)	10,24	1.7	1.065(24)	10,24	1.3	1.162(27)
0.1343	0.1343	0.1343	0.1355	10,24	2.7	1.037(26)	10,24	1.6	1.046(26)	10,24	1.2	1.149(30)
0.1343	0.1343	0.1343	0.1358	10,24	3.1	1.017(29)	10,24	1.5	1.034(27)	10,24	1.1	1.145(34)
0.1343	0.1340	0.1340	0.1343	10,24	1.8	1.120(23)	10,24	1.7	1.120(22)	10,24	1.7	1.203(26)
0.1343	0.1346	0.1346	0.1343	10,24	1.8	1.068(24)	10,24	2.0	1.068(24)	10,24	1.4	1.165(27)
0.1343	0.1350	0.1350	0.1343	10,24	1.8	1.033(25)	10,24	2.4	1.030(26)	10,24	1.2	1.142(29)
0.1343	0.1355	0.1355	0.1343	10,24	1.8	0.990(27)	10,24	3.0	0.974(30)	10,24	1.1	1.119(37)
0.1343	0.1358	0.1358	0.1343	10,24	1.6	0.964(25)	10,24	2.7	0.939(38)	10,24	1.3	1.116(45)
0.1346	0.1340	0.1340	0.1340	11,24	0.9	1.082(13)	–	–	–	11,24	4.9	1.220(38)
0.1346	0.1343	0.1343	0.1343	11,24	1.0	1.045(16)	–	–	–	11,24	3.8	1.184(34)
0.1346	0.1346	0.1346	0.1346	11,24	1.1	1.006(24)	–	–	–	11,24	2.4	1.147(35)
0.1346	0.1350	0.1350	0.1350	11,24	1.7	0.964(56)	–	–	–	11,24	1.4	1.108(49)
0.1346	0.1355	0.1355	0.1355	11,24	2.3	0.924(61)	–	–	–	11,24	1.1	1.089(65)
0.1346	0.1358	0.1358	0.1358	11,24	1.3	0.946(58)	–	–	–	11,24	1.0	1.14(11)
0.1346	0.1346	0.1346	0.1340	11,24	1.1	1.037(19)	11,24	0.9	1.028(18)	11,24	3.2	1.174(34)
0.1346	0.1346	0.1346	0.1343	11,24	1.1	1.022(21)	11,24	1.0	1.017(21)	11,24	2.8	1.161(33)
0.1346	0.1346	0.1346	0.1350	11,24	1.2	0.985(32)	11,24	1.4	0.994(30)	11,24	1.9	1.133(38)
0.1346	0.1346	0.1346	0.1355	11,24	1.1	0.959(39)	11,24	1.6	0.982(40)	11,24	1.6	1.120(45)
0.1346	0.1346	0.1346	0.1358	11,24	0.9	0.940(30)	11,24	1.7	0.976(50)	11,24	1.6	1.118(50)
0.1346	0.1340	0.1340	0.1346	11,24	0.8	1.054(14)	11,24	1.0	1.062(16)	11,24	4.4	1.198(35)
0.1346	0.1343	0.1343	0.1346	11,24	0.9	1.030(18)	11,24	1.1	1.035(18)	11,24	3.3	1.173(34)
0.1346	0.1350	0.1350	0.1346	11,24	1.6	0.979(39)	11,24	1.4	0.970(44)	11,24	1.5	1.120(42)
0.1346	0.1355	0.1355	0.1346	11,24	1.8	0.956(64)	11,24	1.6	0.933(53)	11,24	1.2	1.101(56)
0.1346	0.1358	0.1358	0.1346	11,24	1.8	0.933(66)	11,24	1.2	0.912(45)	11,24	1.2	1.119(59)
0.1350	0.1340	0.1340	0.1340	11,24	1.7	1.026(21)	–	–	–	11,24	0.9	1.094(19)
0.1350	0.1343	0.1343	0.1343	11,24	2.1	0.993(24)	–	–	–	11,24	1.0	1.059(20)
0.1350	0.1346	0.1346	0.1346	11,24	2.8	0.960(26)	–	–	–	11,24	1.2	1.027(24)
0.1350	0.1350	0.1350	0.1350	11,24	3.8	0.915(34)	–	–	–	11,24	1.6	0.992(32)
0.1350	0.1355	0.1355	0.1355	11,24	3.6	0.846(35)	–	–	–	11,24	0.9	0.954(30)
0.1350	0.1358	0.1358	0.1358	11,24	2.8	0.798(57)	–	–	–	11,24	0.4	0.913(47)
0.1350	0.1350	0.1350	0.1340	11,24	3.0	0.961(30)	11,24	3.2	0.936(24)	11,24	1.4	1.016(26)
0.1350	0.1350	0.1350	0.1343	11,24	3.2	0.949(31)	11,24	3.4	0.929(26)	11,24	1.5	1.006(27)
0.1350	0.1350	0.1350	0.1346	11,24	3.5	0.936(32)	11,24	3.6	0.922(29)	11,24	1.5	0.997(28)
0.1350	0.1350	0.1350	0.1355	11,24	3.9	0.881(32)	11,24	4.0	0.905(41)	11,24	1.4	0.974(31)
0.1350	0.1350	0.1350	0.1358	11,24	3.7	0.865(26)	11,24	4.1	0.894(53)	11,24	1.1	0.973(31)
0.1350	0.1340	0.1340	0.1350	11,24	2.2	0.980(22)	11,24	2.3	0.994(28)	11,24	1.1	1.050(20)
0.1350	0.1343	0.1343	0.1350	11,24	2.7	0.959(24)	11,24	2.7	0.972(28)	11,24	1.2	1.029(22)
0.1350	0.1346	0.1346	0.1350	11,24	3.3	0.939(27)	11,24	3.1	0.949(29)	11,24	1.3	1.009(25)
0.1350	0.1355	0.1355	0.1350	11,24	4.1	0.886(42)	11,24	3.3	0.858(31)	11,24	1.1	0.962(32)
0.1350	0.1358	0.1358	0.1350	11,24	4.4	0.869(54)	11,24	1.9	0.838(32)	11,24	0.6	0.947(37)
0.1355	0.1340	0.1340	0.1340	11,24	2.7	0.983(19)	–	–	–	11,24	1.8	1.055(29)
0.1355	0.1343	0.1343	0.1343	11,24	2.5	0.959(27)	–	–	–	11,24	1.5	1.024(33)
0.1355	0.1346	0.1346	0.1346	11,24	2.2	0.930(28)	–	–	–	11,24	1.3	0.989(35)
0.1355	0.1350	0.1350	0.1350	11,24	2.0	0.882(27)	–	–	–	11,24	1.2	0.955(42)
0.1355	0.1355	0.1355	0.1355	11,24	2.0	0.820(36)	–	–	–	11,24	1.6	0.95(10)
0.1355	0.1358	0.1358	0.1358	11,24	1.4	0.854(99)	–	–	–	11,24	1.2	0.94(20)
0.1355	0.1355	0.1355	0.1340	11,24	2.3	0.897(27)	11,24	3.4	0.874(37)	11,24	2.3	0.991(41)
0.1355	0.1355	0.1355	0.1343	11,24	2.1	0.882(25)	11,24	3.2	0.872(41)	11,24	2.0	0.976(47)
0.1355	0.1355	0.1355	0.1346	11,24	1.9	0.867(25)	11,24	2.8	0.869(46)	11,24	1.8	0.961(57)
0.1355	0.1355	0.1355	0.1350	11,24	1.8	0.847(28)	11,24	2.3	0.855(47)	11,24	1.6	0.949(66)
0.1355	0.1355	0.1355	0.1358	11,24	2.4	0.784(68)	11,24	1.6	0.824(48)	11,24	1.8	0.913(88)
0.1355	0.1340	0.1340	0.1355	11,24	2.2	0.943(29)	11,24	3.5	0.930(24)	11,24	2.1	1.013(32)
0.1355	0.1343	0.1343	0.1355	11,24	2.2	0.924(34)	11,24	2.8	0.911(21)	11,24	1.6	0.986(28)
0.1355	0.1346	0.1346	0.1355	11,24	2.2	0.900(34)	11,24	2.2	0.893(21)	11,24	1.3	0.963(34)
0.1355	0.1350	0.1350	0.1355	11,24	2.3	0.875(44)	11,24	1.7	0.863(25)	11,24	1.3	0.943(52)
0.1355	0.1358	0.1358	0.1355	11,24	1.3	0.85(10)	11,24	1.8	0.770(67)	11,24	1.6	0.92(13)

TABLE XXXI: Meson masses on $16^3 \times 48$ lattice in $N_f=2$ full QCD.

K_{sea}	$K_{\text{val},1}$	$K_{\text{val},2}$	$[t_{\min}, t_{\max}]$	χ^2/dof	m_{PS}	$[t_{\min}, t_{\max}]$	χ^2/dof	mv
0.1340	0.1340	0.1340	9,24	3.3	0.6200(21)	9,24	2.0	0.7727(41)
0.1340	0.1343	0.1343	9,24	2.9	0.5917(20)	9,24	1.6	0.7527(49)
0.1340	0.1346	0.1346	9,24	2.4	0.5623(19)	9,24	1.4	0.7324(60)
0.1340	0.1350	0.1350	9,24	1.9	0.5212(22)	9,24	1.6	0.7050(78)
0.1340	0.1355	0.1355	9,24	1.8	0.4656(27)	9,24	2.5	0.672(12)
0.1340	0.1358	0.1358	9,24	2.1	0.4288(29)	9,24	2.5	0.653(13)
0.1340	0.1340	0.1343	9,24	3.1	0.6060(20)	9,24	1.8	0.7627(45)
0.1340	0.1340	0.1346	9,24	2.9	0.5917(20)	9,24	1.6	0.7527(50)
0.1340	0.1340	0.1350	9,24	2.6	0.5724(19)	9,24	1.4	0.7392(59)
0.1340	0.1340	0.1355	9,24	2.3	0.5476(20)	9,24	1.3	0.7220(73)
0.1340	0.1340	0.1358	9,24	2.1	0.5324(22)	9,24	1.4	0.7116(80)
0.1343	0.1340	0.1340	9,24	2.2	0.5819(40)	9,24	3.5	0.7291(73)
0.1343	0.1343	0.1343	9,24	2.3	0.5528(40)	9,24	4.2	0.7090(88)
0.1343	0.1346	0.1346	9,24	2.3	0.5225(39)	9,24	4.9	0.689(10)
0.1343	0.1350	0.1350	9,24	2.5	0.4802(37)	9,24	5.9	0.665(13)
0.1343	0.1355	0.1355	9,24	2.9	0.4226(31)	9,24	5.6	0.626(18)
0.1343	0.1358	0.1358	9,24	3.1	0.3836(33)	9,24	4.4	0.595(19)
0.1343	0.1343	0.1340	9,24	2.2	0.5674(40)	9,24	3.8	0.7191(80)
0.1343	0.1343	0.1346	9,24	2.3	0.5378(40)	9,24	4.5	0.6992(96)
0.1343	0.1343	0.1350	9,24	2.4	0.5175(39)	9,24	5.0	0.687(11)
0.1343	0.1343	0.1355	9,24	2.5	0.4913(39)	9,24	5.6	0.671(12)
0.1343	0.1343	0.1358	9,24	2.8	0.4751(38)	9,24	5.6	0.661(14)
0.1346	0.1340	0.1340	9,24	1.6	0.5556(20)	9,24	1.5	0.7011(34)
0.1346	0.1343	0.1343	9,24	1.3	0.5254(20)	9,24	1.7	0.6789(46)
0.1346	0.1346	0.1346	9,24	0.9	0.4939(20)	9,24	1.8	0.6573(58)
0.1346	0.1350	0.1350	9,24	0.6	0.4496(20)	9,24	2.2	0.6297(70)
0.1346	0.1355	0.1355	9,24	0.8	0.3891(24)	9,24	2.8	0.5947(84)
0.1346	0.1358	0.1358	9,24	1.2	0.3482(36)	9,24	2.9	0.572(12)
0.1346	0.1346	0.1340	9,24	1.2	0.5254(20)	9,24	1.7	0.6790(47)
0.1346	0.1346	0.1343	9,24	1.1	0.5099(19)	9,24	1.7	0.6680(52)
0.1346	0.1346	0.1350	9,24	0.7	0.4721(20)	9,24	2.0	0.6434(66)
0.1346	0.1346	0.1355	9,24	0.6	0.4438(21)	9,24	2.4	0.6262(77)
0.1346	0.1346	0.1358	9,24	0.6	0.4262(22)	9,24	3.0	0.6152(85)
0.1350	0.1340	0.1340	10,24	2.2	0.5107(22)	10,24	1.1	0.6469(56)
0.1350	0.1343	0.1343	10,24	2.2	0.4793(24)	10,24	1.1	0.6233(62)
0.1350	0.1346	0.1346	10,24	2.2	0.4466(27)	10,24	1.0	0.5990(71)
0.1350	0.1350	0.1350	10,24	2.3	0.4003(33)	10,24	0.9	0.5660(91)
0.1350	0.1355	0.1355	10,24	2.9	0.3353(46)	10,24	1.0	0.529(13)
0.1350	0.1358	0.1358	10,24	3.7	0.2904(67)	10,24	1.3	0.510(19)
0.1350	0.1350	0.1340	10,24	2.2	0.4578(26)	10,24	1.1	0.6075(69)
0.1350	0.1350	0.1343	10,24	2.2	0.4410(28)	10,24	1.0	0.5950(74)
0.1350	0.1350	0.1346	10,24	2.3	0.4239(30)	10,24	0.9	0.5825(80)
0.1350	0.1350	0.1355	10,24	2.5	0.3691(39)	10,24	0.9	0.547(11)
0.1350	0.1350	0.1358	10,24	2.7	0.3490(44)	10,24	1.1	0.535(13)
0.1355	0.1340	0.1340	10,24	3.2	0.4680(36)	11,24	0.9	0.5922(57)
0.1355	0.1343	0.1343	10,24	3.2	0.4357(36)	11,24	0.8	0.5685(63)
0.1355	0.1346	0.1346	10,24	3.1	0.4012(37)	11,24	0.7	0.5457(72)
0.1355	0.1350	0.1350	10,24	2.9	0.3511(43)	11,24	0.8	0.5166(81)
0.1355	0.1355	0.1355	10,24	2.6	0.2806(64)	11,24	0.8	0.479(11)
0.1355	0.1358	0.1358	10,24	3.3	0.2321(81)	11,24	1.1	0.448(21)
0.1355	0.1355	0.1340	10,24	2.9	0.3843(43)	11,24	0.7	0.5356(77)
0.1355	0.1355	0.1343	10,24	2.7	0.3651(44)	11,24	0.7	0.5245(78)
0.1355	0.1355	0.1346	10,24	2.7	0.3452(47)	11,24	0.7	0.5132(79)
0.1355	0.1355	0.1350	10,24	2.6	0.3174(53)	11,24	0.8	0.4981(85)
0.1355	0.1355	0.1358	10,24	2.8	0.2579(73)	11,24	0.7	0.465(14)

TABLE XXXII: Baryon masses on $16^3 \times 48$ lattice in $N_f=2$ full QCD.

K_{sea}	$K_{\text{val},1}$	$K_{\text{val},2}$	$K_{\text{val},3}$	$[t_{\min}, t_{\max}]$	χ^2/dof	m_{Σ}	$[t_{\min}, t_{\max}]$	χ^2/dof	m_{Λ}	$[t_{\min}, t_{\max}]$	χ^2/dof	m_{dec}
0.1340	0.1340	0.1340	0.1340	10,24	2.2	1.166(20)	—	—	—	10,24	5.1	1.256(20)
0.1340	0.1343	0.1343	0.1343	10,24	2.3	1.128(21)	—	—	—	10,24	3.8	1.224(17)
0.1340	0.1346	0.1346	0.1346	10,24	2.2	1.089(20)	—	—	—	10,24	2.8	1.192(15)
0.1340	0.1350	0.1350	0.1350	10,24	1.7	1.037(18)	—	—	—	10,24	2.0	1.149(13)
0.1340	0.1355	0.1355	0.1355	10,24	1.3	0.979(18)	—	—	—	10,24	1.4	1.096(13)
0.1340	0.1358	0.1358	0.1358	10,24	1.7	0.955(18)	—	—	—	10,24	1.2	1.067(16)
0.1340	0.1340	0.1340	0.1343	10,24	2.1	1.152(20)	10,24	2.4	1.155(22)	10,24	4.9	1.242(20)
0.1340	0.1340	0.1340	0.1346	10,24	2.0	1.138(20)	10,24	2.7	1.144(23)	10,24	4.3	1.231(19)
0.1340	0.1340	0.1340	0.1350	10,24	1.9	1.120(18)	10,24	3.0	1.129(24)	10,24	3.6	1.218(17)
0.1340	0.1340	0.1340	0.1355	10,24	1.7	1.097(16)	10,24	2.9	1.109(22)	10,24	2.5	1.202(16)
0.1340	0.1340	0.1340	0.1358	10,24	1.5	1.083(15)	10,24	2.3	1.097(18)	10,24	1.9	1.193(15)
0.1340	0.1343	0.1343	0.1340	10,24	2.5	1.142(22)	10,24	2.1	1.139(20)	10,24	4.4	1.231(19)
0.1340	0.1346	0.1346	0.1340	10,24	2.8	1.118(24)	10,24	2.0	1.113(19)	10,24	3.5	1.211(17)
0.1340	0.1350	0.1350	0.1340	10,24	2.9	1.083(24)	10,24	1.6	1.077(17)	10,24	2.5	1.183(14)

TABLE XXXII: (Continued)

K_{sea}	$K_{\text{val},1}$	$K_{\text{val},2}$	$K_{\text{val},3}$	$t_{\text{min}}, t_{\text{max}}$	χ^2/dof	m_{Σ}	$t_{\text{min}}, t_{\text{max}}$	χ^2/dof	m_{Λ}	$t_{\text{min}}, t_{\text{max}}$	χ^2/dof	m_{dec}
0.1340	0.1355	0.1355	0.1340	10,24	2.2	1.040(21)	10,24	1.1	1.035(16)	10,24	1.5	1.149(12)
0.1340	0.1358	0.1358	0.1340	10,24	1.6	1.019(18)	10,24	1.2	1.011(16)	10,24	1.2	1.130(11)
0.1343	0.1340	0.1340	0.1340	10,24	1.0	1.100(14)	–	–	–	10,24	2.0	1.203(15)
0.1343	0.1343	0.1343	0.1343	10,24	0.7	1.063(13)	–	–	–	10,24	2.4	1.176(16)
0.1343	0.1346	0.1346	0.1346	10,24	0.7	1.025(13)	–	–	–	10,24	2.9	1.150(18)
0.1343	0.1350	0.1350	0.1350	10,24	0.8	0.972(15)	–	–	–	10,24	3.1	1.110(27)
0.1343	0.1355	0.1355	0.1355	10,24	1.5	0.902(23)	–	–	–	10,24	2.5	1.044(36)
0.1343	0.1358	0.1358	0.1358	10,24	2.0	0.863(30)	–	–	–	10,24	2.1	1.004(40)
0.1343	0.1343	0.1343	0.1340	10,24	0.8	1.076(13)	10,24	0.8	1.075(13)	10,24	2.3	1.183(15)
0.1343	0.1343	0.1343	0.1346	10,24	0.7	1.050(13)	10,24	0.7	1.051(13)	10,24	2.6	1.166(16)
0.1343	0.1343	0.1343	0.1350	10,24	0.6	1.032(13)	10,24	0.8	1.035(12)	10,24	2.9	1.155(16)
0.1343	0.1343	0.1343	0.1355	10,24	0.8	1.008(14)	10,24	1.0	1.015(13)	10,24	3.4	1.139(19)
0.1343	0.1343	0.1343	0.1358	10,24	1.0	0.993(15)	10,24	1.4	1.003(15)	10,24	3.5	1.125(23)
0.1343	0.1340	0.1340	0.1343	10,24	0.8	1.087(14)	10,24	0.9	1.088(13)	10,24	2.1	1.192(15)
0.1343	0.1346	0.1346	0.1343	10,24	0.7	1.039(13)	10,24	0.7	1.037(13)	10,24	2.8	1.158(16)
0.1343	0.1350	0.1350	0.1343	10,24	0.9	1.005(13)	10,24	0.7	1.001(14)	10,24	3.4	1.135(20)
0.1343	0.1355	0.1355	0.1343	10,24	1.4	0.961(17)	10,24	1.0	0.953(18)	10,24	3.1	1.093(32)
0.1343	0.1358	0.1358	0.1343	10,24	2.2	0.932(19)	10,24	1.4	0.925(25)	10,24	2.6	1.065(38)
0.1346	0.1340	0.1340	0.1340	11,24	2.4	1.064(10)	–	–	–	11,24	1.8	1.153(16)
0.1346	0.1343	0.1343	0.1343	11,24	2.3	1.028(12)	–	–	–	11,24	1.8	1.122(16)
0.1346	0.1346	0.1346	0.1346	11,24	2.2	0.991(14)	–	–	–	11,24	1.8	1.091(17)
0.1346	0.1350	0.1350	0.1350	11,24	1.8	0.938(16)	–	–	–	11,24	1.7	1.053(19)
0.1346	0.1355	0.1355	0.1355	11,24	1.1	0.862(20)	–	–	–	11,24	1.2	1.008(30)
0.1346	0.1358	0.1358	0.1358	11,24	1.7	0.821(30)	–	–	–	11,24	0.9	0.981(40)
0.1346	0.1346	0.1346	0.1340	11,24	2.3	1.017(11)	11,24	2.3	1.014(13)	11,24	1.8	1.110(18)
0.1346	0.1346	0.1346	0.1343	11,24	2.2	1.004(12)	11,24	2.2	1.002(13)	11,24	1.8	1.099(18)
0.1346	0.1346	0.1346	0.1350	11,24	2.0	0.972(15)	11,24	2.1	0.975(13)	11,24	1.9	1.075(18)
0.1346	0.1346	0.1346	0.1355	11,24	1.8	0.945(15)	11,24	1.9	0.953(14)	11,24	2.0	1.061(20)
0.1346	0.1346	0.1346	0.1358	11,24	1.7	0.926(15)	11,24	1.6	0.939(16)	11,24	2.1	1.055(22)
0.1346	0.1340	0.1340	0.1346	11,24	2.4	1.039(12)	11,24	2.4	1.041(10)	11,24	1.8	1.130(17)
0.1346	0.1343	0.1343	0.1346	11,24	2.3	1.015(13)	11,24	2.3	1.016(12)	11,24	1.8	1.109(17)
0.1346	0.1350	0.1350	0.1346	11,24	2.0	0.957(14)	11,24	1.9	0.954(16)	11,24	1.9	1.062(19)
0.1346	0.1355	0.1355	0.1346	11,24	1.7	0.908(18)	11,24	1.4	0.901(16)	11,24	1.7	1.034(23)
0.1346	0.1358	0.1358	0.1346	11,24	1.1	0.873(21)	11,24	1.4	0.869(20)	11,24	1.5	1.019(30)
0.1350	0.1340	0.1340	0.1340	11,24	2.1	0.965(11)	–	–	–	11,24	1.4	1.031(14)
0.1350	0.1343	0.1343	0.1343	11,24	1.7	0.925(10)	–	–	–	11,24	1.3	0.995(15)
0.1350	0.1346	0.1346	0.1346	11,24	1.6	0.884(11)	–	–	–	11,24	1.2	0.958(16)
0.1350	0.1350	0.1350	0.1350	11,24	1.7	0.828(12)	–	–	–	11,24	1.3	0.903(18)
0.1350	0.1355	0.1355	0.1355	11,24	1.1	0.759(16)	–	–	–	11,24	1.1	0.826(33)
0.1350	0.1358	0.1358	0.1358	11,24	1.0	0.715(25)	–	–	–	11,24	0.9	0.758(49)
0.1350	0.1350	0.1350	0.1340	11,24	1.5	0.879(13)	11,24	1.4	0.8708(92)	11,24	1.2	0.947(16)
0.1350	0.1350	0.1350	0.1343	11,24	1.6	0.864(13)	11,24	1.5	0.8577(98)	11,24	1.2	0.934(16)
0.1350	0.1350	0.1350	0.1346	11,24	1.7	0.849(13)	11,24	1.5	0.845(11)	11,24	1.3	0.920(17)
0.1350	0.1350	0.1350	0.1355	11,24	1.3	0.802(12)	11,24	1.7	0.807(16)	11,24	1.2	0.876(20)
0.1350	0.1350	0.1350	0.1358	11,24	1.1	0.787(13)	11,24	1.7	0.792(15)	11,24	1.0	0.857(23)
0.1350	0.1340	0.1340	0.1350	11,24	1.5	0.916(10)	11,24	1.5	0.9247(97)	11,24	1.2	0.988(14)
0.1350	0.1343	0.1343	0.1350	11,24	1.4	0.890(10)	11,24	1.5	0.897(11)	11,24	1.2	0.964(15)
0.1350	0.1346	0.1346	0.1350	11,24	1.5	0.864(11)	11,24	1.6	0.868(12)	11,24	1.2	0.938(16)
0.1350	0.1355	0.1355	0.1350	11,24	1.5	0.784(17)	11,24	1.2	0.778(14)	11,24	1.1	0.851(25)
0.1350	0.1358	0.1358	0.1350	11,24	1.3	0.755(17)	11,24	1.2	0.747(16)	11,24	0.8	0.811(36)
0.1355	0.1340	0.1340	0.1340	11,24	2.7	0.891(16)	–	–	–	11,24	1.1	0.981(17)
0.1355	0.1343	0.1343	0.1343	11,24	3.1	0.851(18)	–	–	–	11,24	1.2	0.948(22)
0.1355	0.1346	0.1346	0.1346	11,24	3.6	0.814(20)	–	–	–	11,24	1.3	0.919(30)
0.1355	0.1350	0.1350	0.1350	11,24	3.5	0.771(24)	–	–	–	11,24	1.4	0.892(39)
0.1355	0.1355	0.1355	0.1355	11,24	2.0	0.707(29)	–	–	–	11,24	1.9	0.864(53)
0.1355	0.1358	0.1358	0.1358	11,24	1.4	0.666(47)	–	–	–	11,24	2.2	0.806(65)
0.1355	0.1355	0.1355	0.1340	11,24	3.0	0.791(27)	11,24	2.8	0.761(22)	11,24	1.4	0.889(39)
0.1355	0.1355	0.1355	0.1343	11,24	2.8	0.776(26)	11,24	2.7	0.749(23)	11,24	1.5	0.883(42)
0.1355	0.1355	0.1355	0.1346	11,24	2.6	0.760(26)	11,24	2.6	0.738(24)	11,24	1.5	0.877(44)
0.1355	0.1355	0.1355	0.1350	11,24	2.3	0.737(28)	11,24	2.4	0.724(27)	11,24	1.6	0.870(47)
0.1355	0.1355	0.1355	0.1358	11,24	1.8	0.686(30)	11,24	1.8	0.703(29)	11,24	2.0	0.845(57)
0.1355	0.1340	0.1340	0.1355	11,24	5.7	0.818(27)	11,24	2.2	0.839(23)	11,24	1.4	0.923(34)
0.1355	0.1343	0.1343	0.1355	11,24	5.3	0.794(27)	11,24	2.6	0.815(25)	11,24	1.3	0.907(37)
0.1355	0.1346	0.1346	0.1355	11,24	4.4	0.773(26)	11,24	2.8	0.793(27)	11,24	1.3	0.893(40)
0.1355	0.1350	0.1350	0.1355	11,24	3.1	0.746(27)	11,24	2.7	0.759(26)	11,24	1.4	0.878(43)
0.1355	0.1358	0.1358	0.1355	11,24	1.7	0.692(32)	11,24	1.6	0.669(34)	11,24	2.3	0.825(55)

TABLE XXXIII: Meson masses on $20^3 \times 48$ lattice in $N_f=2$ full QCD.

K_{sea}	$K_{\text{val},1}$	$K_{\text{val},2}$	$[t_{\text{min}}, t_{\text{max}}]$	χ^2/dof	m_{PS}	$[t_{\text{min}}, t_{\text{max}}]$	χ^2/dof	m_V
0.1340	0.1340	0.1340	9,24	0.8	0.61630(55)	9,24	1.1	0.7715(12)
0.1340	0.1343	0.1343	9,24	0.7	0.58799(56)	9,24	1.1	0.7507(12)
0.1340	0.1346	0.1346	9,24	0.7	0.55869(56)	9,24	1.1	0.7297(13)
0.1340	0.1350	0.1350	9,24	0.7	0.51777(58)	9,24	1.1	0.7016(13)
0.1340	0.1355	0.1355	9,24	0.7	0.46262(62)	9,24	1.0	0.6665(15)
0.1340	0.1358	0.1358	9,24	0.8	0.42623(65)	9,24	1.1	0.6454(17)
0.1340	0.1340	0.1343	9,24	0.7	0.60226(55)	9,24	1.1	0.7611(12)
0.1340	0.1340	0.1346	9,24	0.7	0.58800(56)	9,24	1.1	0.7507(12)
0.1340	0.1340	0.1350	9,24	0.7	0.56861(56)	9,24	1.1	0.7368(13)
0.1340	0.1340	0.1355	9,24	0.7	0.54373(57)	9,24	1.1	0.7196(13)
0.1340	0.1340	0.1358	9,24	0.7	0.52839(58)	9,24	1.1	0.7094(14)
0.1343	0.1340	0.1340	9,24	0.5	0.58180(61)	9,24	0.7	0.7312(11)
0.1343	0.1343	0.1343	9,24	0.5	0.55270(62)	9,24	0.7	0.7098(11)
0.1343	0.1346	0.1346	9,24	0.6	0.52248(64)	9,24	0.7	0.6884(12)
0.1343	0.1350	0.1350	9,24	0.7	0.48003(66)	9,24	0.8	0.6600(13)
0.1343	0.1355	0.1355	9,24	0.8	0.42223(70)	9,24	1.0	0.6247(15)
0.1343	0.1358	0.1358	9,24	1.0	0.38363(78)	9,24	1.3	0.6037(18)
0.1343	0.1343	0.1340	9,24	0.5	0.56738(62)	9,24	0.7	0.7205(11)
0.1343	0.1343	0.1346	9,24	0.6	0.53775(63)	9,24	0.7	0.6991(12)
0.1343	0.1343	0.1350	9,24	0.6	0.51735(64)	9,24	0.7	0.6850(12)
0.1343	0.1343	0.1355	9,24	0.6	0.49109(67)	9,24	0.8	0.6676(13)
0.1343	0.1343	0.1358	9,24	0.7	0.47473(68)	9,24	0.9	0.6575(14)
0.1346	0.1340	0.1340	9,24	0.7	0.55142(68)	9,24	2.4	0.6940(14)
0.1346	0.1343	0.1343	9,24	0.7	0.52143(69)	9,24	2.2	0.6723(14)
0.1346	0.1346	0.1346	9,24	0.7	0.49020(71)	9,24	2.0	0.6505(14)
0.1346	0.1350	0.1350	9,24	0.7	0.44611(74)	9,24	1.7	0.6216(15)
0.1346	0.1355	0.1355	9,24	0.7	0.38534(80)	9,24	1.6	0.5859(18)
0.1346	0.1358	0.1358	9,24	0.6	0.34391(86)	9,24	1.8	0.5654(21)
0.1346	0.1346	0.1340	9,24	0.7	0.52145(69)	9,24	2.2	0.6723(14)
0.1346	0.1346	0.1343	9,24	0.7	0.50599(70)	9,24	2.1	0.6614(14)
0.1346	0.1346	0.1350	9,24	0.7	0.46857(72)	9,24	1.8	0.6361(15)
0.1346	0.1346	0.1355	9,24	0.7	0.44043(74)	9,24	1.8	0.6184(16)
0.1346	0.1346	0.1358	9,24	0.7	0.42278(76)	9,24	1.9	0.6083(16)
0.1350	0.1340	0.1340	10,24	0.7	0.51024(48)	10,24	0.6	0.6432(12)
0.1350	0.1343	0.1343	10,24	0.7	0.47915(50)	10,24	0.6	0.6201(13)
0.1350	0.1346	0.1346	10,24	0.7	0.44662(52)	10,24	0.5	0.5968(14)
0.1350	0.1350	0.1350	10,24	0.9	0.40037(55)	10,24	0.4	0.5656(15)
0.1350	0.1355	0.1355	10,24	1.2	0.33560(59)	10,24	0.6	0.5270(21)
0.1350	0.1358	0.1358	10,24	1.6	0.28996(69)	10,24	0.9	0.5046(28)
0.1350	0.1350	0.1340	10,24	0.7	0.45773(52)	10,24	0.5	0.6048(13)
0.1350	0.1350	0.1343	10,24	0.7	0.44109(53)	10,24	0.5	0.5931(14)
0.1350	0.1350	0.1346	10,24	0.8	0.42399(54)	10,24	0.5	0.5813(14)
0.1350	0.1350	0.1355	10,24	1.0	0.36926(57)	10,24	0.5	0.5464(18)
0.1350	0.1350	0.1358	10,24	1.3	0.34947(59)	10,24	0.6	0.5353(20)
0.1355	0.1340	0.1340	10,24	1.1	0.46084(54)	11,24	1.2	0.5798(13)
0.1355	0.1343	0.1343	10,24	1.1	0.42809(56)	11,24	1.3	0.5551(14)
0.1355	0.1346	0.1346	10,24	1.0	0.39354(57)	11,24	1.3	0.5301(16)
0.1355	0.1350	0.1350	10,24	1.0	0.34367(61)	11,24	1.2	0.4964(19)
0.1355	0.1355	0.1355	10,24	1.1	0.27133(72)	11,24	0.9	0.4541(27)
0.1355	0.1358	0.1358	10,24	1.2	0.2160(10)	11,24	0.8	0.4285(41)
0.1355	0.1355	0.1340	10,24	1.1	0.37591(61)	11,24	1.3	0.5178(18)
0.1355	0.1355	0.1343	10,24	1.1	0.35701(62)	11,24	1.3	0.5052(19)
0.1355	0.1355	0.1346	10,24	1.0	0.33730(63)	11,24	1.2	0.4924(20)
0.1355	0.1355	0.1350	10,24	1.0	0.30947(66)	11,24	1.1	0.4754(22)
0.1355	0.1355	0.1358	10,24	1.2	0.24554(81)	11,24	0.8	0.4413(33)

TABLE XXXIV: Baryon masses on $20^3 \times 48$ lattice in $N_f=2$ full QCD.

K_{sea}	$K_{\text{val},1}$	$K_{\text{val},2}$	$K_{\text{val},3}$	$[t_{\text{min}}, t_{\text{max}}]$	χ^2/dof	m_{Σ}	$[t_{\text{min}}, t_{\text{max}}]$	χ^2/dof	m_{Λ}	$[t_{\text{min}}, t_{\text{max}}]$	χ^2/dof	m_{dec}
0.1340	0.1340	0.1340	0.1340	10,24	1.1	1.1566(26)	—	—	—	10,24	1.4	1.2492(36)
0.1340	0.1343	0.1343	0.1343	10,24	1.1	1.1202(26)	—	—	—	10,24	1.5	1.2175(37)
0.1340	0.1346	0.1346	0.1346	10,24	1.1	1.0831(26)	—	—	—	10,24	1.6	1.1856(40)
0.1340	0.1350	0.1350	0.1350	10,24	1.1	1.0325(27)	—	—	—	10,24	1.7	1.1428(45)
0.1340	0.1355	0.1355	0.1355	10,24	1.1	0.9666(28)	—	—	—	10,24	1.7	1.0890(54)
0.1340	0.1358	0.1358	0.1358	10,24	0.9	0.9255(31)	—	—	—	10,24	1.6	1.0561(63)
0.1340	0.1340	0.1340	0.1343	10,24	1.1	1.1436(26)	10,24	1.1	1.1453(26)	10,24	1.3	1.2360(36)
0.1340	0.1340	0.1340	0.1346	10,24	1.1	1.1305(26)	10,24	1.1	1.1340(26)	10,24	1.4	1.2253(37)
0.1340	0.1340	0.1340	0.1350	10,24	1.1	1.1127(26)	10,24	1.1	1.1190(27)	10,24	1.5	1.2110(38)
0.1340	0.1340	0.1340	0.1355	10,24	1.0	1.0898(27)	10,24	1.2	1.1001(27)	10,24	1.6	1.1931(40)
0.1340	0.1340	0.1340	0.1358	10,24	1.0	1.0757(27)	10,24	1.3	1.0889(27)	10,24	1.8	1.1824(42)
0.1340	0.1343	0.1343	0.1340	10,24	1.1	1.1332(26)	10,24	1.1	1.1314(26)	10,24	1.4	1.2254(37)
0.1340	0.1346	0.1346	0.1340	10,24	1.1	1.1097(26)	10,24	1.1	1.1058(26)	10,24	1.5	1.2041(38)

TABLE XXXV: Meson masses on $12^3 \times 48$ lattice in quenched QCD.

$K_{\text{val},1}$	$K_{\text{val},2}$	$[t_{\text{min}}, t_{\text{max}}]$	χ^2/dof	m_{PS}	$[t_{\text{min}}, t_{\text{max}}]$	χ^2/dof	m_V
0.13260	0.13260	10,24	0.6	0.4906(17)	10,24	1.2	0.6079(43)
0.13290	0.13290	10,24	0.6	0.4616(18)	10,24	1.3	0.5875(48)
0.13331	0.13331	10,24	0.7	0.4201(20)	10,24	1.3	0.5606(58)
0.13384	0.13384	10,24	0.9	0.3620(24)	10,24	1.2	0.5285(79)
0.13432	0.13432	10,24	1.0	0.3018(30)	10,24	0.9	0.502(12)
0.13465	0.13465	10,24	0.9	0.2519(38)	10,24	0.4	0.484(20)
0.13260	0.13290	10,24	0.6	0.4763(18)	10,24	1.3	0.5977(45)
0.13260	0.13331	10,24	0.7	0.4562(19)	10,24	1.3	0.5840(49)
0.13260	0.13384	10,24	0.8	0.4296(20)	10,24	1.2	0.5669(56)
0.13260	0.13432	10,24	0.9	0.4048(23)	10,24	1.0	0.5518(65)
0.13260	0.13465	10,24	1.1	0.3870(26)	10,24	0.8	0.5396(79)
0.13290	0.13331	10,24	0.7	0.4412(19)	10,24	1.3	0.5740(52)
0.13290	0.13384	10,24	0.8	0.4139(21)	10,24	1.2	0.5571(60)
0.13290	0.13432	10,24	0.9	0.3884(24)	10,24	1.1	0.5422(70)
0.13290	0.13465	10,24	1.0	0.3700(27)	10,24	0.8	0.5302(85)
0.13331	0.13384	10,24	0.8	0.3919(22)	10,24	1.3	0.5442(67)
0.13331	0.13432	10,24	1.0	0.3651(25)	10,24	1.1	0.5297(80)
0.13331	0.13465	10,24	1.0	0.3458(28)	10,24	0.8	0.5180(96)
0.13384	0.13432	10,24	1.0	0.3332(27)	10,24	1.0	0.5147(97)
0.13384	0.13465	10,24	1.0	0.3121(30)	10,24	0.7	0.504(12)
0.13432	0.13465	10,24	0.9	0.2782(33)	10,24	0.6	0.492(15)

TABLE XXXVI: Baryon masses on $12^3 \times 48$ lattice in quenched QCD.

$K_{\text{val},1}$	$K_{\text{val},2}$	$K_{\text{val},3}$	$[t_{\text{min}}, t_{\text{max}}]$	χ^2/dof	m_Σ	$[t_{\text{min}}, t_{\text{max}}]$	χ^2/dof	m_Λ	$[t_{\text{min}}, t_{\text{max}}]$	χ^2/dof	m_{dec}
0.13260	0.13260	0.13260	11,24	0.7	0.9394(76)	–	–	–	11,24	0.7	1.014(11)
0.13260	0.13260	0.13290	11,24	0.7	0.9264(79)	11,24	0.7	0.9294(78)	11,24	0.7	1.003(11)
0.13260	0.13260	0.13331	11,24	0.8	0.9083(86)	11,24	0.8	0.9159(83)	11,24	0.7	0.989(12)
0.13260	0.13260	0.13384	11,24	0.9	0.8841(98)	11,24	0.9	0.8983(94)	11,24	0.7	0.970(13)
0.13260	0.13260	0.13432	11,24	1.1	0.861(12)	11,24	0.9	0.882(11)	11,24	0.8	0.952(14)
0.13260	0.13260	0.13465	11,24	1.4	0.841(14)	11,24	0.8	0.869(13)	11,24	1.0	0.937(16)
0.13290	0.13290	0.13260	11,24	0.8	0.9180(81)	11,24	0.7	0.9148(82)	11,24	0.7	0.993(12)
0.13290	0.13290	0.13290	11,24	0.8	0.9048(85)	–	–	–	11,24	0.7	0.984(12)
0.13290	0.13290	0.13331	11,24	0.9	0.8865(92)	11,24	0.9	0.8911(90)	11,24	0.7	0.969(13)
0.13290	0.13290	0.13384	11,24	1.0	0.862(10)	11,24	0.9	0.873(10)	11,24	0.7	0.950(14)
0.13290	0.13290	0.13432	11,24	1.2	0.838(12)	11,24	0.9	0.857(12)	11,24	0.7	0.931(15)
0.13290	0.13290	0.13465	11,24	1.5	0.818(15)	11,24	0.8	0.843(14)	11,24	0.9	0.916(18)
0.13331	0.13331	0.13260	11,24	0.9	0.8884(92)	11,24	0.9	0.8804(95)	11,24	0.7	0.965(13)
0.13331	0.13331	0.13290	11,24	0.9	0.8750(96)	11,24	0.9	0.8703(98)	11,24	0.6	0.955(13)
0.13331	0.13331	0.13331	11,24	1.0	0.856(10)	–	–	–	11,24	0.6	0.942(14)
0.13331	0.13331	0.13384	11,24	1.1	0.831(12)	11,24	1.0	0.838(12)	11,24	0.6	0.922(15)
0.13331	0.13331	0.13432	11,24	1.2	0.806(14)	11,24	1.0	0.821(14)	11,24	0.7	0.903(17)
0.13331	0.13331	0.13465	11,24	1.6	0.784(17)	11,24	0.8	0.806(16)	11,24	0.8	0.887(20)
0.13384	0.13384	0.13260	11,24	1.0	0.849(12)	11,24	1.1	0.834(13)	11,24	0.6	0.927(15)
0.13384	0.13384	0.13290	11,24	1.0	0.835(12)	11,24	1.1	0.824(13)	11,24	0.6	0.917(16)
0.13384	0.13384	0.13331	11,24	1.0	0.816(13)	11,24	1.1	0.809(13)	11,24	0.6	0.903(16)
0.13384	0.13384	0.13384	11,24	1.0	0.789(14)	–	–	–	11,24	0.7	0.887(18)
0.13384	0.13384	0.13432	11,24	1.1	0.762(17)	11,24	0.9	0.771(17)	11,24	0.7	0.866(21)
0.13384	0.13384	0.13465	11,24	1.4	0.736(21)	11,24	0.8	0.755(21)	11,24	0.8	0.849(25)
0.13432	0.13432	0.13260	11,24	0.9	0.810(16)	11,24	1.4	0.788(19)	11,24	0.6	0.890(20)
0.13432	0.13432	0.13290	11,24	0.9	0.795(16)	11,24	1.3	0.777(19)	11,24	0.6	0.880(21)
0.13432	0.13432	0.13331	11,24	0.9	0.775(18)	11,24	1.2	0.761(19)	11,24	0.6	0.866(22)
0.13432	0.13432	0.13384	11,24	0.9	0.747(20)	11,24	1.0	0.738(21)	11,24	0.7	0.848(23)
0.13432	0.13432	0.13432	11,24	0.8	0.716(25)	–	–	–	11,24	0.8	0.832(27)
0.13432	0.13432	0.13465	11,24	0.9	0.682(33)	11,24	0.7	0.695(32)	11,24	0.8	0.810(31)
0.13465	0.13465	0.13260	11,24	1.1	0.774(22)	11,24	1.0	0.746(36)	11,24	0.5	0.858(28)
0.13465	0.13465	0.13290	11,24	1.1	0.758(23)	11,24	1.1	0.733(35)	11,24	0.6	0.848(28)
0.13465	0.13465	0.13331	11,24	1.0	0.735(25)	11,24	1.1	0.713(34)	11,24	0.6	0.833(29)
0.13465	0.13465	0.13384	11,24	0.9	0.703(30)	11,24	1.0	0.683(37)	11,24	0.7	0.813(31)
0.13465	0.13465	0.13432	11,24	0.7	0.665(40)	11,24	0.8	0.653(44)	11,24	0.8	0.794(34)
0.13465	0.13465	0.13465	11,24	0.6	0.633(55)	–	–	–	11,24	1.0	0.784(38)

TABLE XXXVII: Meson masses on $16^3 \times 48$ lattice in quenched QCD.

$K_{\text{val},1}$	$K_{\text{val},2}$	$[t_{\text{min}}, t_{\text{max}}]$	χ^2/dof	m_{PS}	$[t_{\text{min}}, t_{\text{max}}]$	χ^2/dof	m_V
0.13260	0.13260	[10,24]	0.6	0.48454(94)	[10,24]	1.3	0.6024(20)
0.13290	0.13290	[10,24]	0.6	0.45480(97)	[10,24]	1.3	0.5805(23)
0.13331	0.13331	[10,24]	0.6	0.4119(10)	[10,24]	1.2	0.5506(27)
0.13384	0.13384	[10,24]	0.6	0.3511(12)	[10,24]	1.1	0.5121(36)
0.13432	0.13432	[10,24]	0.9	0.2871(15)	[10,24]	0.9	0.4778(55)
0.13465	0.13465	[10,24]	1.3	0.2332(23)	[10,24]	0.6	0.4531(88)
0.13260	0.13290	[10,24]	0.6	0.46982(95)	[10,24]	1.3	0.5915(21)
0.13260	0.13331	[10,24]	0.5	0.44919(99)	[10,24]	1.3	0.5766(23)
0.13260	0.13384	[10,24]	0.5	0.4216(10)	[10,24]	1.2	0.5574(27)
0.13260	0.13432	[10,24]	0.6	0.3956(12)	[10,24]	1.2	0.5405(32)
0.13260	0.13465	[10,24]	0.6	0.3775(14)	[10,24]	1.0	0.5291(38)
0.13290	0.13331	[10,24]	0.5	0.4337(10)	[10,24]	1.3	0.5656(25)
0.13290	0.13384	[10,24]	0.5	0.4054(11)	[10,24]	1.2	0.5464(28)
0.13290	0.13432	[10,24]	0.6	0.3786(12)	[10,24]	1.1	0.5294(34)
0.13290	0.13465	[10,24]	0.7	0.3597(14)	[10,24]	1.0	0.5180(40)
0.13331	0.13384	[10,24]	0.6	0.3825(11)	[10,24]	1.1	0.5314(31)
0.13331	0.13432	[10,24]	0.7	0.3543(12)	[10,24]	1.1	0.5143(37)
0.13331	0.13465	[10,24]	0.7	0.3343(14)	[10,24]	1.0	0.5029(45)
0.13384	0.13432	[10,24]	0.7	0.3206(13)	[10,24]	1.0	0.4950(44)
0.13384	0.13465	[10,24]	0.8	0.2986(16)	[10,24]	0.9	0.4835(53)
0.13432	0.13465	[10,24]	0.9	0.2625(19)	[10,24]	0.8	0.4663(68)

TABLE XXXVIII: Baryon masses on $16^3 \times 48$ lattice in quenched QCD.

$K_{\text{val},1}$	$K_{\text{val},2}$	$K_{\text{val},3}$	$[t_{\text{min}}, t_{\text{max}}]$	χ^2/dof	m_{Σ}	$[t_{\text{min}}, t_{\text{max}}]$	χ^2/dof	m_{Λ}	$[t_{\text{min}}, t_{\text{max}}]$	χ^2/dof	m_{dec}
0.13260	0.13260	0.13260	[11,24]	0.9	0.9081(44)	—	—	—	[11,24]	1.7	0.9865(55)
0.13260	0.13260	0.13290	[11,24]	0.9	0.8948(45)	[11,24]	0.9	0.8969(45)	[11,24]	1.7	0.9746(56)
0.13260	0.13260	0.13331	[11,24]	0.9	0.8762(46)	[11,24]	0.9	0.8817(47)	[11,24]	1.7	0.9602(59)
0.13260	0.13260	0.13384	[11,24]	0.8	0.8512(49)	[11,24]	0.9	0.8622(51)	[11,24]	1.7	0.9415(64)
0.13260	0.13260	0.13432	[11,24]	0.7	0.8273(56)	[11,24]	0.9	0.8454(56)	[11,24]	1.8	0.9247(72)
0.13260	0.13260	0.13465	[11,24]	0.6	0.8107(67)	[11,24]	0.8	0.8351(65)	[11,24]	1.6	0.9146(86)
0.13290	0.13290	0.13260	[11,24]	0.9	0.8847(46)	[11,24]	0.9	0.8824(46)	[11,24]	1.7	0.9642(58)
0.13290	0.13290	0.13290	[11,24]	0.9	0.8712(47)	—	—	—	[11,24]	1.7	0.9549(60)
0.13290	0.13290	0.13331	[11,24]	0.9	0.8523(48)	[11,24]	0.9	0.8559(49)	[11,24]	1.7	0.9388(63)
0.13290	0.13290	0.13384	[11,24]	0.8	0.8266(52)	[11,24]	0.9	0.8363(53)	[11,24]	1.7	0.9197(69)
0.13290	0.13290	0.13432	[11,24]	0.7	0.8019(61)	[11,24]	0.9	0.8192(59)	[11,24]	1.6	0.9025(78)
0.13290	0.13290	0.13465	[11,24]	0.6	0.7849(73)	[11,24]	0.8	0.8086(69)	[11,24]	1.5	0.8922(94)
0.13331	0.13331	0.13260	[11,24]	0.9	0.8526(50)	[11,24]	0.9	0.8461(49)	[11,24]	1.7	0.9351(64)
0.13331	0.13331	0.13290	[11,24]	0.9	0.8388(51)	[11,24]	0.9	0.8348(51)	[11,24]	1.7	0.9242(67)
0.13331	0.13331	0.13331	[11,24]	0.9	0.8193(53)	—	—	—	[11,24]	1.6	0.9108(72)
0.13331	0.13331	0.13384	[11,24]	0.8	0.7925(59)	[11,24]	0.9	0.7994(58)	[11,24]	1.6	0.8893(78)
0.13331	0.13331	0.13432	[11,24]	0.7	0.7665(70)	[11,24]	0.9	0.7819(66)	[11,24]	1.4	0.8715(91)
0.13331	0.13331	0.13465	[11,24]	0.7	0.7490(84)	[11,24]	0.8	0.7706(78)	[11,24]	1.3	0.861(11)
0.13384	0.13384	0.13260	[11,24]	0.9	0.8111(58)	[11,24]	0.7	0.7954(60)	[11,24]	1.6	0.8969(78)
0.13384	0.13384	0.13290	[11,24]	0.9	0.7967(60)	[11,24]	0.8	0.7838(62)	[11,24]	1.5	0.8855(82)
0.13384	0.13384	0.13331	[11,24]	0.9	0.7761(64)	[11,24]	0.8	0.7680(66)	[11,24]	1.4	0.8697(88)
0.13384	0.13384	0.13384	[11,24]	0.9	0.7475(74)	—	—	—	[11,24]	1.3	0.852(10)
0.13384	0.13384	0.13432	[11,24]	0.8	0.7195(90)	[11,24]	0.9	0.7294(85)	[11,24]	1.2	0.831(12)
0.13384	0.13384	0.13465	[11,24]	0.8	0.701(11)	[11,24]	0.9	0.717(10)	[11,24]	1.1	0.821(15)
0.13432	0.13432	0.13260	[11,24]	1.0	0.7749(75)	[11,24]	0.7	0.7442(84)	[11,24]	1.3	0.862(11)
0.13432	0.13432	0.13290	[11,24]	1.0	0.7596(79)	[11,24]	0.7	0.7324(88)	[11,24]	1.2	0.851(11)
0.13432	0.13432	0.13331	[11,24]	1.0	0.7376(86)	[11,24]	0.7	0.7161(95)	[11,24]	1.1	0.834(13)
0.13432	0.13432	0.13384	[11,24]	0.9	0.707(10)	[11,24]	0.8	0.695(11)	[11,24]	1.0	0.814(15)
0.13432	0.13432	0.13432	[11,24]	0.9	0.677(13)	—	—	—	[11,24]	1.0	0.800(18)
0.13432	0.13432	0.13465	[11,24]	0.9	0.656(16)	[11,24]	1.0	0.665(16)	[11,24]	1.0	0.786(22)
0.13465	0.13465	0.13260	[11,24]	0.9	0.754(11)	[11,24]	0.8	0.707(12)	[11,24]	1.1	0.844(17)
0.13465	0.13465	0.13290	[11,24]	0.9	0.738(11)	[11,24]	0.8	0.695(12)	[11,24]	1.0	0.832(17)
0.13465	0.13465	0.13331	[11,24]	1.0	0.715(13)	[11,24]	0.8	0.679(13)	[11,24]	1.0	0.815(19)
0.13465	0.13465	0.13384	[11,24]	1.1	0.682(15)	[11,24]	0.9	0.658(15)	[11,24]	0.9	0.795(23)
0.13465	0.13465	0.13432	[11,24]	1.1	0.650(19)	[11,24]	1.0	0.638(18)	[11,24]	0.9	0.778(29)
0.13465	0.13465	0.13465	[11,24]	1.1	0.623(23)	—	—	—	[11,24]	0.9	0.776(40)

TABLE XXXIX: Meson masses on $20^3 \times 48$ lattice in quenched QCD.

$K_{\text{val},1}$	$K_{\text{val},2}$	$[t_{\text{min}}, t_{\text{max}}]$	χ^2/dof	m_{PS}	$[t_{\text{min}}, t_{\text{max}}]$	χ^2/dof	m_V
0.13260	0.13260	[10,24]	0.7	0.48376(66)	[10,24]	1.0	0.6008(16)
0.13290	0.13290	[10,24]	0.6	0.45385(69)	[10,24]	1.0	0.5790(18)
0.13331	0.13331	[10,24]	0.4	0.41066(74)	[10,24]	1.0	0.5492(21)
0.13384	0.13384	[10,24]	0.5	0.34897(96)	[10,24]	1.1	0.5117(29)
0.13432	0.13432	[10,24]	0.6	0.2845(11)	[10,24]	0.9	0.4773(43)
0.13465	0.13465	[10,24]	0.9	0.2296(15)	[10,24]	1.0	0.4566(74)
0.13260	0.13290	[10,24]	0.6	0.46895(67)	[10,24]	1.0	0.5899(17)
0.13260	0.13331	[10,24]	0.5	0.44819(70)	[10,24]	1.0	0.5751(18)
0.13260	0.13384	[10,24]	0.4	0.42006(80)	[10,24]	1.0	0.5564(21)
0.13260	0.13432	[10,24]	0.4	0.39385(85)	[10,24]	1.0	0.5399(25)
0.13260	0.13465	[10,24]	0.4	0.37486(97)	[10,24]	1.3	0.5299(29)
0.13290	0.13331	[10,24]	0.5	0.43262(71)	[10,24]	1.0	0.5641(19)
0.13290	0.13384	[10,24]	0.3	0.40370(84)	[10,24]	1.0	0.5454(22)
0.13290	0.13432	[10,24]	0.4	0.37669(87)	[10,24]	1.1	0.5288(26)
0.13290	0.13465	[10,24]	0.4	0.35697(99)	[10,24]	1.2	0.5188(31)
0.13331	0.13384	[10,24]	0.4	0.38048(90)	[10,24]	1.1	0.5304(24)
0.13331	0.13432	[10,24]	0.3	0.35215(91)	[10,24]	1.0	0.5136(29)
0.13331	0.13465	[10,24]	0.5	0.3312(10)	[10,24]	1.2	0.5036(35)
0.13384	0.13432	[10,24]	0.4	0.31839(97)	[10,24]	1.0	0.4944(35)
0.13384	0.13465	[10,24]	0.6	0.2952(11)	[10,24]	1.1	0.4845(42)
0.13432	0.13465	[10,24]	0.8	0.2582(12)	[10,24]	0.9	0.4669(55)

TABLE XL: Baryon masses on $20^3 \times 48$ lattice in quenched QCD.

$K_{\text{val},1}$	$K_{\text{val},2}$	$K_{\text{val},3}$	$[t_{\text{min}}, t_{\text{max}}]$	χ^2/dof	m_Σ	$[t_{\text{min}}, t_{\text{max}}]$	χ^2/dof	m_Λ	$[t_{\text{min}}, t_{\text{max}}]$	χ^2/dof	m_{dec}
0.13260	0.13260	0.13260	[11,24]	1.1	0.9001(27)	—	—	—	[11,24]	0.7	0.9765(44)
0.13260	0.13260	0.13290	[11,24]	1.1	0.8866(27)	[11,24]	1.1	0.8885(27)	[11,24]	0.7	0.9643(45)
0.13260	0.13260	0.13331	[11,24]	1.1	0.8678(28)	[11,24]	1.1	0.8727(28)	[11,24]	0.7	0.9501(47)
0.13260	0.13260	0.13384	[11,24]	0.9	0.8429(31)	[11,24]	1.1	0.8525(31)	[11,24]	0.8	0.9323(51)
0.13260	0.13260	0.13432	[11,24]	0.8	0.8192(34)	[11,24]	0.9	0.8342(35)	[11,24]	1.0	0.9173(55)
0.13260	0.13260	0.13465	[11,24]	0.6	0.8047(39)	[11,24]	0.8	0.8240(42)	[11,24]	1.3	0.9087(63)
0.13290	0.13290	0.13260	[11,24]	1.1	0.8759(28)	[11,24]	1.1	0.8739(28)	[11,24]	0.7	0.9539(46)
0.13290	0.13290	0.13290	[11,24]	1.1	0.8622(29)	—	—	—	[11,24]	0.7	0.9453(48)
0.13290	0.13290	0.13331	[11,24]	1.0	0.8431(30)	[11,24]	1.1	0.8462(30)	[11,24]	0.7	0.9292(50)
0.13290	0.13290	0.13384	[11,24]	0.9	0.8177(33)	[11,24]	1.1	0.8258(33)	[11,24]	0.7	0.9114(54)
0.13290	0.13290	0.13432	[11,24]	0.7	0.7933(36)	[11,24]	0.9	0.8072(38)	[11,24]	0.9	0.8963(58)
0.13290	0.13290	0.13465	[11,24]	0.6	0.7788(41)	[11,24]	0.8	0.7969(46)	[11,24]	1.1	0.8872(67)
0.13331	0.13331	0.13260	[11,24]	1.1	0.8426(31)	[11,24]	1.0	0.8370(31)	[11,24]	0.7	0.9257(51)
0.13331	0.13331	0.13290	[11,24]	1.1	0.8286(32)	[11,24]	1.0	0.8251(32)	[11,24]	0.7	0.9152(52)
0.13331	0.13331	0.13331	[11,24]	1.0	0.8088(34)	—	—	—	[11,24]	0.7	0.9035(55)
0.13331	0.13331	0.13384	[11,24]	0.9	0.7827(36)	[11,24]	1.0	0.7880(37)	[11,24]	0.7	0.8833(59)
0.13331	0.13331	0.13432	[11,24]	0.7	0.7572(41)	[11,24]	0.8	0.7688(44)	[11,24]	0.8	0.8681(65)
0.13331	0.13331	0.13465	[11,24]	0.6	0.7427(47)	[11,24]	0.7	0.7583(51)	[11,24]	0.9	0.8584(75)
0.13384	0.13384	0.13260	[11,24]	1.1	0.7995(38)	[11,24]	0.9	0.7861(36)	[11,24]	0.7	0.8907(59)
0.13384	0.13384	0.13290	[11,24]	1.0	0.7849(39)	[11,24]	0.9	0.7739(38)	[11,24]	0.7	0.8802(61)
0.13384	0.13384	0.13331	[11,24]	1.0	0.7643(42)	[11,24]	0.9	0.7570(40)	[11,24]	0.7	0.8660(65)
0.13384	0.13384	0.13384	[11,24]	1.0	0.7348(46)	—	—	—	[11,24]	0.6	0.8519(73)
0.13384	0.13384	0.13432	[11,24]	0.7	0.7099(57)	[11,24]	0.9	0.7153(55)	[11,24]	0.7	0.8331(81)
0.13384	0.13384	0.13465	[11,24]	0.7	0.6959(63)	[11,24]	0.8	0.7042(63)	[11,24]	0.7	0.8226(97)
0.13432	0.13432	0.13260	[11,24]	0.8	0.7595(53)	[11,24]	0.6	0.7354(58)	[11,24]	0.8	0.8610(74)
0.13432	0.13432	0.13290	[11,24]	0.7	0.7442(55)	[11,24]	0.6	0.7227(61)	[11,24]	0.8	0.8503(77)
0.13432	0.13432	0.13331	[11,24]	0.7	0.7225(58)	[11,24]	0.7	0.7052(65)	[11,24]	0.7	0.8359(83)
0.13432	0.13432	0.13384	[11,24]	0.7	0.6937(65)	[11,24]	0.7	0.6830(71)	[11,24]	0.7	0.8180(96)
0.13432	0.13432	0.13432	[11,24]	0.8	0.6631(75)	—	—	—	[11,24]	0.7	0.807(12)
0.13432	0.13432	0.13465	[11,24]	0.8	0.6501(82)	[11,24]	0.7	0.6521(84)	[11,24]	0.8	0.790(14)
0.13465	0.13465	0.13260	[11,24]	0.5	0.7368(71)	[11,24]	0.5	0.7105(78)	[11,24]	0.8	0.841(10)
0.13465	0.13465	0.13290	[11,24]	0.5	0.7214(73)	[11,24]	0.5	0.6987(82)	[11,24]	0.7	0.830(11)
0.13465	0.13465	0.13331	[11,24]	0.5	0.6997(77)	[11,24]	0.5	0.6822(88)	[11,24]	0.7	0.815(12)
0.13465	0.13465	0.13384	[11,24]	0.4	0.6710(87)	[11,24]	0.5	0.6605(99)	[11,24]	0.8	0.797(14)
0.13465	0.13465	0.13432	[11,24]	0.6	0.642(10)	[11,24]	0.6	0.638(11)	[11,24]	0.9	0.780(18)
0.13465	0.13465	0.13465	[11,24]	0.5	0.627(14)	—	—	—	[11,24]	1.1	0.775(23)

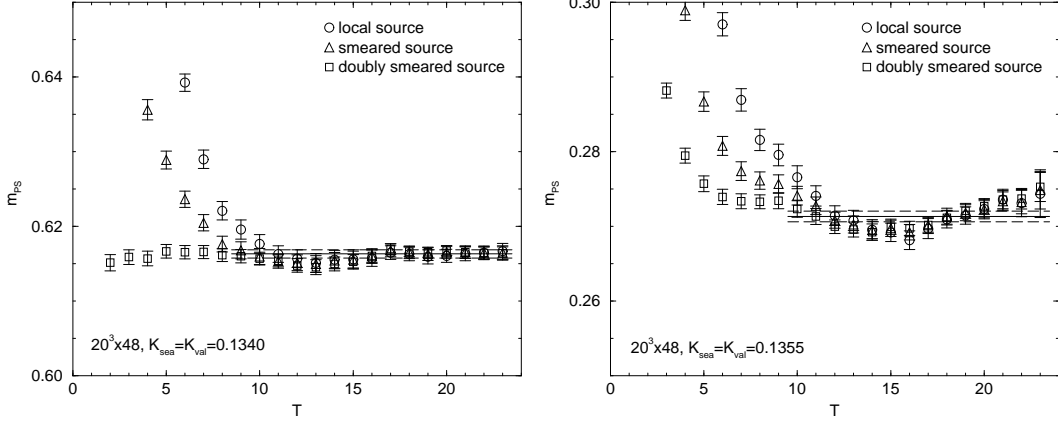


FIG. 1: Effective mass of PS meson at $K_{\text{sea}} = K_{\text{val}} = 0.1340$ (left figure) and 0.1355 (right figure) on $20^3 \times 48$ lattice in full QCD. We use the local sink operator for all data.

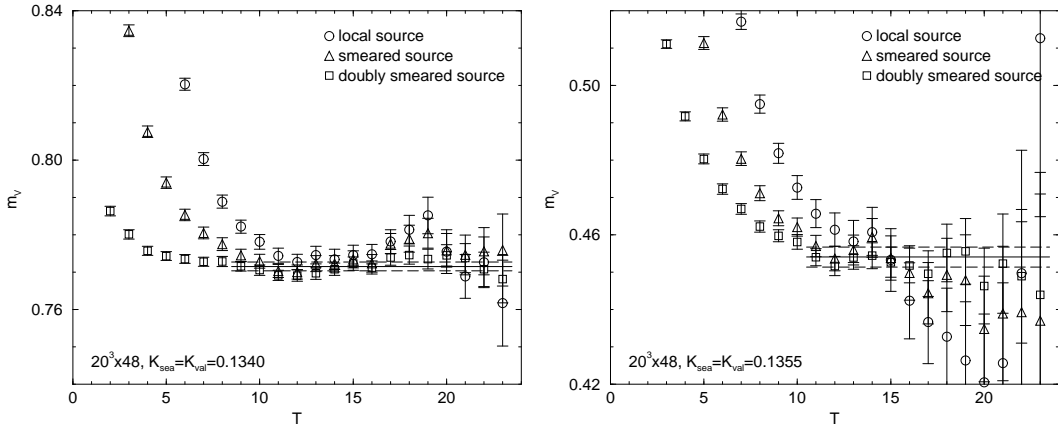


FIG. 2: Effective mass of vector meson at $K_{\text{sea}} = K_{\text{val}} = 0.1340$ (left figure) and 0.1355 (right figure) on $20^3 \times 48$ lattice in full QCD. We use the local sink operator for all data.

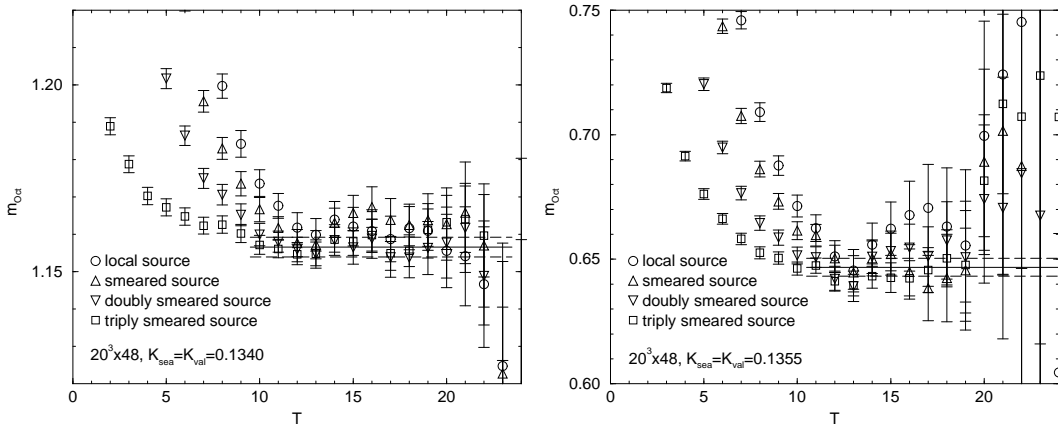


FIG. 3: Effective mass of octet baryon at $K_{\text{sea}} = K_{\text{val}} = 0.1340$ (left figure) and 0.1355 (right figure) on $20^3 \times 48$ lattice in full QCD. We use the local sink operator for all data.

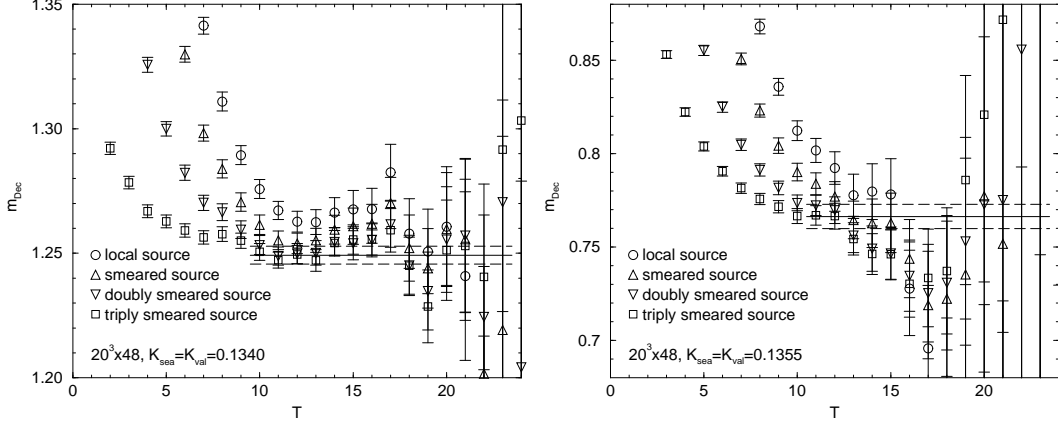


FIG. 4: Effective mass of decuplet baryon at $K_{\text{sea}} = K_{\text{val}} = 0.1340$ (left figure) and 0.1355 (right figure) on $20^3 \times 48$ lattice in full QCD. We use the local sink operator for all data.

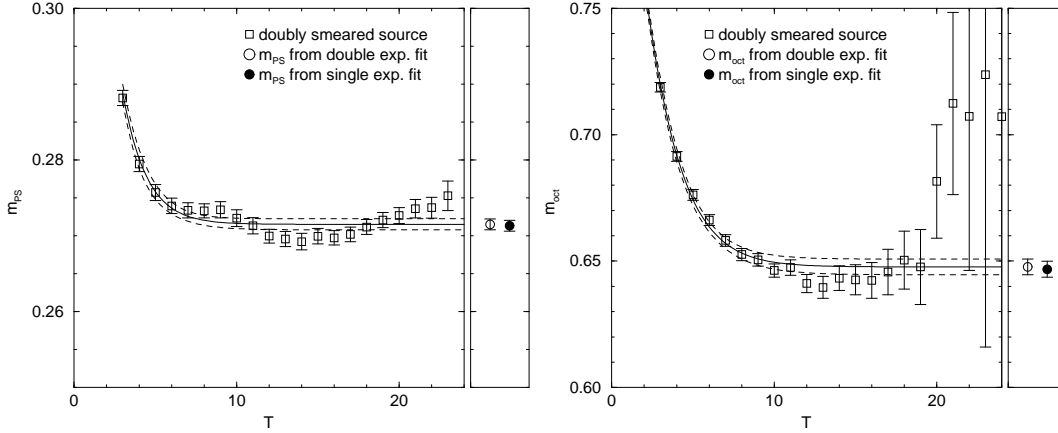


FIG. 5: Double exponential fits to PS meson (left figure) and octet baryon masses (right figure) at $K_{\text{sea}} = 0.1355$. Right panel in each figure shows fitted masses determined from double exponential (open symbol) and single exponential fit (filled symbol). The local sink operator is used for all data.

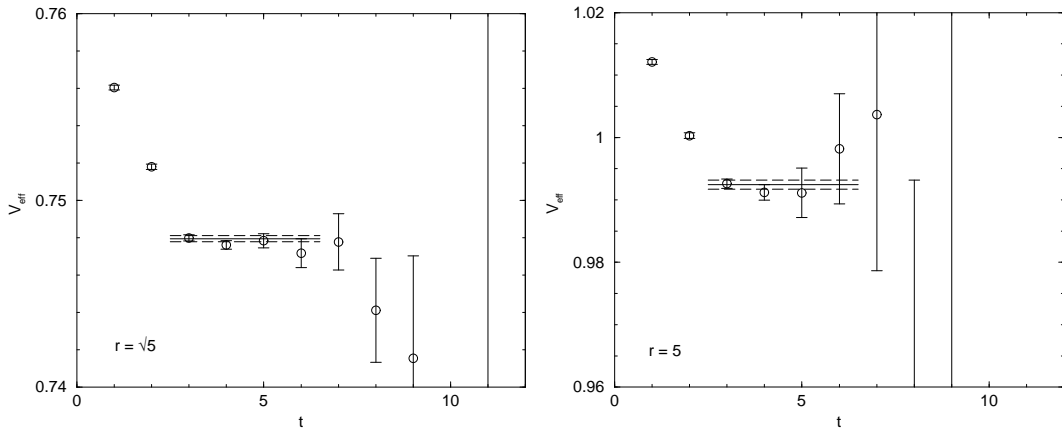


FIG. 6: Effective potential energies $V_{\text{eff}}(r, t)$ as a function of temporal separation t at $K_{\text{sea}} = 0.1350$ on $20^3 \times 48$ lattice.

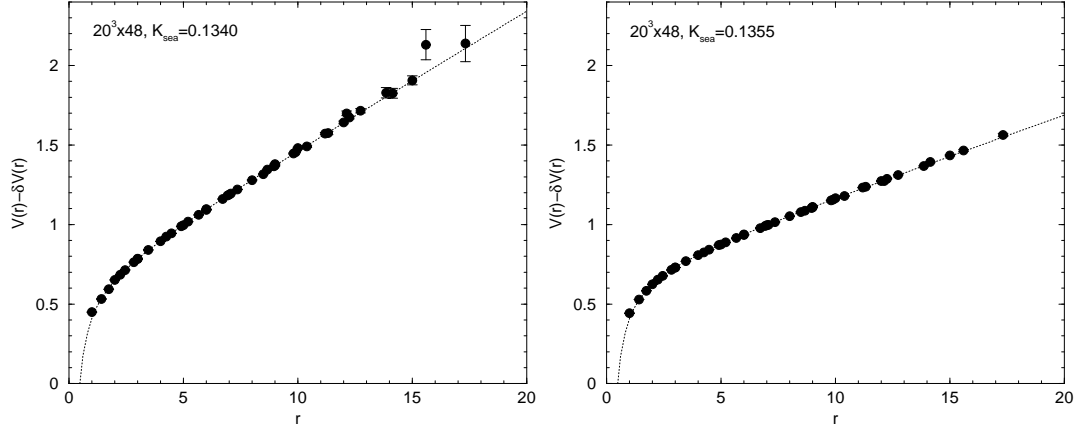


FIG. 7: Static quark potential on $20^3 \times 48$ lattice. Left and right figures show data at $K_{\text{sea}} = 0.1340$ and 0.1355 , respectively.

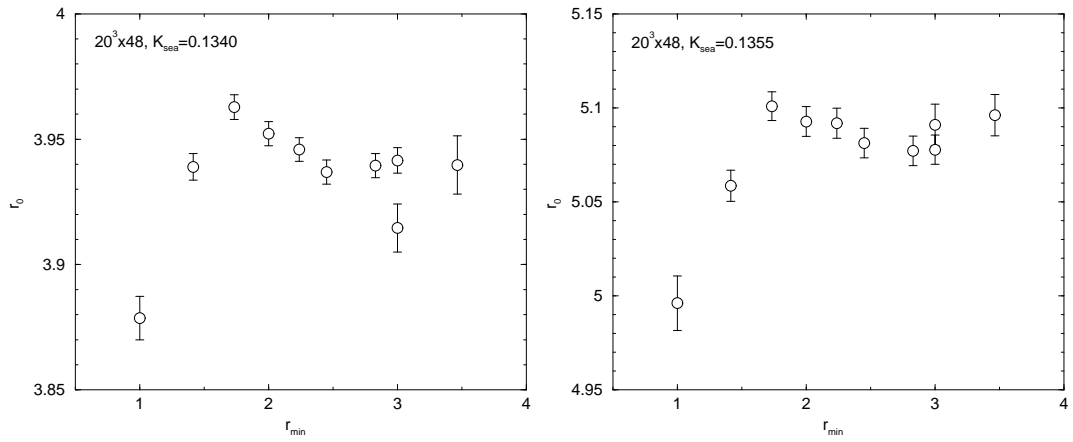


FIG. 8: Sommer scale on $20^3 \times 48$ lattice as a function of r_{min} . Left and right figures show data at $K_{\text{sea}} = 0.1340$ and 0.1355 .

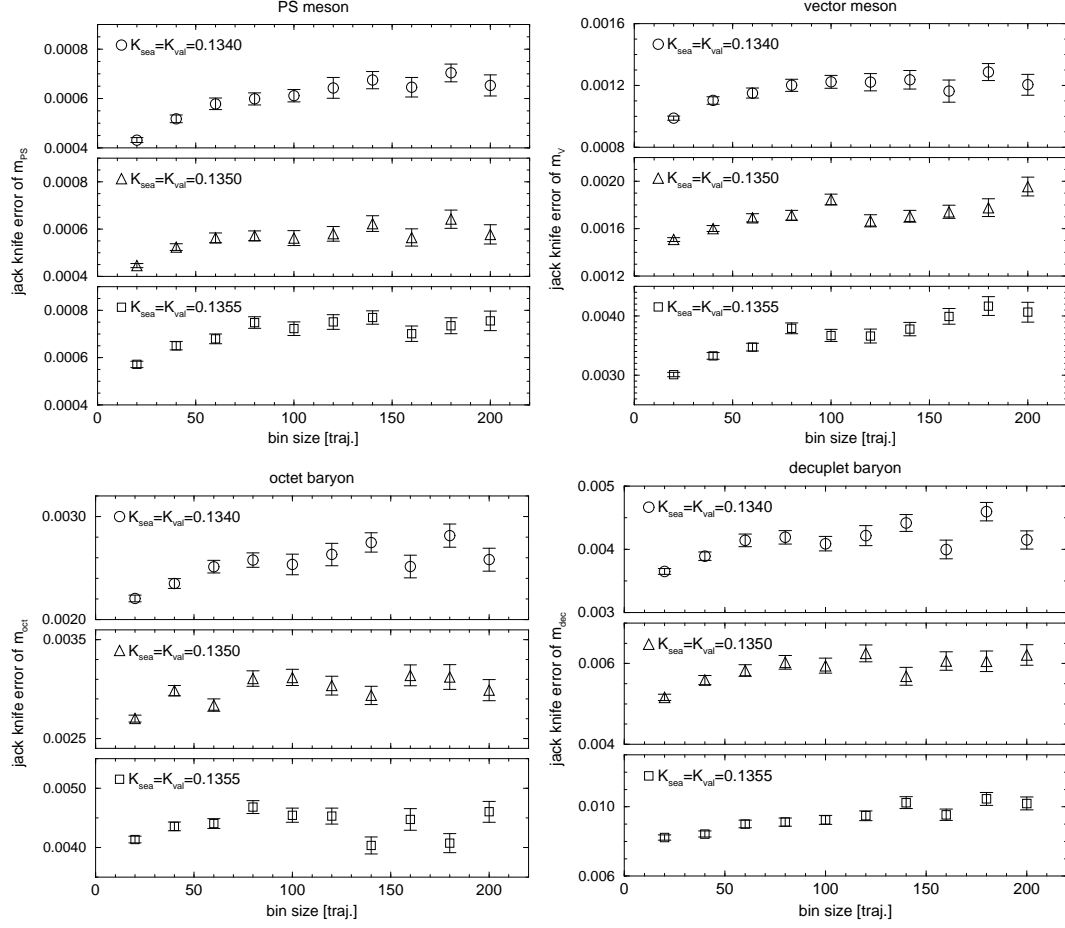


FIG. 9: Bin size dependence of jack-knife error of hadron masses on $20^3 \times 48$ lattice in full QCD.

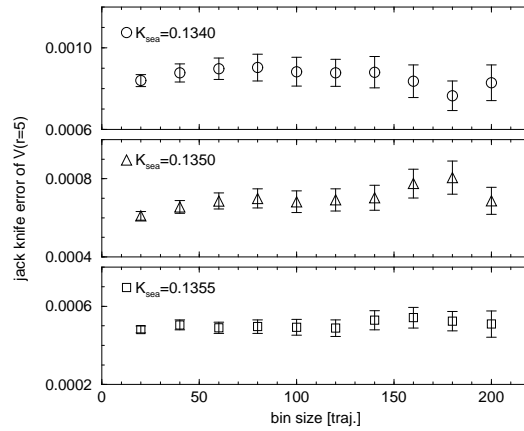


FIG. 10: Bin size dependence of jack-knife error of static potential at $r = 5$ on $20^3 \times 48$ lattice in full QCD.

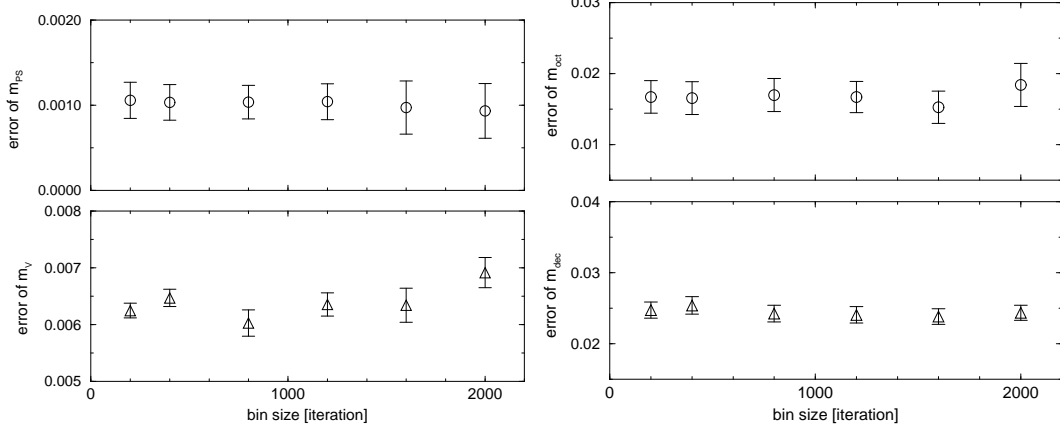


FIG. 11: Bin size dependence of jack-knife error of meson (left figures) and baryon masses (right figures) with $K_{\text{val}} = 0.13432$, which corresponds to $m_{\text{PS, val}}/m_{\text{V, val}} \simeq 0.6$, on $20^3 \times 48$ lattice in quenched QCD.

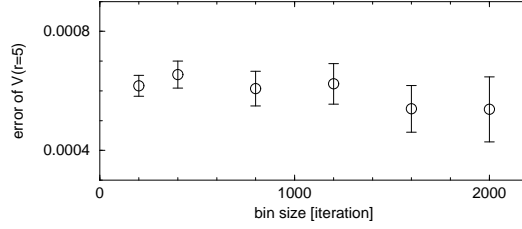


FIG. 12: Bin size dependence of jack-knife error of static potential at $r=5$ on $20^3 \times 48$ lattice in quenched QCD.

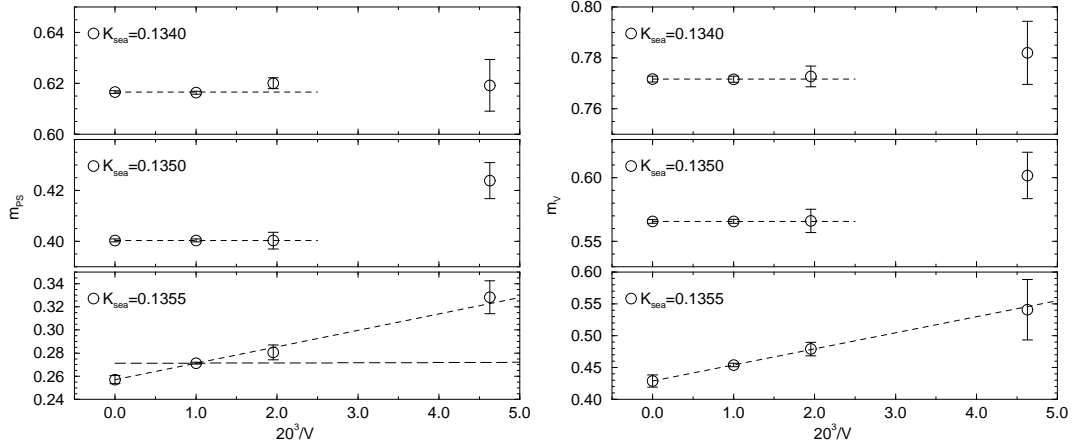


FIG. 13: Diagonal data of PS (left figure) and vector meson masses (right figure) as a function of $20^3/V$. Meson masses in the infinite volume limit at $K_{\text{sea}}=0.1340$ and 0.1350 are determined by the constant fit to data on two larger volumes, while we assume the linear dependence Eq. (27) at $K_{\text{sea}}=0.1355$. We also plot the prediction from the analytic formula[38] for the PS meson mass at the lightest sea quark mass, by long dashed line.

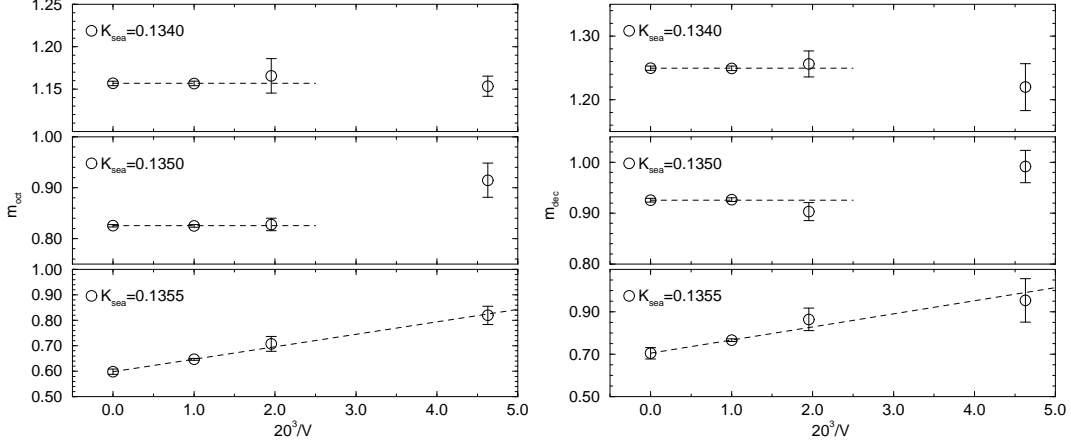


FIG. 14: Diagonal data of octet (left figure) and decuplet baryon masses (right figure) as a function of $20^3/V$.

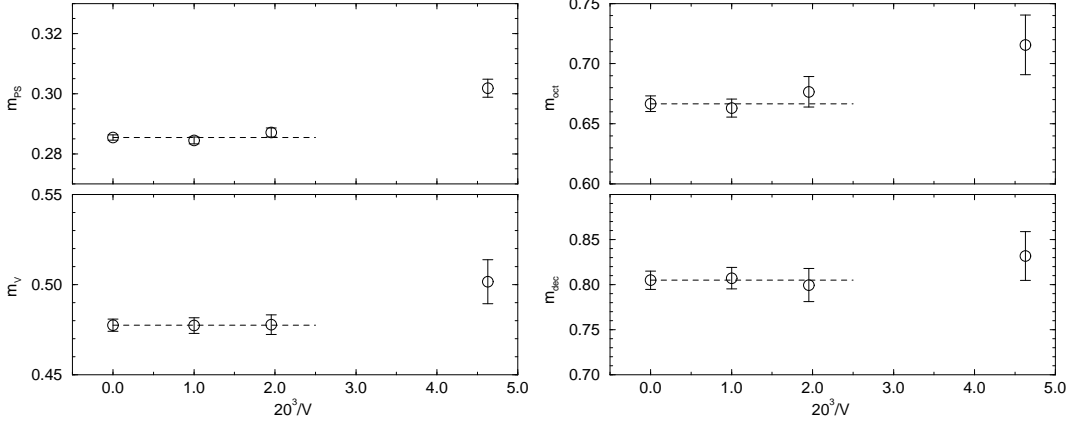


FIG. 15: Volume size dependence of meson (left figure) and baryon masses (right figure) at $K_{\text{val}} = 0.13432$ in quenched simulations.

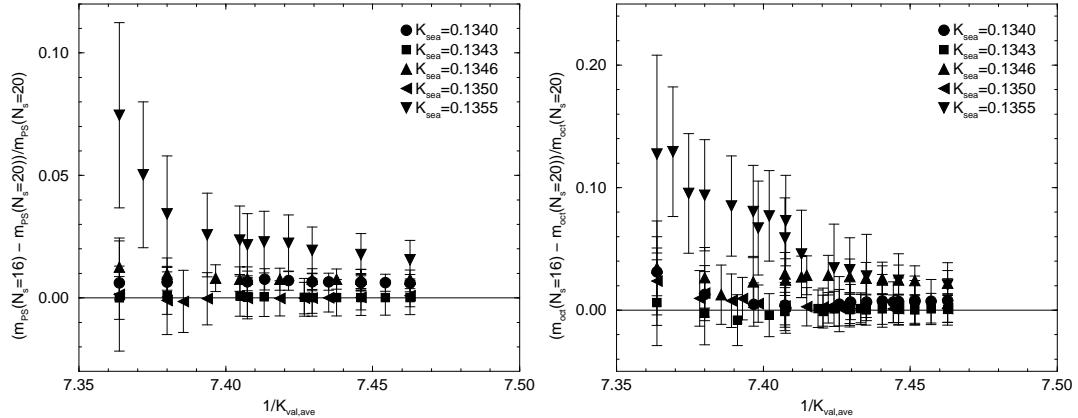


FIG. 16: Valence quark mass dependence of relative difference between hadron masses measured on 16^3 and 20^3 lattices. Left and right figure show data for the PS meson and the octet baryon, respectively. We define $K_{\text{val,ave}}$ by $1/K_{\text{val,ave}} = (1/K_{\text{val},1} + 1/K_{\text{val},2})/2$ for meson masses $m(K_{\text{sea}}; K_{\text{val},1}, K_{\text{val},2})$ and $1/K_{\text{val,ave}} = (1/K_{\text{val},1} + 1/K_{\text{val},2} + 1/K_{\text{val},3})/3$ for baryon masses $m(K_{\text{sea}}; K_{\text{val},1}, K_{\text{val},2}, K_{\text{val},3})$.

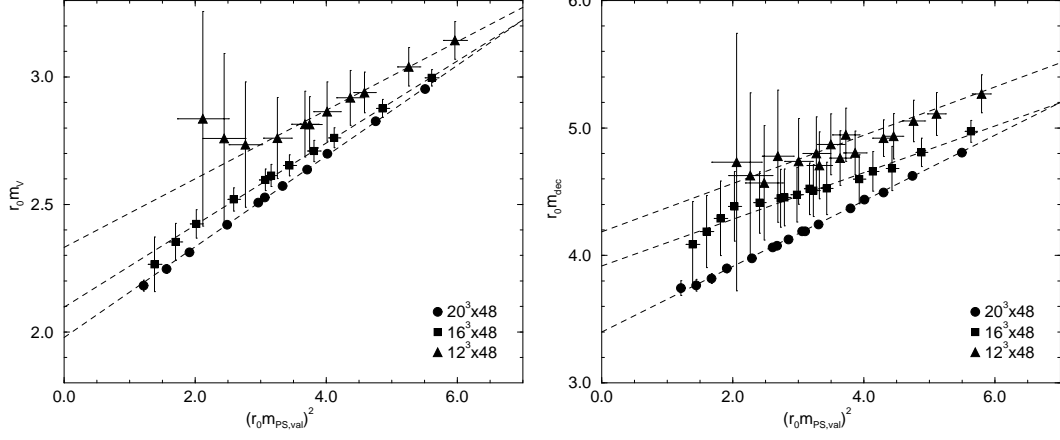


FIG. 17: Vector meson (left figure) and decuplet baryon masses (right figure) at $K_{\text{sea}}=0.1355$ on three spatial volumes as a function of PS meson mass squared. Linear fit curve to each data set is shown as a guide for eyes.

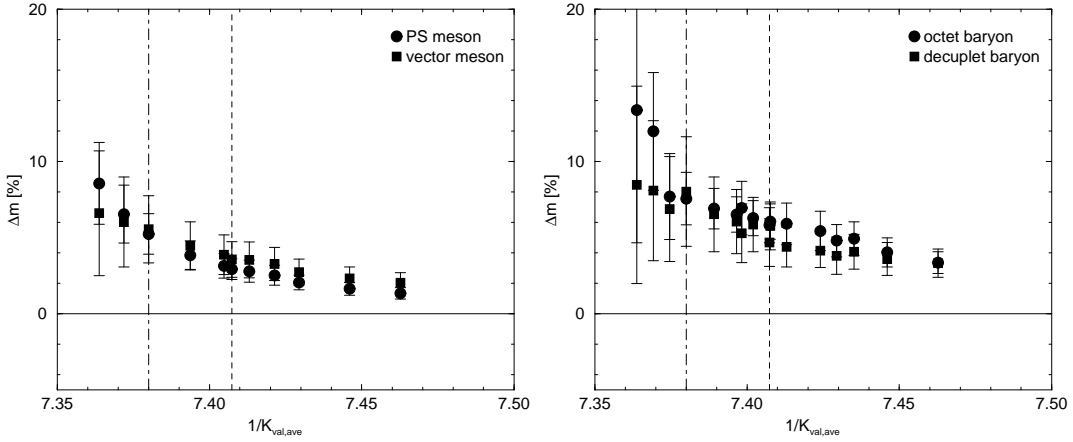


FIG. 18: Relative size of FSE for meson (left figure) and baryon masses (right figure) at $K_{\text{sea}}=0.1355$ on $20^3 \times 48$. Dot-dashed and dashed lines show the location where $K_{\text{val,ave}}=K_{\text{sea}}$ and 0.1350, respectively. The latter roughly corresponds to the strange quark mass.

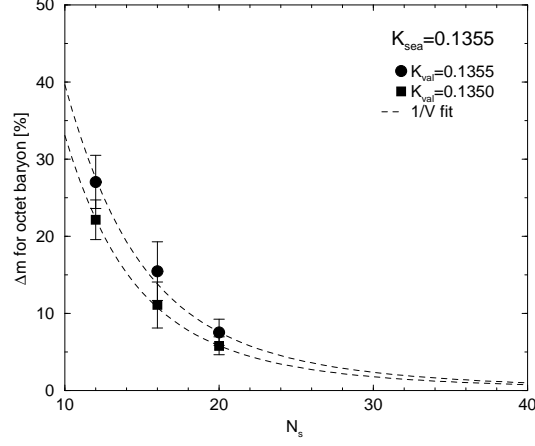


FIG. 19: Magnitude of FSE on octet baryon mass at $K_{\text{sea}}=0.1355$ as a function of spatial linear extent in lattice units. Circles are results for diagonal data, while squares represent those at $K_{\text{val}}=0.1350$.

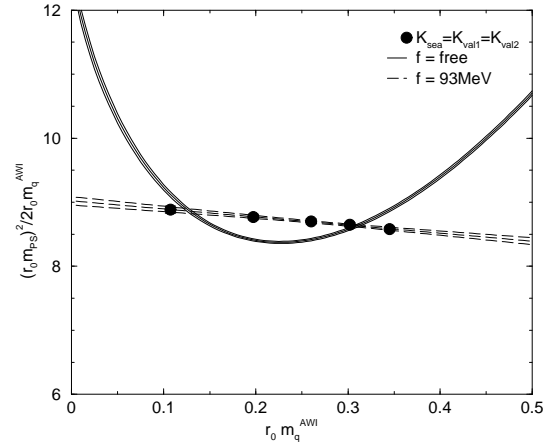


FIG. 20: Test of logarithmic singularity in quark mass dependence of PS meson mass. We use the quark mass defined through the axial vector Ward identity in this plot. Solid and dashed lines are fit curves of Eq. (29) assuming f to be a free parameter or fixed to the experimental value.

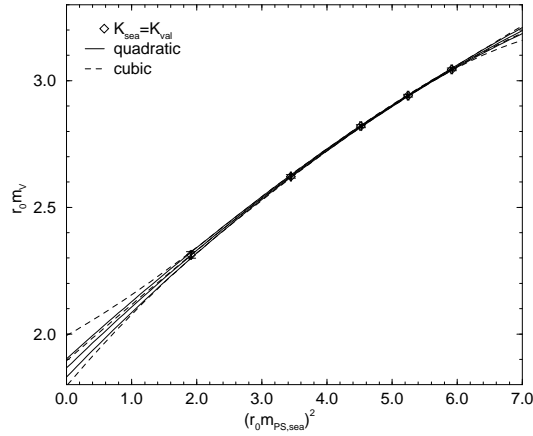


FIG. 21: Comparison of quadratic and cubic diagonal fits in method-A.

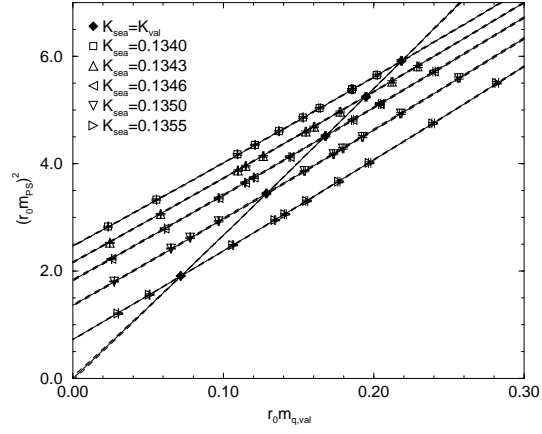


FIG. 22: Combined chiral extrapolation of PS meson masses in terms of VWI quark mass.

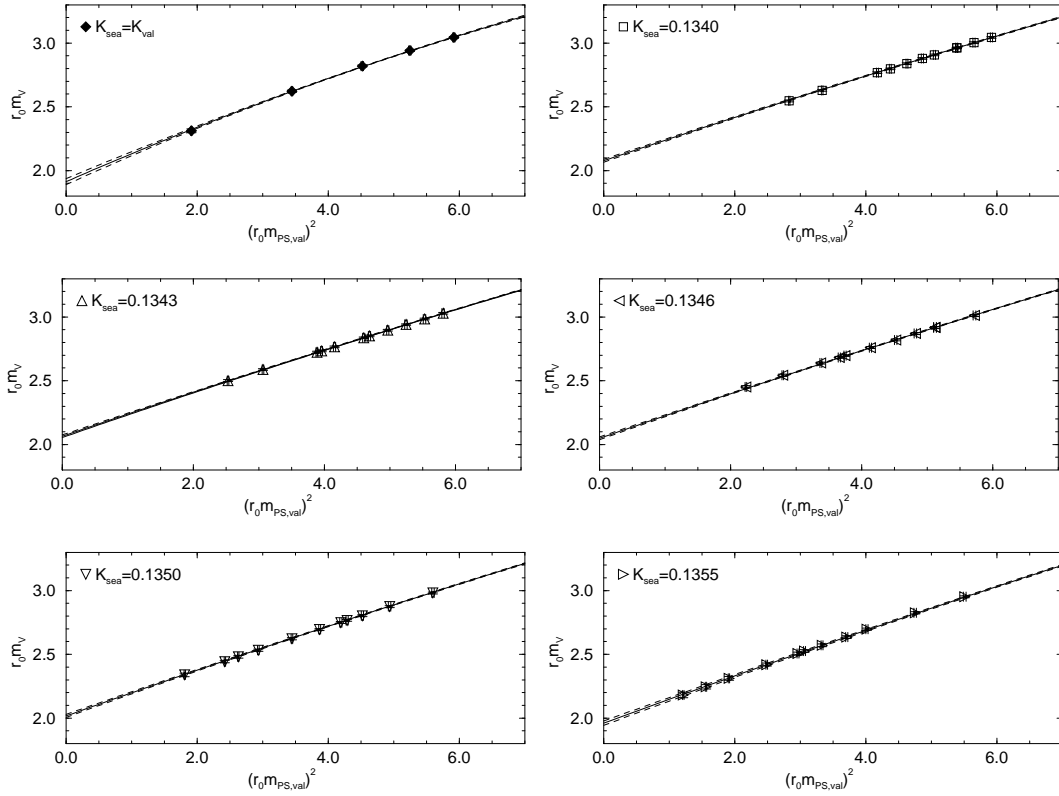


FIG. 23: Combined chiral extrapolation of vector meson masses.

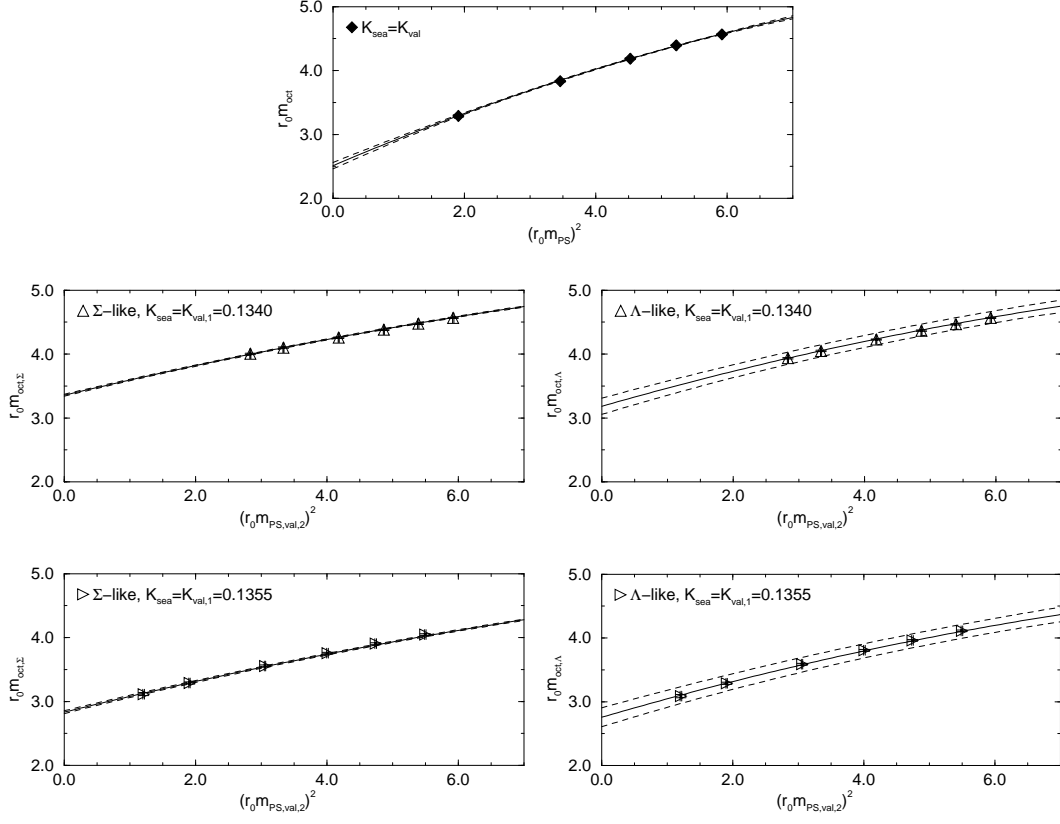


FIG. 24: Combined chiral extrapolation of octet baryon masses. Top figure shows extrapolation of diagonal data. Middle and bottom figures are data at $K_{\text{sea}} = K_{\text{val},1} = 0.1340$ and 0.1355 for Σ -like (left panels) and Λ -like baryons (right panels).

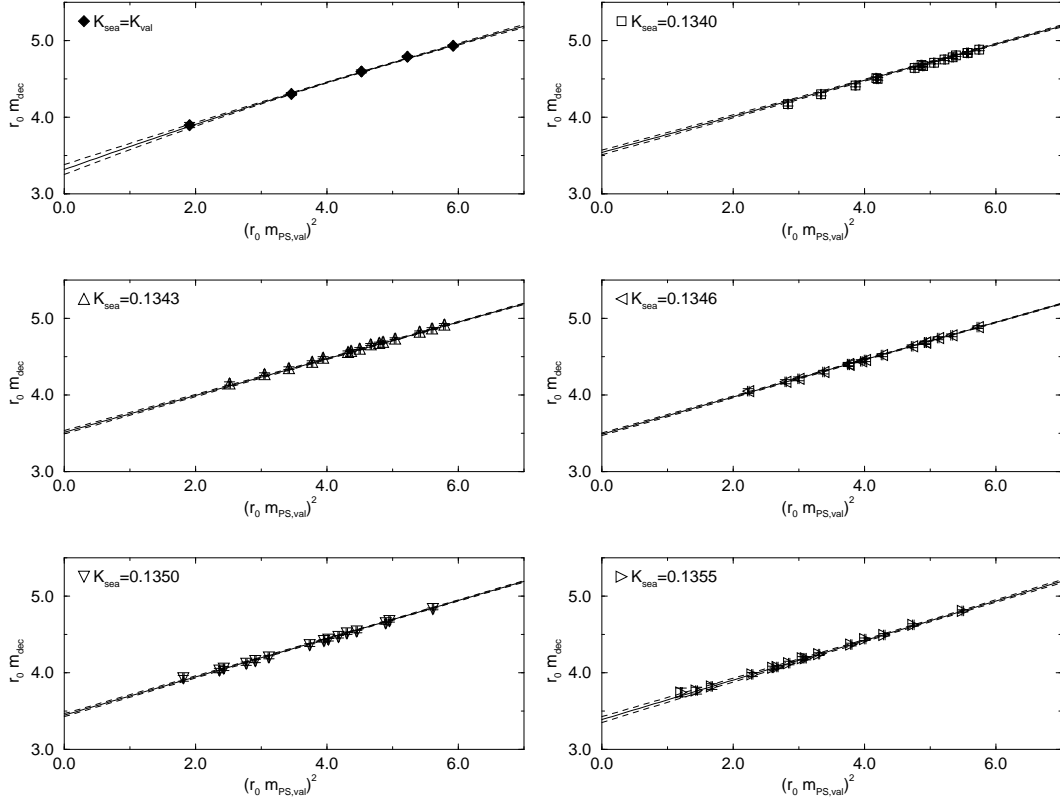


FIG. 25: Combined chiral extrapolation of decuplet baryon masses.

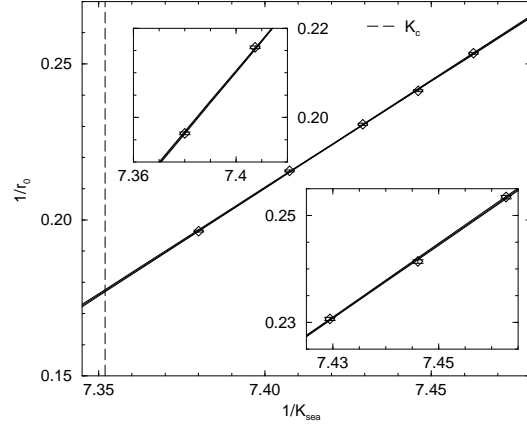


FIG. 26: Chiral extrapolation of r_0 . The vertical line shows where $K_{\text{sea}} = K_c$.

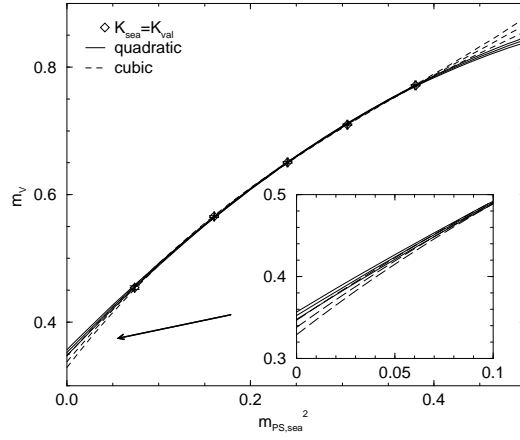


FIG. 27: Comparison of quadratic and cubic diagonal fits in method-B.

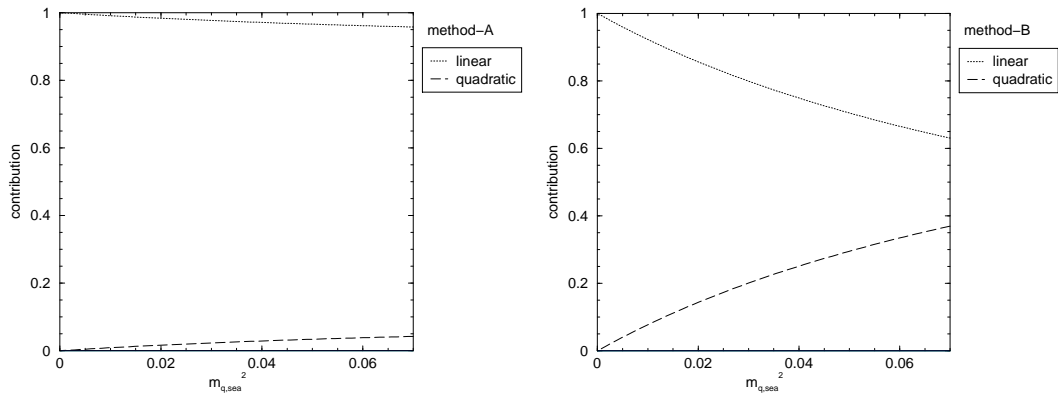


FIG. 28: Relative magnitude of contribution of linear and quadratic terms in quadratic diagonal fit of PS meson masses.

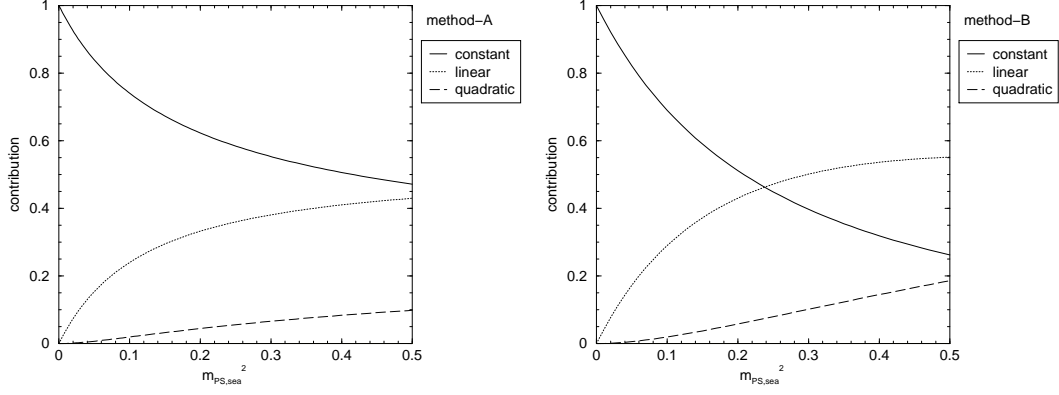


FIG. 29: Relative magnitude of contribution of constant, linear and quadratic terms in quadratic diagonal fit of vector meson masses.

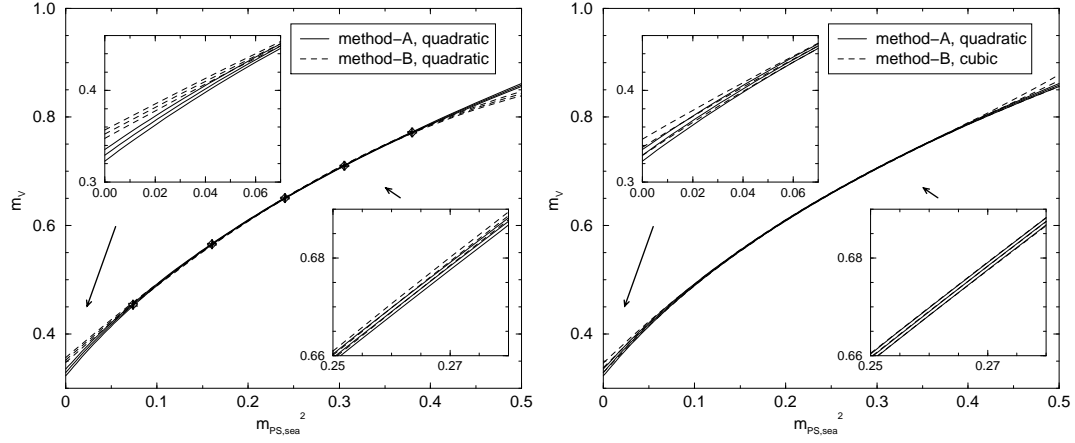


FIG. 30: Comparison of diagonal fits in method-A and B.

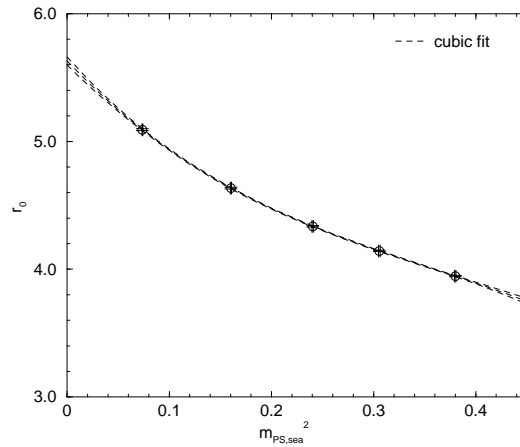


FIG. 31: Chiral extrapolation of r_0 in terms of $m_{PS,sea}^2$.

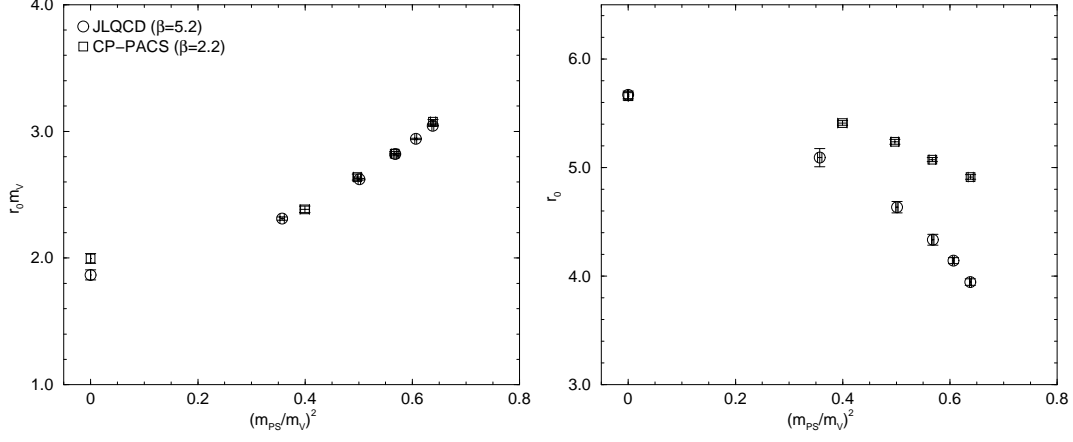


FIG. 32: Comparison of sea quark mass dependence of $r_0 m_V$ (left figure) and r_0 in lattice units (right figure) with those in CP-PACS data. We estimate $r_0 m_V$ in the chiral limit in the CP-PACS data from linear fit in terms of $(r_0 m_{PS})^2$.

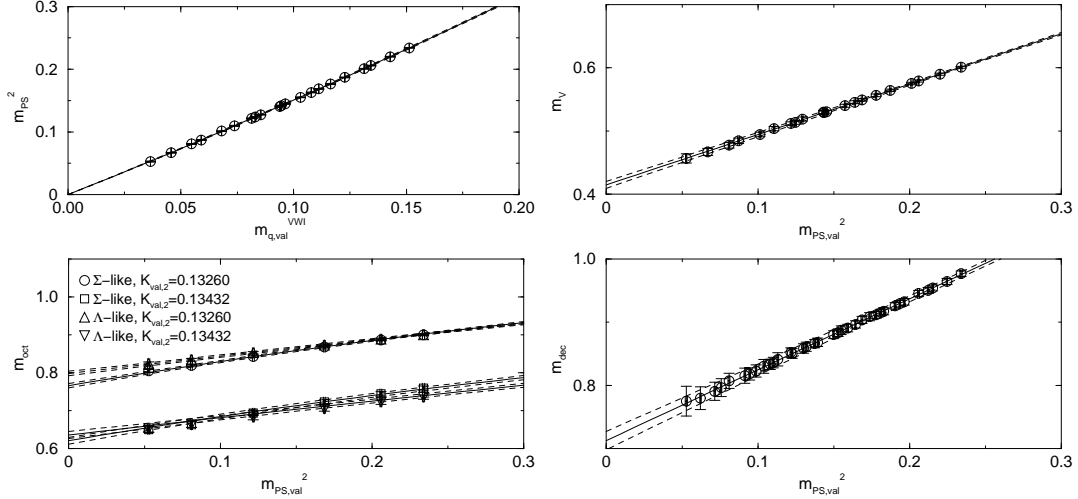


FIG. 33: Chiral extrapolation of meson (top figures) and baryon masses (bottom figures) in quenched QCD. For octet baryon masses, we plot only data at $K_{val,2}=0.13260$ and 0.13432 for simplicity.

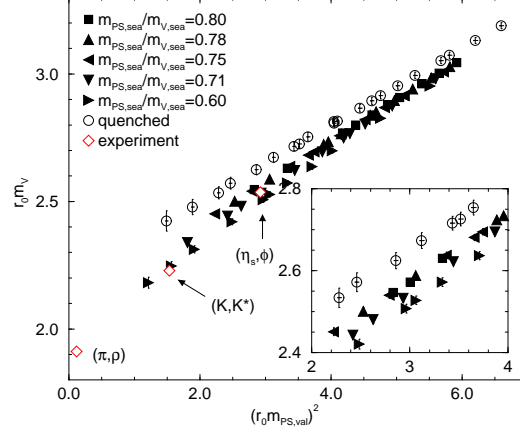


FIG. 34: Vector meson mass as a function of PS meson mass squared at each sea quark mass in full QCD and in quenched QCD. The experimental values of meson masses are also plotted using our result $r_0 = 0.497$ fm, which is determined from Eq. (54) and K_{ud} and a in Table XVI.

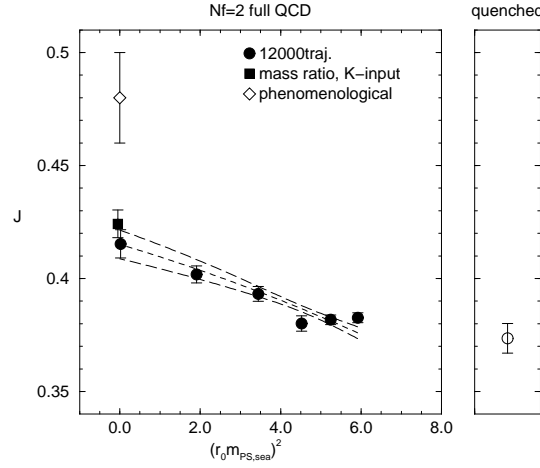


FIG. 35: J parameter defined by Eq. (68) in full (left panel) and quenched QCD (right panel). Dashed lines are reproduced from combined chiral fit, Eq. (41). We also plot values calculated from an phenomenological definition, Eq. (69), using experimental spectrum (open diamond) and our results in Table XX (filled square).

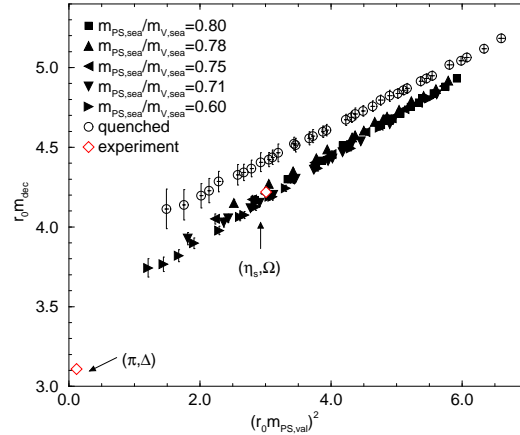


FIG. 36: Decuplet baryon masses as a function of PS meson mass squared at each sea quark mass in full and quenched QCD.

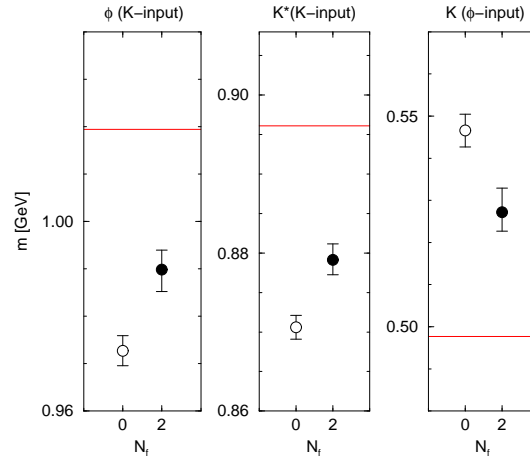


FIG. 37: Comparison of strange meson masses between full and quenched QCD. Experimental values are shown by horizontal lines.

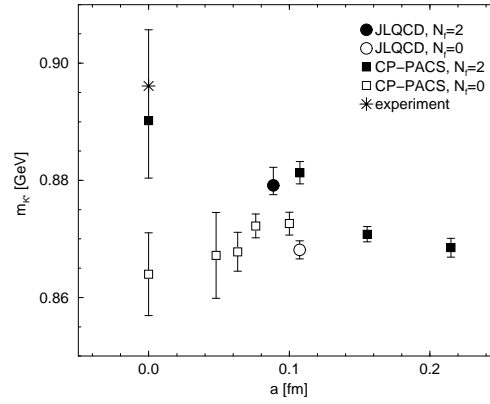


FIG. 38: Mass of K^* meson with K -input as a function of lattice spacing.

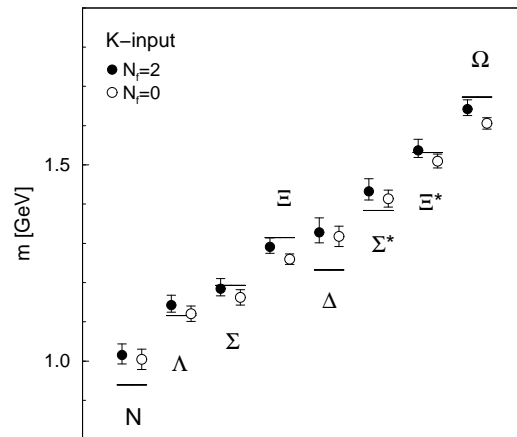


FIG. 39: Baryon spectrum with K -input. Experimental values are shown by horizontal lines.

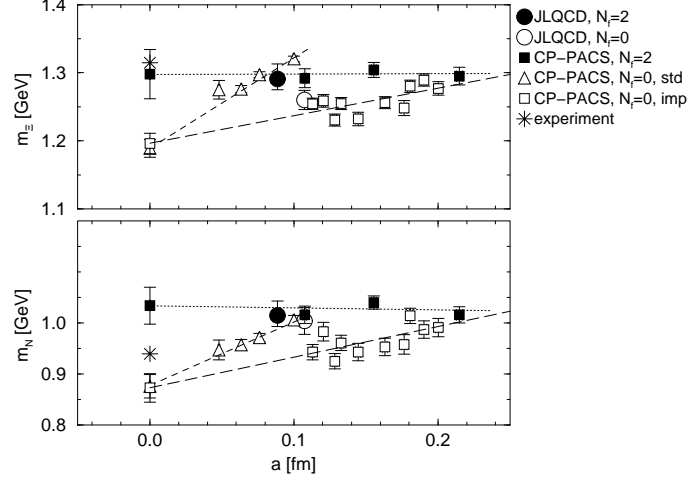


FIG. 40: Nucleon mass (bottom panel) and Ξ baryon mass with K -input (top panel) as a function of lattice spacing. Open triangles represent the CP-PACS results in quenched QCD using the standard plaquette gauge and the Wilson quark actions, while open squares are obtained with the renormalization group improved gauge and the tadpole improved clover actions.

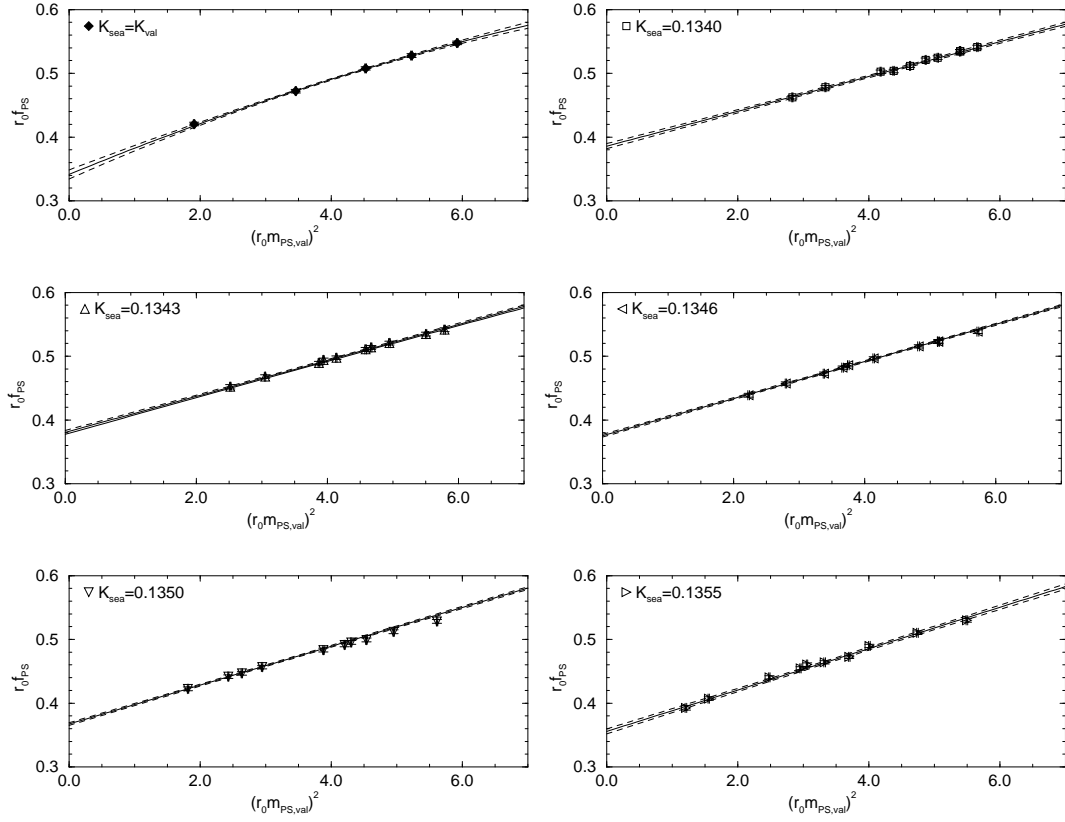


FIG. 41: Combined chiral extrapolation of PS meson decay constants.

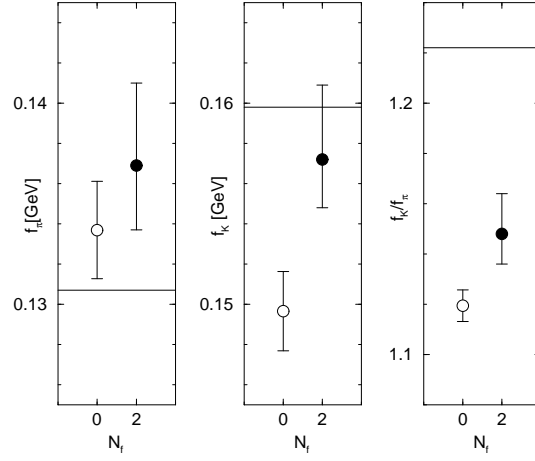


FIG. 42: Comparison of f_π (left panel), f_K (center panel) and f_K/f_π (right panel) between full and quenched QCD. We use K -input for f_K and f_K/f_π . Experimental values are shown by horizontal lines.

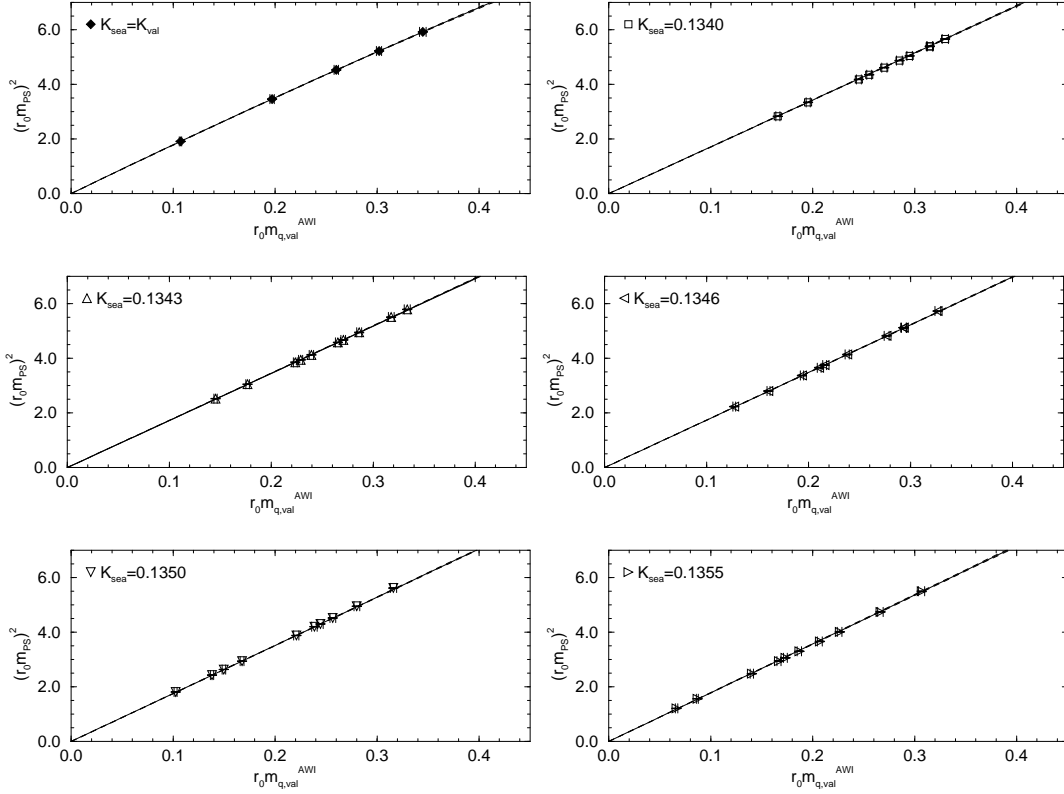


FIG. 43: Combined chiral extrapolation of PS meson masses in terms of AWI quark mass.

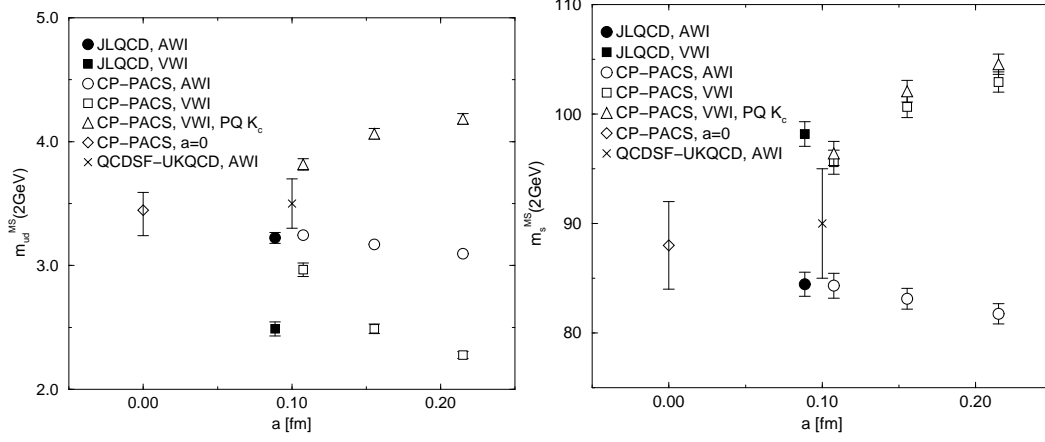


FIG. 44: Comparison of light (left figure) and strange quark mass with K -input (right figure) in two-flavor QCD. Triangles represent the CP-PACS results of the VWI quark mass using K_c determined by partially quenched chiral extrapolations. The CP-PACS result in the continuum limit was obtained by combined linear extrapolation of three data. We note that SESAM- $T\chi L$'s results in Ref. [7] are consistent with these results within large error arising from their continuum extrapolation.

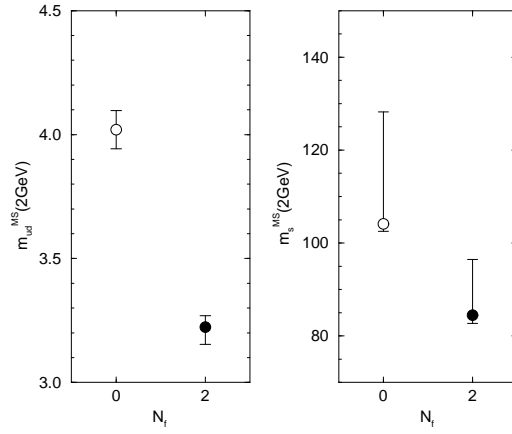


FIG. 45: Comparison of light (left panel) and strange quark mass (right panel) in full and quenched QCD.